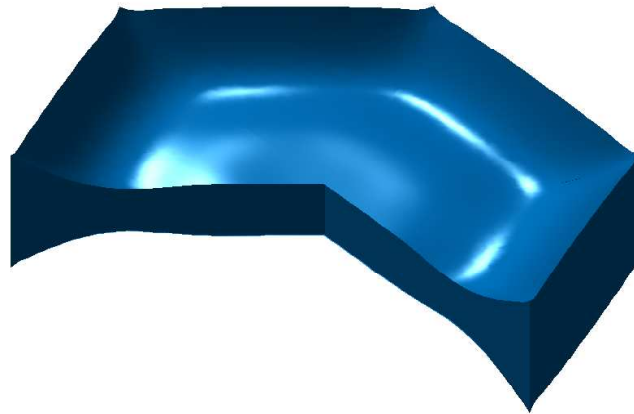


# A Mathematical Analysis of Foam Films



**Dipl. Math. techn. Christian Schick**

Dem Fachbereich Mathematik  
der Universität Kaiserslautern  
zur Verleihung des akademischen Grades  
Doktor der Naturwissenschaften  
(Doctor rerum naturalium, Dr. rer. nat.)  
vorgelegte Dissertation

Referent: Prof. Dr. Dr. h.c. H. Neunzert  
Korreferent: Prof. Dr. A. Unterreiter

Kaiserslautern, 27.04.2004

The image on the title page shows the shape of a three-dimensional hexagonal lamella (ref. page 43) of a pure liquid at time  $t = 0.001$ . The solution has been computed using the model derived in Chapter 3 for the initial condition given in Section 5.1.

Meinen Eltern



An dieser Stelle möchte ich all jenen danken, die mich beim Zustandekommen der vorliegenden Arbeit unterstützt haben. An erster Stelle zu nennen ist hierbei Prof. Helmut Neunzert für die Möglichkeit, am Fraunhofer-Institut für Techno- und Wirtschaftsmathematik in Kaiserslautern zu promovieren, und für die Unterstützung, die ich durch ihn in den vergangenen drei Jahren erfahren habe. Danken möchte ich auch Prof. Andreas Unterreiter für die fruchtbaren Diskussionen, die ich mit ihm führen durfte, sowie für die Übernahme des Korreferats.

Ein besonderer Dank gilt Dr. Jörg Kuhnert, Prof. Michael Junk, Dr. Thomas Götz und Prof. Reinhardt Illner für eine Vielzahl wertvoller Hinweise und Anregungen. Des weiteren danke ich den übrigen Mitarbeitern der Arbeitsgruppe Technomathematik sowie der Abteilung Transportvorgänge des Fraunhofer ITWM für die gute und freundschaftliche Zusammenarbeit. Im speziellen geht mein Dank an Nicole Marheineke und Markus von Nida für das Korrekturlesen der Arbeit sowie zahlreiche hilfreiche Anmerkungen und Diskussionen.

Die finanzielle Unterstützung dieser Arbeit erfolgte im Rahmen des Forschungsprojekts *Umweltfreundliches Betanken* des Fraunhofer ITWM in Verbindung mit dem Bundesministerium für Bildung und Forschung (BMBF) und der Volkswagen AG. Ich möchte mich dafür bei den beteiligten Parteien bedanken.

Mein ganz besonderer Dank gilt meinen Eltern, die mich während des gesamten Studiums und der Promotion stets mit viel positiver Energie unterstützt haben.



---

# Table of Contents

<b>Table of Contents</b>	<b>vi</b>
<b>Preface</b>	<b>xi</b>
<b>1 An introduction to foams</b>	<b>1</b>
1.1 Basic notations . . . . .	1
1.2 Foam scales . . . . .	3
1.3 Basic properties of foam . . . . .	4
1.3.1 Laplace's law . . . . .	4
1.3.2 Plateau's laws . . . . .	4
1.4 Foam stability . . . . .	5
1.4.1 Surfactants . . . . .	5
1.4.2 Volatile components . . . . .	6
1.4.3 Molecular forces . . . . .	7
1.4.4 Surface viscosity . . . . .	8
1.5 Aspects of foam research . . . . .	8
1.5.1 Foam creation . . . . .	8
1.5.2 Geometry . . . . .	9
1.5.3 Rheology . . . . .	10
1.5.4 Decay and coarsening . . . . .	11
1.5.5 Foam drainage . . . . .	11
1.5.6 Film drainage . . . . .	12
1.6 Model of a real foam . . . . .	13
1.7 Foams in gasoline and diesel fuel . . . . .	13
<b>2 Derivation of the thin film equations (TFE)</b>	<b>15</b>
2.1 Newtonian fluid . . . . .	16
2.1.1 Physical model . . . . .	16

2.1.2	Definition of interface parameters . . . . .	17
2.1.3	Interface conditions . . . . .	17
2.1.4	Nondimensionalization . . . . .	18
2.1.5	Asymptotic expansion . . . . .	20
2.1.6	Special cases . . . . .	24
2.2	Surfactant . . . . .	26
2.2.1	Physical model . . . . .	26
2.2.2	Conditions at the free interfaces . . . . .	27
2.2.3	Influence on the surface tension . . . . .	29
2.2.4	Nondimensionalization . . . . .	30
2.2.5	Asymptotic expansion . . . . .	31
2.2.6	Surface tension . . . . .	33
2.3	Volatile component . . . . .	33
2.3.1	Physical model . . . . .	33
2.3.2	Interface conditions . . . . .	34
2.3.3	Determination of the evaporation rate . . . . .	35
2.3.4	Influence on the surface tension . . . . .	36
2.3.5	Nondimensionalization . . . . .	36
2.3.6	Asymptotic analysis . . . . .	37
2.3.7	Surface tension and evaporation rate . . . . .	38
2.4	Summary . . . . .	39
2.4.1	Pure liquid . . . . .	39
2.4.2	Presence of a surfactant . . . . .	39
2.4.3	Presence of a volatile component . . . . .	40
<b>3</b>	<b>Analysis of a foam film in fuel</b>	<b>41</b>
3.1	Setting of the problem . . . . .	41
3.2	Initial and boundary conditions . . . . .	44
3.2.1	One-dimensional problem . . . . .	45
3.2.2	Two-dimensional problem . . . . .	48
3.2.3	Initial conditions . . . . .	50
3.3	Discussion of parameter sizes . . . . .	50
3.4	Resulting model for fuel foam . . . . .	53
3.5	Analytical discussion of the problem . . . . .	56
3.5.1	Classification of the PDE . . . . .	56
3.5.2	An existence and uniqueness result for the linearized problem	57



3.5.3	Discussion of the nonlinear problem . . . . .	66
3.6	A numerical scheme for the solution of the lamella problem . . . . .	68
3.6.1	A Galerkin finite element approach . . . . .	68
3.7	Discussion of the error . . . . .	73
3.8	Summary . . . . .	74
<b>4</b>	<b>The limit <math>\varepsilon \rightarrow 0</math></b>	<b>75</b>
4.1	Domain splitting approach . . . . .	76
4.2	Inertia-free case . . . . .	77
4.2.1	General model . . . . .	77
4.2.2	Pure liquid . . . . .	78
4.2.3	Presence of a surfactant . . . . .	82
4.2.4	Presence of a volatile component . . . . .	86
4.3	Non-planar lamella . . . . .	89
4.3.1	Governing equations . . . . .	89
4.3.2	Generalized splitting approach . . . . .	89
4.3.3	Pure liquid . . . . .	90
4.3.4	Presence of a surfactant . . . . .	92
4.3.5	Presence of a volatile component . . . . .	94
4.4	Generalization to 2D . . . . .	95
4.4.1	Example: Foam film stabilized by a surfactant . . . . .	96
<b>5</b>	<b>Results and applications</b>	<b>98</b>
5.1	General remarks . . . . .	98
5.2	Pure liquid . . . . .	99
5.2.1	Influence of inertia . . . . .	101
5.2.2	Choice of initial conditions . . . . .	101
5.2.3	Dependence on $\kappa$ . . . . .	103
5.2.4	Behaviour for $\varepsilon \rightarrow 0$ . . . . .	104
5.2.5	Two-dimensional problem . . . . .	106
5.3	Influence of a surfactant . . . . .	109
5.3.1	Evolution of the film thickness . . . . .	109
5.3.2	Approximation for $\varepsilon \rightarrow 0$ . . . . .	110
5.3.3	Two-dimensional problem . . . . .	113
5.4	Influence of a volatile component . . . . .	118
5.5	Extensions . . . . .	122
5.5.1	Coupling with a global foam model . . . . .	122

5.5.2	Application of an enhanced evaporation model . . . . .	123
5.5.3	Continuous thermodynamics . . . . .	123
	<b>Conclusion</b>	<b>124</b>
	<b>Nomenclature</b>	<b>127</b>
	<b>References</b>	<b>130</b>
	<b>Index</b>	<b>134</b>

# Preface

With the increase of computing power over the past years, numerical simulation has become a major constituent in the derivation of new theories and the development and optimization of industrial products. In some areas, e.g. the automotive industry, it is already a key element for the evaluation of new designs, allowing for efficient virtual experiments and thus reducing development time and costs. Moreover, simulation can provide data that is hard or impossible to obtain in a physical experiment and therefore serves as a source of deeper insights into complex phenomena.

However, the conduction of numerical experiments is a science of its own. The core of any numerical simulation is a mathematical model of the involved process, whose quality is crucial to the result of the simulation. The challenge in the development of such a model is to find the optimal compromise between accuracy and computational demand. It should reproduce all the important phenomena occurring in the real problem while allowing for an efficient numerical solution.

This thesis is embedded in the research project *Umweltfreundliches Betanken* of the *Fraunhofer Institut für Techno- und Wirtschaftsmathematik (ITWM)* in Kaiserslautern, supported by the *German Federal Ministry of Education and Research (BMBF)* in cooperation with the *Volkswagen AG* as an industrial partner. The primary goal is to assist in the design process of car fuel tanks through the simulation of tank-filling processes. A full simulation of such a complex dynamical process is facilitated by the use of state-of-the-art numerical methods such as the *Finite Pointset Method (FPM)* (ref. [25] and [26]), a meshfree method based on a local least squares approximation, allowing for the efficient simulation of free flows in complex geometries.

An important issue arising in the filling process is the undesirable formation of foam in the tank. Its presence can lead to a premature termination of the fueling if the tank is partly occupied by foam instead of mere fuel. The consideration of this effect in the simulation requires an appropriate mathematical model. Modelling the foam in its entirety as two-phase flow of a continuous liquid phase and dispersed gaseous bubbles is certainly a straightforward approach, but leads to

an insurmountable computational effort. However, the formulation of a unified macroscopic foam model is difficult due to the many aspects resulting from the complex foam structure, e.g. drainage and decay. One approach for a more sophisticated model is based on the decomposition of the problem into isolated subproblems dealing with single aspects. An analysis of the corresponding models provides a thorough understanding of the occurring effects. Moreover, the coupling of their solutions yields information regarding the macroscopic problem.

In this work, we deal with one of the fundamental questions in this context, namely the breakup of foam. This is of particular interest as fuel foam is very short-lived. To obtain an insight into this problem, the mechanisms leading to the rupture of a single foam lamella have to be studied. Therefore, the aim of this thesis is to develop and analyze a model describing the evolution of such a lamella, paying special attention to the processes leading to its thinning. Moreover, strategies to couple this lamella model to a macroscopic foam model are discussed, and suitable coupling parameters determined.

The thinning of free foam films has previously been studied in several works, including [34], [3], [8] and [9]. Our approach differs from the models presented in these references in several points:

- All of these models are based on the decomposition of the film into several regions for which simplified equations are derived. However, the approximations involved in this approach require the lamella to be very thin and are only applicable to a limited range of problems. We will develop a more general model suitable also for relatively thick films and are therefore able to cover a longer time span of the thinning process.
- Inertia is completely neglected in all of the above works. We found that inertial effects can play an important role in the lamella evolution and have included them in our model.
- The previous models are restricted to two-dimensional films; we consider the more general three-dimensional case.

This work is organized as follows: We start with an overview of the physical and chemical properties of foams, presenting the various aspects in foam research and some of the previous work that has been done in these areas.

In the second chapter, a mathematical model describing the dynamics of foam lamellae is developed. Starting from a free surface flow governed by the incompressible Navier-Stokes equations, an asymptotic analysis with respect to the lamella thickness yields a set of equations on a simpler fixed geometry which

we call *thin film equations*. A similar approximation is done for the equations describing surfactant and volatile component.

Chapter 3 deals with a real foam film made up of fuel. The parameters of the foam are determined for this case, and conclusions about the relative magnitude of the considered physical effects are drawn. Foam lamellae are surrounded by Plateau borders, whose influence on the film is realized by posing appropriate boundary conditions. The central film-thinning problem is formulated and investigated theoretically, leading to an existence and uniqueness result for the linearized model. Finally, a Galerkin scheme is developed for the numerical examination of the problem.

In the case of a very thin lamella, for which the ratio  $\varepsilon$  between thickness and length of the film tends to zero, a domain splitting approach is used to derive a set of simpler models which can be more efficiently solved than the full problem considered in Chapter 3. Such an approach is discussed in Chapter 4 first for an inertia-free film and then generalized to the case where inertia is included.

Chapter 5 discusses numerical results for the film-thinning problem and examines the mechanisms involved in the process. The influence of surfactants and volatile components on the stability of the foam is examined and compared. Moreover, some suggestions for extensions to the thin film models derived in this work are discussed.

We close the work with some final conclusions.



# Chapter 1

## An introduction to foams

### 1.1 Basic notations

**Definition 1** *A colloidal dispersion is a system containing two phases, of which one is continuous and the other phase is dispersed in the first. Moreover, the order of magnitude of the dispersed particles is larger than molecular size.*

Examples for such dispersions are polystyrene (gas dispersed in a solid), ceramics (solid in solid), smoke (solid in gas), mist (liquid in gas) or soap foam (gas in liquid).

**Definition 2** *Foams are colloidal dispersions in which the dispersed phase is a gas. We call the dispersed gas particles bubbles or cells.*

We distinguish between *solid foams* and *liquid foams*. Solid foams are often used in order to create light but strong materials (for example aluminium foam), since they retain much of the strength of the original material. Liquid foams have been much longer utilized industrially and are for example used when one wants to create a large volume out of a small amount of liquid. This effect is used in fire extinguishers or in the oil drilling industry, where foam is pumped into oil fields in order to press out as much oil as possible.

In this thesis, however, we are concerned with another effect of liquid foam, namely that it often emerges in unwanted situations as for example in a car tank during the filling process, or when opening a bottle of shaken beer. Therefore, in the remainder of this thesis, *foam* always denotes a liquid foam.

**Definition 3** *The liquid content  $\varphi$  of a foam is the volume fraction of its liquid part. It is customary to speak of emulsions if  $\varphi$  is of the magnitude 0.9 and larger,*

and of foams if it is about 0.1–0.2 or lower. However, these ranges are not strict, and there is a smooth transition between emulsions and foams as shown in Figure 1.1 (left).

Moreover, we say a foam is dry if the liquid content is close to  $\varphi = 0$  and wet if it is closer to  $\varphi = 0.2$ . As before, the transition is smooth.

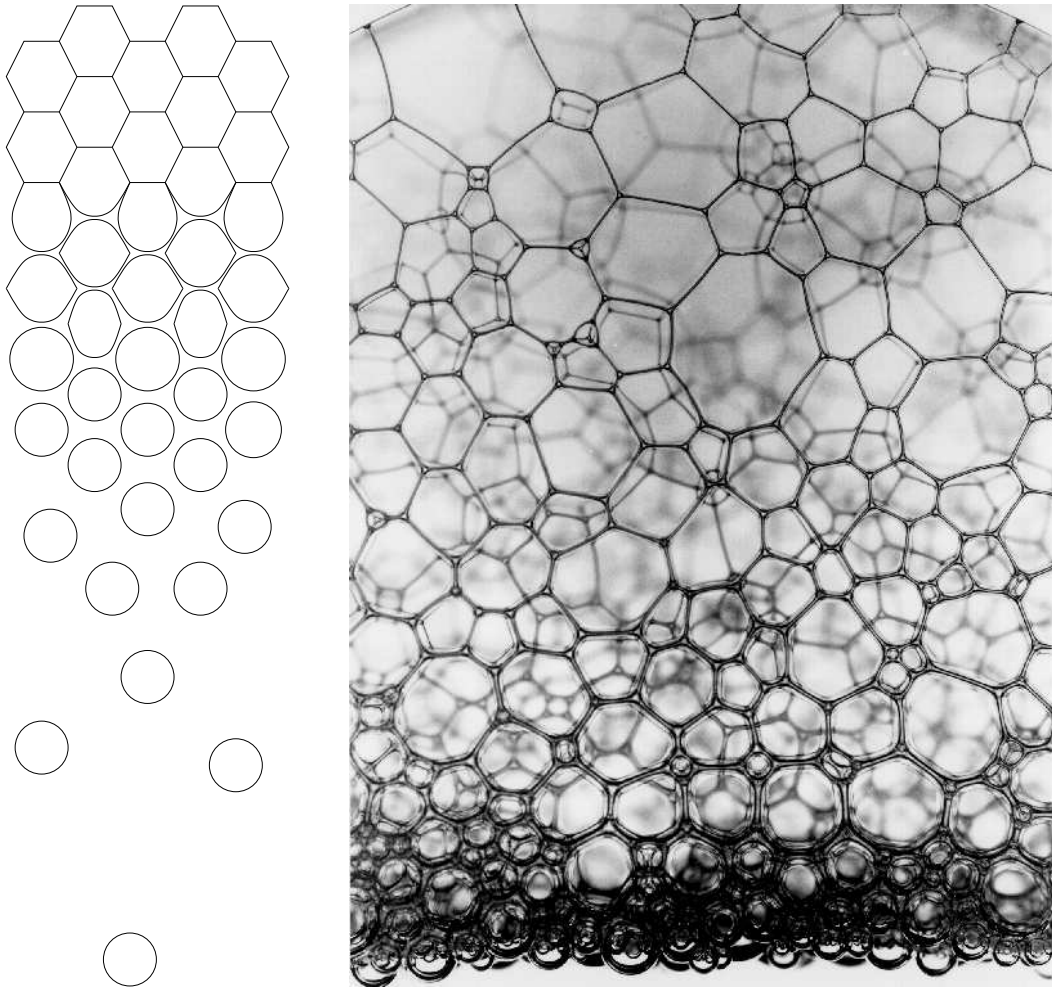


Figure 1.1: LEFT: Transition from dry foam (top) to emulsion (bottom). RIGHT: Photograph of a real foam (Courtesy of <http://www.physics.ucla.edu/~dws/foam.html>)

The geometry of a foam (in the broad sense including emulsions) and its bubbles depends strongly on its liquid content. In an emulsion, where bubbles do not interfere with each other, their shape is spherical. When the liquid content is lower, bubbles become packed together and are deformed to become more polyhedral in shape. The limit at which the bubbles just touch each other such that



their shape is still spherical is sometimes called *Kugelschaum* (which is German for *spherical foam*). In the dry limit, i.e.  $\varphi \rightarrow 0$ , the bubbles become perfect (curved) polyhedra. This is also called *Polyederschaum*.

**Definition 4** Consider a foam with a liquid content that is lower than that of *Kugelschaum* such that bubbles have a polyhedral shape.

The (more or less flat) faces of these polyhedral bubbles are called lamellae or (foam) films.

The edges of the bubbles are called Plateau borders. There are always three lamellae meeting in a Plateau border (see Figure 1.2 (left)).

The vertices of the bubbles are called nodes. There are always four Plateau borders meeting in a node (see Figure 1.2 (right)); generated using the free software “surface evolver” by Ken Brakke, available at [6].

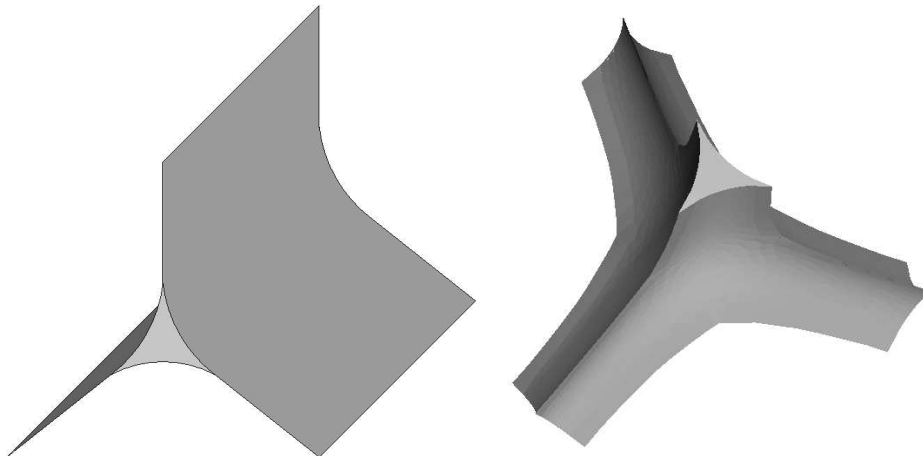


Figure 1.2: LEFT: Plateau border. RIGHT: Node.

For very wet foams these definitions lose their meaning.

**Remark** In dry foams, most of the liquid contained in the foam is located in the Plateau borders and nodes.

## 1.2 Foam scales

A conventional fluid may be considered on two different scales: on the one hand we have the *microscopic scale* at which atoms and molecules interact via molecular

forces, and on the other hand the *macroscopic scale*. This is the scale where the fluid appears at a continuous phase and which is usually the interesting one for flow simulations.

In a foam, however, we have an additional scale. There is the microscopic scale at which molecules interact, the macroscopic scale at which the foam appears as a continuous fluid, and there is the scale at which the size of bubbles is of order one. We will refer to this as the *mesoscopic scale*.

## 1.3 Basic properties of foam

The shape of a foam in equilibrium at the mesoscopic scale, i.e. the shape of the bubbles, is mainly determined by some basic laws. These are crucial for the complete examination of foams and are therefore stated in the following.

### 1.3.1 Laplace's law

Laplace's law of capillary pressure states that at a gas-liquid interface, the pressure-difference between the two phases is

$$p_1 - p_2 = \sigma \left( \frac{1}{R_1} + \frac{1}{R_2} \right), \quad (1.1)$$

where  $\sigma$  is the surface tension of the liquid and  $R_1, R_2$  are the principal radii of the interface. If there is a pressure difference between two bubbles, this leads to a curvature of the separating lamella, which is cambered into the bubble with lower pressure.

### 1.3.2 Plateau's laws

Plateau's laws state that in a stable stationary foam a Plateau border is always a junction of three lamellae, and the angle between them is always  $120^\circ$ . Furthermore there are always exactly four Plateau borders meeting in a node at an angle of approximately  $109,5^\circ$  (the tetrahedral angle). This is a consequence of the ambition of the liquid to reduce its surface energy and has been mathematically proven by Jean Taylor in 1976 [36].

## 1.4 Foam stability

Foams are inherently unstable. Since every liquid tries to minimize its surface area due to its surface tension, it would be energetically much more favorable for a lamella to become a spherical drop. So we have to ask the question: What makes a foam stable?

At this point, we will present some effects that can have a stabilizing effect on foams in different circumstances.

### 1.4.1 Surfactants

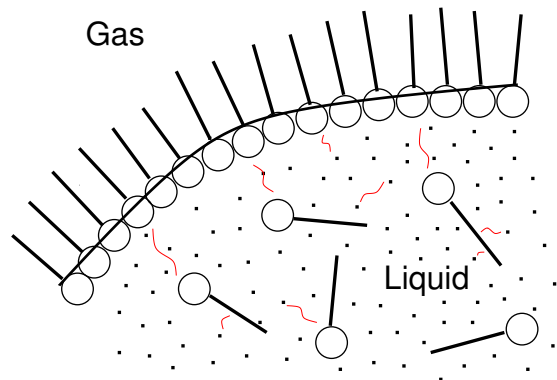


Figure 1.3: Surfactants in a solution.

Pure water does nearly not foam at all. This changes dramatically if soap is added. The reason for this is that soap consists of surface-active agents or so-called *surfactants*. These are long molecules composed of a hydrophilic “head” and a hydrophobic “tail” which therefore accumulate at the surface of the liquid, thus reducing the surface tension (see Figure 1.3). The crucial point is that the surface tension is no longer constant as in a pure liquid but varies with the surfactant concentration; a lower concentration corresponds to a higher surface tension. The following examples show how this leads to a stabilization of the foam.

**Example** *Assume a flat foam film in equilibrium, which is disturbed in such a way that a dent is formed (Figure 1.4). Liquid flows outwards and pulls the surfactant with it. Hence, a gradient in the surfactant concentration evolves which leads to a surface force pointing into the dent, the so-called Marangoni force. Liquid from the bulk is dragged along due to viscosity which ultimately levels the dent and stabilizes the film.*

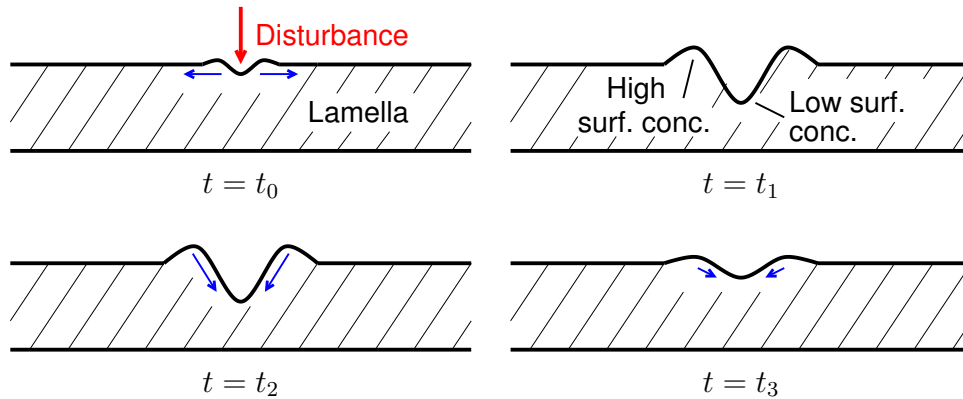


Figure 1.4: Stabilization due to Marangoni forces. TOP LEFT: A lamella is hit by a disturbance, liquid flows outward (velocity in blue). TOP RIGHT: A dent has formed, surfactant has been dragged out of it. BOTTOM LEFT: Liquid starts to flow back due to Marangoni force. BOTTOM RIGHT: Dent has been smoothed out.

**Example** Consider a lamella close to the Plateau border (Figure 1.5). Due to Laplace's law, there is a lower pressure in the Plateau border than in the lamella. This causes a flow of liquid out of the lamella, thinning it. The same mechanism as in the previous example yields a Marangoni force retarding the flow and hence slowing the thinning, which increases the lifetime of the film.

### 1.4.2 Volatile components

Consider a liquid composed of several components with different surface tensions, of which one or more are volatile. Since the lamellae have a much larger ratio of surface to volume than the Plateau borders, the concentration of the volatile components in an a priori well-mixed solution will decrease much faster in the lamellae. As the surface tension of the solution depends on its composition, this may lead to a Marangoni force which either accelerates or retards the flow of liquid into the Plateau border, depending on the surface tensions of the components. If the volatile components have a lower surface tension than the rest, the system is called *Marangoni positive*. In this case, the evaporation leads to a stabilization of the foam. Otherwise, the system is called *Marangoni negative* and the opposite effect occurs (see for example [44]).

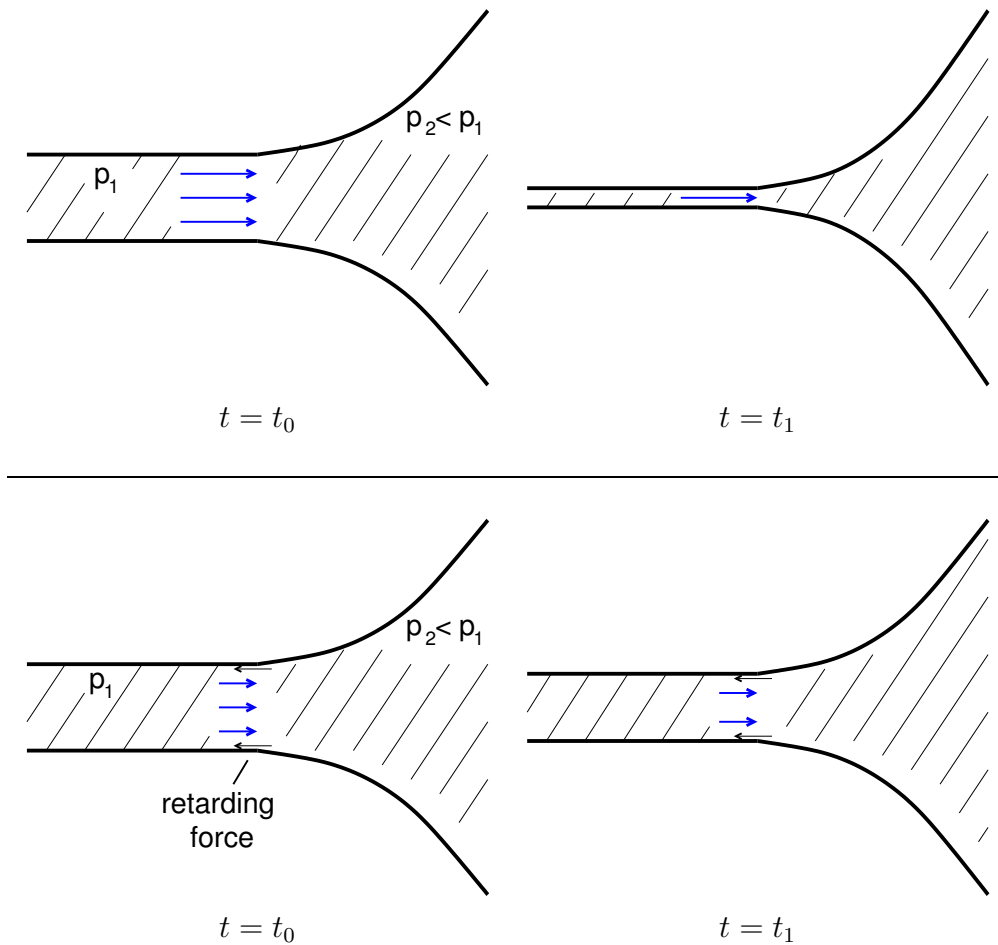


Figure 1.5: Slowing of film thinning. TOP LEFT: Liquid flows into the Plateau border due to pressure difference, no surfactant present. TOP RIGHT: The lamella thins very fast and becomes unstable. BOTTOM LEFT: Surfactant present; Marangoni force retards the flow. BOTTOM RIGHT: Film thinning happens much slower.

### 1.4.3 Molecular forces

If a lamella becomes very thin, molecular forces between surfactants on either side of the film may appear. An electric double layer can form at both sides of the lamella, which repel each other if the foam is thin enough. This leads to a stabilization of the film. More about the stabilization of foam films by molecular forces can be found for example in [5].

### 1.4.4 Surface viscosity

A common concept for the stability of foams that is widely used in applications is the so-called *surface viscosity*. The basic idea behind it is that if liquids containing surfactants form thin films, they have a sandwich-like structure. The outer layers (adjacent to the gas phase) have a high surfactant concentration and do therefore have a higher viscosity than the liquid in the interior layer. These viscous outer layers act as a kind of skin that keeps the lamella stable.

**Remark** *It has to be noted that the concept of surface viscosity is different from the common Newtonian viscosity, which is not existent for two-dimensional surfaces. A drawback to this idea is that surface viscosity is not correlated to the fluid viscosity and needs to be measured in a complicated way.*

Although surface viscosity can be used to explain aspects of foam stability and has been successfully applied in simulations, we are convinced that it is only a symptom of the effects originating from Marangoni forces acting in the film and not an independent physical property. Therefore, we prefer to deal with Marangoni forces directly and discard the concept of surface viscosity in this thesis.

## 1.5 Aspects of foam research

At this point, we want to give a short overview on research topics arising in connection with foam and classify this thesis in this context. Due to the complex nature of foam, there are miscellaneous aspects in its behaviour on the different scales which lead to a variety of physical and mathematical challenges. A general overview on foams, experimental studies and applications is given in [5]. This book is a good starting point, while it concentrates on phenomenological studies and simple heuristic models.

### 1.5.1 Foam creation

Foam is created when gas and liquid are mixed. This may happen when a liquid is stirred such that gas is introduced due to perturbations at the surface (for example when washing the dishes), or when gas dissolved in a liquid is released due to a pressure drop (for example when opening a beer bottle).

While there are many studies of “foaminess” of solutions in controlled experimental environments (for example [5]), to our knowledge there exists currently

no rigid mathematical model of foam creation that can be utilized in simulations of real foams.

### 1.5.2 Geometry

Numerous researchers are interested in the geometry of foams. As mentioned above, the geometry strongly depends on the liquid content of the foam (Kugelschaum vs. Polyederschaum). The aim is to find feasible foam geometries, usually under the condition that they have some interesting properties.

There are a number of very interesting geometrical problems arising with (infinitely dry) foam. Although their significance for the simulation of a real foam may not be that great, we at least want to mention one of them, the so-called *Kelvin problem*. The challenge of this problem is to find the space-filling arrangement of similar cells of unit volume that has the minimal surface area. The problem is closely related to the *Kepler problem*, which is to find the densest packing of unit spheres.

Although in two dimensions this problem has a very simple solution, the honeycomb structure (Figure 1.6), it could only be proved very recently by Tom Hales that this is indeed the optimal geometry [18]. Notably, he also proved the Kepler conjecture in three dimensions [19], which was one of Hilbert's famous 23 mathematical problems.

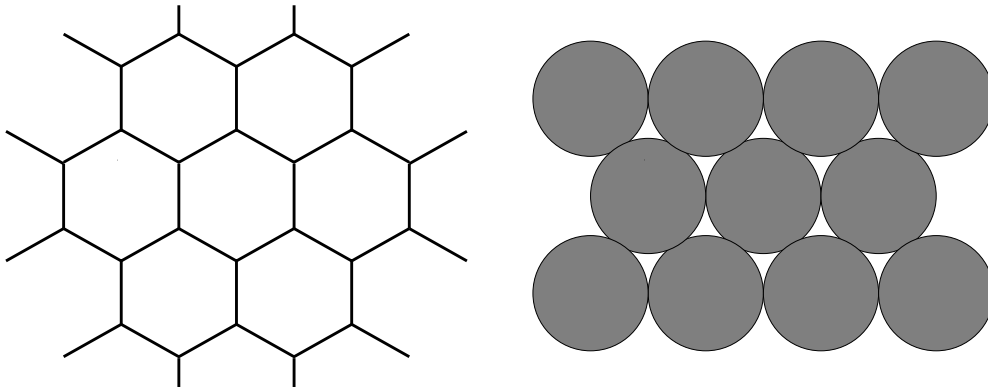


Figure 1.6: LEFT: Honeycomb structure. RIGHT: Sphere packing.

The three-dimensional Kelvin problem is even more complex (and still unsolved). In 1887, Lord Kelvin proposed a possible solution [37], a slightly curved 14-sided truncated octahedron which is now called the *Kelvin cell* (Figure 1.7). This solution could not be improved for more than one hundred years, until in 1994

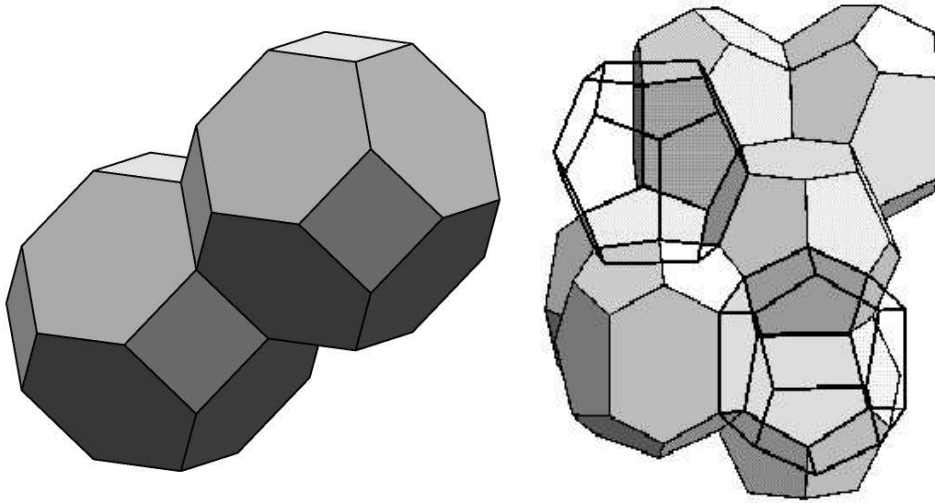


Figure 1.7: LEFT: Kelvin cell. RIGHT: Weaire-Phelan cells.

Weaire and Phelan found a structure consisting of six 14-sided polyhedra and two 12-sided polyhedra [41] that has a slightly smaller surface (per volume) (Figure 1.7). It should be noted, that the Kelvin cell is still the optimal known solution if only one kind of bubbles is allowed, and that there is still no proof of optimality for either of the solutions.

### 1.5.3 Rheology

Often, one is not interested in the structure of a foam or small-scale behaviour such as the flow of liquid through lamellae and Plateau borders, but one wants to study the flow of a foam at the macroscopic scale, i.e. consider the foam as a continuous fluid. In order to do this, one has to find the rheological properties of the foam which depend in turn on the mesoscopic properties of the foam such as its geometry and its liquid content.

A very dry foam, for example, has some properties which are similar to those of a solid, while a wet foam is much closer to a Newtonian fluid. The aim is to find a simple rheological model with as few coefficients as possible that can be determined in a simple way.

An overview on foam flows and the rheology of foam can be found for example in [24] and [43].



### 1.5.4 Decay and coarsening

In general, foams have only a limited lifetime and will by and by decay. As we will discuss in the following sections, the liquid content of a foam reduces due to gravity and the lamellae become thinner until they eventually rupture (theoretically the films may just become infinitesimally thin, but the thinner a lamella is, the less stable it becomes and at some time it will rupture due to outer disturbances, unless in a very controlled environment).

If a lamella bursts, bubbles will rearrange until they reach a new equilibrium, changing the topology of the foam. This is especially the case if a lamella between two bubbles ruptures. In this case, the two bubbles merge to one larger bubble; this process is called *coarsening*.

Coarsening can have two causes: the bursting of a lamella between two cells, but also diffusion of gas through the lamellae. These are not totally impervious, but gas diffuses through them slowly, if there is a pressure difference between neighbouring cells. Since smaller bubbles in general have a higher pressure, these cells become even smaller until they vanish, such that small bubbles disappear with time, while large bubbles become even larger.

### 1.5.5 Foam drainage

A newly formed foam is usually not in equilibrium, but liquid immediately begins to drain out of it due to gravity. This process is called *foam drainage*.

Commonly, the lamellae are considered to be thin and their contribution to the drainage is neglected. Instead, the drainage is assumed to happen entirely in a network of Plateau borders and nodes. If one furthermore assumes a Poiseuille-type flow through this network, together with some more simplifications (see for example [42]), the following *foam drainage equation* for the cross-sectional area of the Plateau border network can be derived:

$$\frac{\partial \alpha}{\partial \tau} + \frac{\partial}{\partial \xi} \left( \alpha^2 - \frac{\sqrt{\alpha}}{2} \frac{\partial \alpha}{\partial \xi} \right) = 0 \quad (1.2)$$

This is a dimensionless equation in one space dimension, as in this simplest case  $\alpha$  is assumed to be only dependent on the height;  $\alpha$  is essentially the liquid content of the foam at a given height and time. Equation (1.2) is a kind of Darcy law for porous media, which is not very surprising considering the structure of a foam.

More about history, experiments and the derivation of this equation can be found in the reviews of Andy Kraynik [23] and Denis Weaire et al. [42]. A mathematical examination and the analysis of special solutions is given in [21] and [39].

A more general form of the foam drainage equation, allowing for slip conditions at the gas-liquid-interfaces, is discussed in [22].

### 1.5.6 Film drainage

Unlike foam drainage, which describes the flow of liquid through Plateau borders due to gravity, *film drainage* denotes the flow of liquid out of a lamella into the Plateau borders due to capillary suction (Figure 1.8).

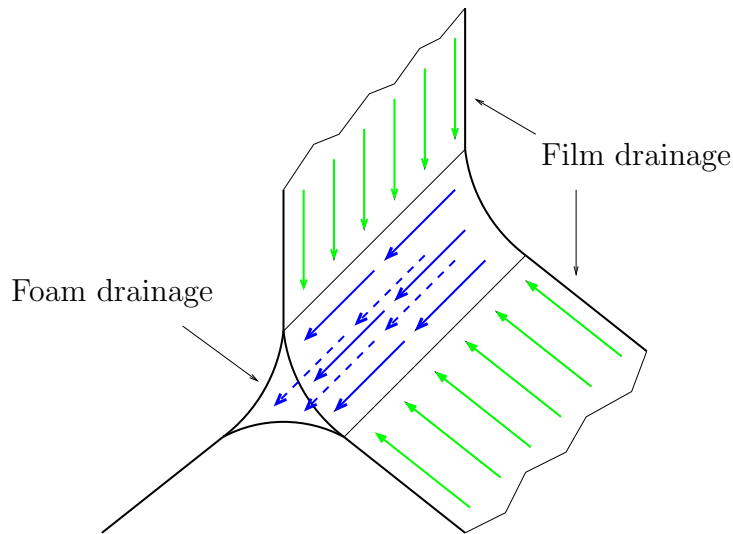


Figure 1.8: Foam drainage vs. film drainage.

The thickness of foam films and their rate of thinning are of great importance for foam stability and the lifetime of foams. Film drainage is the crucial effect that leads to the thinning of a lamella.

We have mentioned above that film drainage is usually neglected in foam drainage models, as it is assumed that the lamellae are very thin and do therefore not contribute much to the overall drainage. However, for wet films this is not necessarily true, such that an examination of film drainage may lead to an improved model for foam drainage.

In this thesis, we will concern ourselves with the stability and decay of foam arising in car tanks during the tank-filling process. Therefore, the main focus of this work is placed on film drainage. In particular, we will consider the thinning of a single three-dimensional lamella stabilized by the Marangoni effect caused by the presence of a surfactant or a volatile component. A similar problem has

already been studied in the dissertation of C. Breward, but in a more theoretical and less general point of view [9].

Early studies of film thinning have been done by Mysels, Shinoda and Frankel in [29]. Schwartz and Princen studied dynamics of films pulled out of Plateau borders in order to compute the effective viscosity of foams [34]. Vaynblat et al. examined mathematical phenomena in film rupture [38].

Some work has also been done for thin films coating a surface, for example in [4], [32] and [17]. Analytical studies of equations arising in such a context involve [20] and [14].

## 1.6 Model of a real foam

It is important to understand that in a real foam, all of the aspects from the previous section influence each other. Hence, a simulation of a real foam has to take all of these effects into account. Theoretically, it may be possible to compute the dynamics of the complete foam on the mesoscopic scale, i.e. simulate the flow of liquid in the complex foam structure as well as the gas flow in each bubble. However, this approach is computationally much too expensive.

Therefore, one is interested in developing models for the different aspects of foam and then couple these models in order to solve a specific problem. If one only wants to simulate the macroscopic flow of the foam, one may use a homogenization approach in order to obtain the rheological parameters from a mesoscopic model of only a few bubbles. Moreover, creation, drainage and decay may be modularly added.

In the application under consideration, in which this thesis is embedded, the aim is to simulate the foam arising in a tank-filling process. Since the foam has a relatively short lifetime, its decay plays an important role for this task. In this thesis, we are therefore interested in the thinning of foam lamellae in order to predict the local lifetime of foams depending on its state.

## 1.7 Foams in gasoline and diesel fuel

Since we are interested in foam arising in a car tank, we need to know the foaming properties of gas (or gasoline, benzine) and diesel fuel, i.e. which effects and which substances are in which way responsible for the development of foam.

Fuel is a compound of a multitude of chemical substances, therefore this question is very difficult to answer. However, we assume that the effects discussed in Section 1.4 are also responsible for fuel foaming. In particular, we consider the Marangoni effect caused by surfactants and volatile components, as we assume that these are the dominant effects.

**Remark** *In the remainder of this thesis, we will speak of gasoline and diesel, or of fuel if we refer to both of them simultaneously.*

## Chapter 2

# Derivation of the thin film equations (TFE)

The aim of this work is the simulation of the thinning of foam films in order to obtain estimates for the rate of decay of foams. Therefore, we need to establish a model for the evolution of such a film.

In this chapter, we will derive equations describing the flow of liquid inside of a foam lamella and from such a lamella into the Plateau borders. We are dealing with a geometry as in Figure 2.1, a thin film of liquid between two gas bubbles bordered by free liquid-gas interfaces on either side.

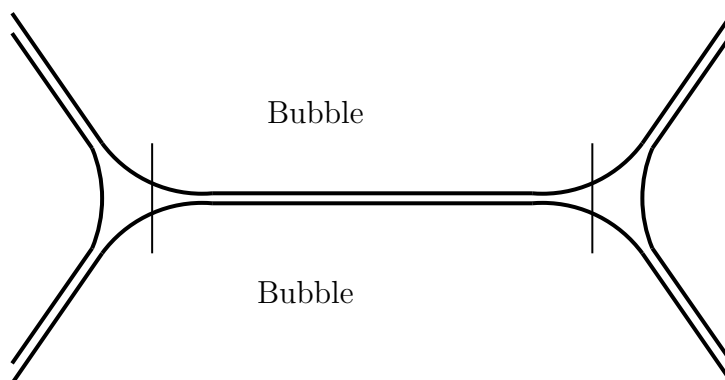


Figure 2.1: Lamella between two bubbles

In the following, we will consider a thin parametrizable lamella with a center-face  $H(x, y, t)$  and thickness  $h(x, y, t)$ . The interfaces between liquid and air are situated at  $H(x, y, t) \pm \frac{1}{2}h(x, y, t)$  (see Figure 2.2). We will present the basic

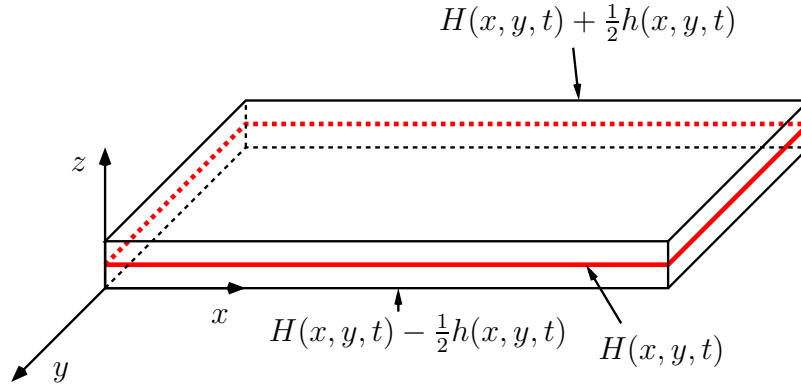


Figure 2.2: Thin liquid film

equations describing the behaviour of a Newtonian liquid, a surfactant and a volatile component. These will be the basis for the derivation of the thin film equations which will be studied further in this thesis.

## 2.1 Newtonian fluid

### 2.1.1 Physical model

In the following, we will present the basic model for the simulation of an incompressible Newtonian fluid. We are dealing with the filling of a car tank, hence the liquid under consideration is gasoline or Diesel, both of which are compounds of several hydrocarbons. However, at the moment we are only interested in the fact that we can consider them as incompressible Newtonian fluids, so the flow is described by the *Navier-Stokes equations* whose derivation can be found in any standard fluid dynamics book, for example [15].

$$u_x + v_y + w_z = 0 \quad (2.1)$$

$$\rho(u_t + uu_x + vv_y + ww_z) = -p_x + \mu[u_{xx} + v_{yy} + w_{zz}] + \rho g_1 \quad (2.2)$$

$$\rho(v_t + uv_x + vv_y + vw_z) = -p_y + \mu[v_{xx} + v_{yy} + v_{zz}] + \rho g_2 \quad (2.3)$$

$$\rho(w_t + uw_x + vw_y + ww_z) = -p_z + \mu[w_{xx} + w_{yy} + w_{zz}] + \rho g_3 \quad (2.4)$$

The indices denote derivatives. Equation (2.1) represents conservation of mass and Equations (2.2) – (2.4) represent conservation of momentum in  $x$ -,  $y$ - and  $z$ -direction, respectively. The components of the velocity  $\mathbf{u}_F$  of the fluid are denoted by  $u$ ,  $v$  and  $w$ ,  $p$  is its pressure,  $\rho$  its (constant) density and  $\mu$  its viscosity. The left hand sides of the momentum equations denote inertial forces,

which are balanced on the right hand side by the pressure gradient and viscous forces. Moreover, we consider the gravitational force  $\rho\mathbf{g}$ , which is a body force and acts on the whole fluid.

### 2.1.2 Definition of interface parameters

We need to define conditions at the free interfaces  $h^\pm(x, y, t) := H(x, y, t) \pm \frac{1}{2}h(x, y, t)$  between the liquid and gas phases. Therefore, we first have to determine unit vectors normal and tangential to the interface, as well as the curvature of the interface at a given point. The normal vector pointing from the interface into the gas phase is uniquely defined as follows:

$$\mathbf{n}^\pm = \frac{\pm 1}{\sqrt{1 + (h_x^\pm)^2 + (h_y^\pm)^2}} \begin{pmatrix} -h_x^\pm \\ -h_y^\pm \\ 1 \end{pmatrix}. \quad (2.5)$$

We define the first tangential vector such that it lies in the  $x$ - $z$ -plane:

$$\mathbf{t}_1^\pm = \frac{1}{\sqrt{1 + (h_x^\pm)^2}} \begin{pmatrix} 1 \\ 0 \\ h_x^\pm \end{pmatrix}. \quad (2.6)$$

The second tangential vector  $\mathbf{t}_2$  is chosen in such a way that  $\mathbf{n}$ ,  $\mathbf{t}_1$  and  $\mathbf{t}_2$  form an orthonormal system:

$$\mathbf{t}_2^\pm = \frac{1}{\sqrt{(1 + (h_x^\pm)^2)(1 + (h_x^\pm)^2 + (h_y^\pm)^2)}} \begin{pmatrix} -h_x^\pm h_y^\pm \\ 1 + (h_x^\pm)^2 \\ h_y^\pm \end{pmatrix}. \quad (2.7)$$

Finally the mean curvature of the interface is given by

$$\pm\kappa^\pm = \frac{((h_x^\pm)^2 + 1)h_{yy}^\pm + ((h_y^\pm)^2 + 1)h_{xx}^\pm - 2h_x^\pm h_y^\pm h_{xy}^\pm}{((h_x^\pm)^2 + (h_y^\pm)^2 + 1)^{3/2}}. \quad (2.8)$$

In all of the above expressions, “+” belongs to the upper interface  $h^+$ , and “-” to the lower interface  $h^-$ .

### 2.1.3 Interface conditions

We have the following condition for the evolution of the interfaces:

$$w = h_t^\pm + uh_x^\pm + vh_y^\pm, \quad (2.9)$$

which means that the interface moves with the velocity of the flow. Additionally, there are conditions for the equilibrium of normal and tangential forces:

$$\sigma \kappa^\pm = (\mathbf{n}^\pm)^\top (\mathcal{T} + p^\pm \mathbf{1}) \mathbf{n}^\pm, \quad (2.10)$$

$$\mathbf{t}_1^\pm \cdot \nabla \sigma = (\mathbf{t}_1^\pm)^\top (\mathcal{T} + p^\pm \mathbf{1}) \mathbf{n}^\pm, \quad (2.11)$$

$$\mathbf{t}_2^\pm \cdot \nabla \sigma = (\mathbf{t}_2^\pm)^\top (\mathcal{T} + p^\pm \mathbf{1}) \mathbf{n}^\pm. \quad (2.12)$$

Hereby,  $\mathcal{T}$  is the stress tensor of the fuel, which is for an incompressible Newtonian fluid given by

$$\mathcal{T} = \begin{pmatrix} -p + 2\mu u_x & \mu(u_y + v_x) & \mu(u_z + w_x) \\ \mu(u_y + v_x) & -p + 2\mu v_y & \mu(v_z + w_y) \\ \mu(u_z + w_x) & \mu(v_z + w_y) & -p + 2\mu w_z \end{pmatrix}.$$

Moreover, the term  $p^\pm \mathbf{1}$  represents the stress tensor of the air, where  $p^\pm$  is the pressure in the bubble adjacent to  $h^\pm$ . Here we assume for simplicity that we are dealing with a perfect gas.

The normal condition represents an equilibrium of capillary and pressure forces (Laplace's law), while the tangential conditions balance Marangoni and viscous stress. As before, all of these conditions are given for both interfaces.

We have an additional unknown quantity here, the surface tension  $\sigma$ . In order to close the system, it will be related to the concentrations of surfactant or volatile component, respectively. We will take a closer look at these dependencies in Sections 2.2 and 2.3.

### 2.1.4 Nondimensionalization

We assume that the dimension of the lamella under consideration in  $x$ - and  $y$ -direction is of the magnitude  $L$  and that its typical thickness is  $d = \varepsilon L \ll L$ , where  $\varepsilon$  is a small parameter. We assume furthermore that the curvature of the center-face of the film is small, such that  $H \ll L$ . Finally, we expect that the surface tension varies around a constant value  $\gamma$  in the magnitude  $\Delta\gamma \ll \gamma$ . Based on these assumptions, we introduce the following dimensionless variables:

$$\begin{aligned} x &= Lx' & y &= Ly' & z &= \varepsilon Lz' \\ u &= Uu' & v &= Uv' & w &= \varepsilon Uw' \\ h^\pm &= \varepsilon Lh'^\pm & p &= \frac{\mu U}{L} p' & t &= \frac{L}{U} t' \\ \sigma^\pm &= \gamma + \Delta\gamma \sigma'^\pm \end{aligned} \quad (2.13)$$

Moreover, we introduce the following similarity parameters:



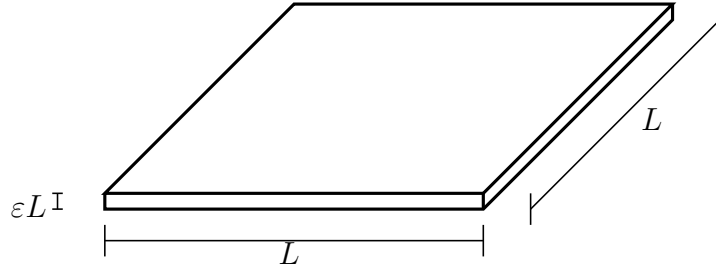


Figure 2.3: Parameter sizes

- The dimensionless Reynolds number  $\text{Re} = \frac{\rho LU}{\mu}$ , which characterizes the relation between inertial and viscous forces.
- The Froude number  $\text{Fr} = \frac{U^2}{L}$ , which has the dimension of an acceleration. The dimensionless ratio  $\frac{g}{\text{Fr}}$  characterizes the relation between gravitational and inertial forces, where  $g$  is the absolute value of the gravitational acceleration.
- The Capillary number  $\text{Ca} = \frac{\mu U}{\gamma}$ , which is the ratio of viscous and capillary forces.
- The Marangoni number  $\text{Ma} = \frac{\Delta\gamma}{\mu U}$ , which describes the relation between Marangoni and viscous forces.

Plugging these into Equations (2.1) – (2.4), we obtain (dropping primes):

$$\begin{aligned}
 u_x + v_y + w_z &= 0, \\
 \varepsilon^2 \text{Re}(u_t + uu_x + vv_y + ww_z) &= u_{zz} + \varepsilon^2 \left( -p_x + u_{xx} + u_{yy} + \frac{g \cdot \text{Re}}{\text{Fr}} e_{gx} \right), \\
 \varepsilon^2 \text{Re}(v_t + uv_x + vv_y + wv_z) &= v_{zz} + \varepsilon^2 \left( -p_y + v_{xx} + v_{yy} + \frac{g \cdot \text{Re}}{\text{Fr}} e_{gy} \right), \\
 \varepsilon^2 \text{Re}(w_t + uw_x + vw_y + ww_z) &= -p_z + w_{zz} + \varepsilon^2 \left( w_{xx} + w_{yy} + \frac{g \cdot \text{Re}}{\text{Fr}} e_{gz} \right).
 \end{aligned}$$

The values  $e_{gx}$ ,  $e_{gy}$  and  $e_{gz}$  are the coefficients of the unit vector in direction of the gravity, that is  $\mathbf{g} = g\mathbf{e}_g$ .

Next, we process similarly for the interface conditions at  $z = h^\pm(x, y, t)$ . The motion of the interface (2.9) becomes

$$w = h_t^\pm + uh_x^\pm + vh_y^\pm. \quad (2.14)$$

The force balances in normal and tangential directions (2.10) – (2.12) are

$$\begin{aligned} & \pm \left( \frac{\varepsilon}{\text{Ca}} + \varepsilon \text{Ma} \sigma^\pm \right) \frac{h_{yy}^\pm (1 + \varepsilon^2 (h_x^\pm)^2) + h_{xx}^\pm (1 + \varepsilon^2 (h_y^\pm)^2) - 2\varepsilon^2 h_x^\pm h_y^\pm h_{xy}^\pm}{(1 + \varepsilon^2 ((h_x^\pm)^2 + (h_y^\pm)^2))^{3/2}} \\ &= p^\pm - p + \frac{1}{1 + \varepsilon^2 ((h_x^\pm)^2 + (h_y^\pm)^2)} \left[ 2\varepsilon^2 u_x (h_x^\pm)^2 + 2\varepsilon^2 (u_y + v_x) h_x^\pm h_y^\pm \right. \\ & \quad \left. - 2(u_z + \varepsilon^2 w_x) h_x^\pm - 2(v_z + \varepsilon^2 w_y) h_y^\pm + 2\varepsilon^2 v_y (h_y^\pm)^2 + 2w_z \right] \end{aligned}$$

in normal direction, and

$$\begin{aligned} & \pm \varepsilon \text{Ma} (\sigma_x^\pm + \sigma_z^\pm h_x^\pm) \\ &= \frac{1}{1 + \varepsilon^2 ((h_x^\pm)^2 + (h_y^\pm)^2)} \left[ -2\varepsilon^2 u_x h_x^\pm - \varepsilon^2 (u_y + v_x) h_y^\pm + 2\varepsilon^2 w_z h_x^\pm \right. \\ & \quad \left. + (u_z + \varepsilon^2 w_x) (1 - \varepsilon^2 (h_x^\pm)^2) - \varepsilon^2 (v_z + \varepsilon^2 w_y) h_x^\pm h_y^\pm \right] \end{aligned}$$

and

$$\begin{aligned} & \pm \varepsilon \text{Ma} (-\varepsilon^2 \sigma_x^\pm h_x^\pm h_y^\pm + (1 + \varepsilon^2 (h_x^\pm)^2) \sigma_y^\pm + h_y^\pm \sigma_z^\pm) \\ &= \frac{1}{1 + \varepsilon^2 ((h_x^\pm)^2 + (h_y^\pm)^2)} \left[ \varepsilon^2 (u_y + v_x) (\varepsilon^2 h_x^\pm (h_y^\pm)^2 - h_x^\pm (1 + \varepsilon^2 (h_x^\pm)^2)) \right. \\ & \quad + 2\varepsilon^4 u_x (h_x^\pm)^2 h_y^\pm - 2\varepsilon^2 (u_z + \varepsilon^2 w_x) h_x^\pm h_y^\pm - 2\varepsilon^2 v_y h_y^\pm (1 + \varepsilon^2 (h_x^\pm)^2) \\ & \quad \left. + (v_z + \varepsilon^2 w_y) (1 + \varepsilon^2 ((h_x^\pm)^2 - (h_y^\pm)^2)) + 2\varepsilon^2 w_z h_y^\pm \right] \end{aligned}$$

in the two tangential directions.

### 2.1.5 Asymptotic expansion

We expand the dimensionless equations in terms of the small parameter  $\varepsilon$ . At the moment, we make the following assumptions on the size of the parameters:

- $\varepsilon^2 \text{Re} \ll 1$ ,
- $\frac{\varepsilon^2 g \text{Re}}{\text{Fr}} \ll 1$ ,
- $\varepsilon \text{Ma} \ll 1$ .

In Section 2.1.6, we will consider which changes we have to make if the assumptions above do not hold.

We make the ansatz  $\phi = \phi_0 + \varepsilon^2 \phi_1 + \dots$ , where  $\phi$  stands for any of the unknowns. Then we obtain in leading order:

$$u_{0x} + v_{0y} + w_{0z} = 0, \quad (2.15)$$

$$u_{0zz} = 0, \quad (2.16)$$

$$v_{0zz} = 0, \quad (2.17)$$

$$w_{0zz} = p_{0z}. \quad (2.18)$$

At the interfaces  $\pm \frac{1}{2}h_0$  we have:

$$\begin{aligned} w_0 &= H_{0t} + u_0 H_{0x} + v_0 H_{0y} \\ &\quad \pm \frac{1}{2}h_{0t} \pm \frac{1}{2}u_0 h_{0x} \pm \frac{1}{2}v_0 h_{0y}, \end{aligned} \quad (2.19)$$

$$\begin{aligned} &\pm \frac{\varepsilon}{\text{Ca}} (H_{0xx} + H_{0yy}) \\ + \frac{\varepsilon}{\text{Ca}} \left( \frac{1}{2}h_{0xx} + \frac{1}{2}h_{0yy} \right) &= p^\pm - p_0 + 2w_{0z} \mp u_{0z} h_{0x} \mp v_{0z} h_{0y}, \end{aligned} \quad (2.20)$$

$$u_{0z} = 0, \quad (2.21)$$

$$v_{0z} = 0. \quad (2.22)$$

These equations can be simplified further. Integrating (2.16) and (2.17) together with boundary conditions (2.21) and (2.22) yields

$$u_{0z} = 0,$$

$$v_{0z} = 0.$$

Plugging these into derivative of (2.15) with respect to  $z$ , we obtain with (2.18):

$$p_{0z} = 0.$$

Hence the horizontal velocities and the pressure are constant across the film.

Next, we integrate (2.15) over  $[H_0 - \frac{1}{2}h_0, z]$  and  $[z, H_0 + \frac{1}{2}h_0]$ , respectively. This yields with (2.19) the following two equations:

$$\begin{aligned} 0 &= (u_{0x} + v_{0y})(z - H_0 + \frac{h_0}{2}) + w_0(z) + \frac{h_{0t}}{2} + u_0 \frac{h_{0x}}{2} + v_0 \frac{h_{0y}}{2} \\ &\quad - H_{0t} - u_0 H_{0x} - v_0 H_{0y} \end{aligned}$$

$$\begin{aligned} 0 &= (u_{0x} + v_{0y})(H_0 + \frac{h_0}{2} - z) - w_0(z) + \frac{h_{0t}}{2} + u_0 \frac{h_{0x}}{2} + v_0 \frac{h_{0y}}{2} \\ &\quad + H_{0t} + u_0 H_{0x} + v_0 H_{0y} \end{aligned}$$

Adding these gives mass conservation:

$$h_{0t} + (u_0 h_0)_x + (v_0 h_0)_y = 0 \quad (2.23)$$

Subtraction leads to an expression for  $w_0$ :

$$w_0 = -z(u_{0x} + v_{0y}) + H_{0t} + (u_0 H_0)_x + (v_0 H_0)_y. \quad (2.24)$$

Finally, we obtain two expressions by adding and subtracting the two boundary conditions (2.20):

$$p_0 = -\frac{\varepsilon}{2\text{Ca}}(h_{0xx} + h_{0yy}) - 2(u_{0x} + v_{0y}) + \frac{p^+ + p^-}{2}, \quad (2.25)$$

$$H_{0xx} + H_{0yy} = \frac{\text{Ca}(p^+ - p^-)}{2\varepsilon}. \quad (2.26)$$

The latter equation yields a temporally constant center-face if we assume that the pressures in the adjacent bubbles are constant. In the following, we will assume for simplicity that  $p^+ = p^- = 0$ . Moreover, we assume that all the Plateau borders lie in the plane  $z = 0$  such that  $H \equiv 0$ .

**Remark** *If  $\text{Ca} \ll \varepsilon$  the scaling for  $p_0$  is no longer valid. In this case, the pressure gradient may enter into the Navier-Stokes equations in leading order and we obtain a lubrication-type equation. This will be considered in Section 2.1.6.*

We now have the three equations (2.23) – (2.25) for the five unknowns  $h_0$ ,  $u_0$ ,  $v_0$ ,  $w_0$  and  $p_0$ . We need two more equations in order to close the system. These will be taken from the next order  $\varepsilon^2$ :

$$\text{Re}(u_{0t} + u_0 u_{0x} + v_0 u_{0y}) = -p_{0x} + u_{0xx} + u_{0yy} + u_{1zz} + \frac{g \cdot \text{Re}}{\text{Fr}} e_{gx}, \quad (2.27)$$

$$\text{Re}(v_{0t} + u_0 v_{0x} + v_0 v_{0y}) = -p_{0y} + v_{0xx} + v_{0yy} + v_{1zz} + \frac{g \cdot \text{Re}}{\text{Fr}} e_{gy}. \quad (2.28)$$

The related boundary conditions on  $\pm \frac{h_0}{2}$  are:

$$\begin{aligned} \pm \frac{\text{Ma}}{\varepsilon} \sigma_x^\pm + \frac{\text{Ma}}{2\varepsilon} \sigma_z^\pm h_{0x} &= u_{1z} + w_{0x} \mp u_{0x} h_{0x} \mp \frac{h_{0y}}{2} (u_{0y} + v_{0x}) \pm w_{0z} h_{0x}, \\ \pm \frac{\text{Ma}}{\varepsilon} \sigma_y^\pm + \frac{\text{Ma}}{2\varepsilon} \sigma_z^\pm h_{0y} &= v_{1z} + w_{0y} \mp v_{0y} h_{0y} \mp \frac{h_{0x}}{2} (u_{0y} + v_{0x}) \pm w_{0z} h_{0y}. \end{aligned}$$

Integration of (2.27) and (2.28) across the film together with these boundary conditions leads to

$$\begin{aligned} & h_0 \left[ p_{0x} - u_{0xx} - u_{0yy} - \frac{g \cdot \text{Re}}{\text{Fr}} e_{gx} + \text{Re}(u_{0t} + u_0 u_{0x} + v_0 u_{0y}) \right] \\ &= \frac{\text{Ma}}{\varepsilon} (\sigma^+ + \sigma^-)_x + \frac{\text{Ma}}{2\varepsilon} h_{0x} (\sigma^+ - \sigma^-)_z - w_{0x}|_{\frac{h_0}{2}} + w_{0x}|_{-\frac{h_0}{2}} \\ & \quad + 2h_{0x}(2u_{0x} + v_{0y}) + h_{0y}(u_{0y} + v_{0x}), \end{aligned} \quad (2.29)$$

$$\begin{aligned} & h_0 \left[ p_{0y} - v_{0xx} - v_{0yy} - \frac{g \cdot \text{Re}}{\text{Fr}} e_{gy} + \text{Re}(v_{0t} + u_0 v_{0x} + v_0 v_{0y}) \right] \\ &= \frac{\text{Ma}}{\varepsilon} (\sigma^+ + \sigma^-)_y + \frac{\text{Ma}}{2\varepsilon} h_{0y} (\sigma^+ - \sigma^-)_z - w_{0y}|_{\frac{h_0}{2}} + w_{0y}|_{-\frac{h_0}{2}} \\ & \quad + 2h_{0y}(u_{0x} + 2v_{0y}) + h_{0x}(u_{0y} + v_{0x}). \end{aligned} \quad (2.30)$$

Under the assumption of symmetry, that is  $\sigma_x^+ = \sigma_x^-$  and  $\sigma_z^+ = -\sigma_z^-$ , together with Equations (2.24) and (2.25), we obtain from (2.23), (2.29) and (2.30) a system of three ODE's for the three unknowns  $h$ ,  $u$  and  $v$  (dropping the subscripts):

$$0 = h_t + (uh)_x + (vh)_y, \quad (2.31)$$

$$\begin{aligned} 0 &= \frac{\text{Ma}}{\varepsilon} (2\sigma_x + h_x \sigma_z) + \frac{\varepsilon}{2\text{Ca}} h (h_{xx} + h_{yy})_x \\ & \quad - \text{Re} h (u_t + uu_x + vv_y) + h \frac{g \text{Re}}{\text{Fr}} e_{gx} \\ & \quad + 4(hu_x)_x + 2(hv_y)_x + (hv_x)_y + (hu_y)_y, \end{aligned} \quad (2.32)$$

$$\begin{aligned} 0 &= \frac{\text{Ma}}{\varepsilon} (2\sigma_y + h_y \sigma_z) + \frac{\varepsilon}{2\text{Ca}} h (h_{xx} + h_{yy})_y \\ & \quad - \text{Re} h (v_t + uv_x + vv_y) + h \frac{g \text{Re}}{\text{Fr}} e_{gy} \\ & \quad + 4(hv_y)_y + 2(hu_x)_y + (hu_y)_x + (hv_x)_x. \end{aligned} \quad (2.33)$$

**Remark** *Note that the surface tension  $\sigma$  still appears in these equations. We will relate this quantity to the surfactant concentration and to the concentration of volatile component in the following sections. If none of these is present, the surface tension is constant and the corresponding terms drop out.*

### 2.1.6 Special cases

Up to now, we have assumed that  $\varepsilon^2 \text{Re} \ll 1$ ,  $\frac{\varepsilon^2 g \text{Re}}{\text{Fr}} \ll 1$  and  $\varepsilon \text{Ma} \ll 1$ . In this section, we will consider some special cases in which these conditions do not hold.

#### Dominant boundary forces

Consider the case when  $\varepsilon \text{Ma}$  is of order one or higher. Since we assume  $\Delta\gamma \ll \gamma$  this means  $\text{Ca} \ll \varepsilon$ . As we can see on Equation (2.25), we have to rescale the pressure and will use the scaling  $p = \frac{\mu U}{\varepsilon^2 L} p'$ . In this case, the dimensionless Navier-Stokes equations in leading order become:

$$u_{0x} + v_{0y} + w_{0z} = 0, \quad (2.34)$$

$$p_{0x} = u_{0zz}, \quad (2.35)$$

$$p_{0y} = v_{0zz}, \quad (2.36)$$

$$p_{0z} = 0. \quad (2.37)$$

The boundary conditions change accordingly (we assume for simplicity  $\sigma_z^\pm = 0$ ; this will be motivated in Sections 2.2.4 and 2.3.5):

$$2w_0 = \pm h_{0t} \pm u_0 h_{0x} \pm v_0 h_{0y} \quad (2.38)$$

$$\frac{\varepsilon^3}{2\text{Ca}}(h_{0xx} + h_{0yy}) = -p_0 \quad (2.39)$$

$$\pm \varepsilon \text{Ma} \sigma_{0x}^\pm = u_{0z} \quad (2.40)$$

$$\pm \varepsilon \text{Ma} \sigma_{0y}^\pm = v_{0z} \quad (2.41)$$

Equation (2.37) yields constant pressure across the film, hence (2.39) gives

$$p_0 = -\frac{\varepsilon^3}{2\text{Ca}}(h_{0xx} + h_{0yy}).$$

Integration of (2.35) and (2.36) across the film using (2.40) and (2.41) gives, together with the expression for the pressure:

$$\begin{aligned} \frac{\varepsilon^2}{2\text{Ca}} h_0 (h_{0xx} + h_{0yy})_x + \text{Ma} (\sigma_0^+ + \sigma_0^-)_x &= 0, \\ \frac{\varepsilon^2}{2\text{Ca}} h_0 (h_{0xx} + h_{0yy})_y + \text{Ma} (\sigma_0^+ + \sigma_0^-)_y &= 0. \end{aligned}$$

Then integrating (2.35) and (2.36) twice with (2.40) and (2.41) yields

$$\begin{aligned} u_0 &= \bar{u} + \frac{\varepsilon \text{Ma}}{2} (\sigma_0^+ - \sigma_0^-)_x z + \frac{\varepsilon^3}{4\text{Ca}} (h_{0xx} + h_{0yy})_x \left( \frac{h_0^2}{12} - z^2 \right), \\ v_0 &= \bar{v} + \frac{\varepsilon \text{Ma}}{2} (\sigma_0^+ - \sigma_0^-)_y z + \frac{\varepsilon^3}{4\text{Ca}} (h_{0xx} + h_{0yy})_y \left( \frac{h_0^2}{12} - z^2 \right), \end{aligned}$$

where

$$\begin{aligned}\bar{u} &= \frac{u_0(\frac{h_0}{2}) + u_0(-\frac{h_0}{2})}{2} + \frac{\varepsilon^3}{4\text{Ca}}(h_{0xx} + h_{0yy})_x \frac{h_0^2}{6}, \\ \bar{v} &= \frac{v_0(\frac{h_0}{2}) + v_0(-\frac{h_0}{2})}{2} + \frac{\varepsilon^3}{4\text{Ca}}(h_{0xx} + h_{0yy})_y \frac{h_0^2}{6}.\end{aligned}$$

Note that the Marangoni term cancels due to symmetry. We observe that we no longer have constant velocities  $u_0$  and  $v_0$  across the film, but that we obtain a parabolic velocity profile as in lubrication theory.

Finally, integrating (2.34) across the film together with (2.38), we obtain mass conservation:

$$h_{0t} + (h_0\bar{u})_x + (h_0\bar{v})_y = 0$$

The final system for  $h$ ,  $\bar{u}$  and  $\bar{v}$  is then given by (using symmetry and leaving the subscripts):

$$\begin{aligned}0 &= h_t + (\bar{u}h)_x + (\bar{v}h)_y \\ 0 &= \frac{2\text{Ma}}{\varepsilon}\sigma_x + \frac{\varepsilon}{2\text{Ca}}h(h_{xx} + h_{yy})_x \\ 0 &= \frac{2\text{Ma}}{\varepsilon}\sigma_y + \frac{\varepsilon}{2\text{Ca}}h(h_{xx} + h_{yy})_y\end{aligned}$$

Apart from the fact that the tangential velocity is no longer constant across the film, this is exactly the same model as we obtained before in (2.31) – (2.33) for the case that inertia and viscosity can be neglected, i.e. the film is dominated by surface forces.

### Model of a fast film

We will now consider the case in which the liquid drains out of the lamella very fast, i.e. the velocity scaling is so large that the condition  $\varepsilon^2\text{Re} \ll 1$  from Section 2.1.5 no longer holds. Assuming that inertia forces enter in leading order, we obtain the following system:

$$\begin{aligned}u_{0x} + v_{0y} + w_{0z} &= 0, \\ \varepsilon^2\text{Re}(u_{0t} + u_0u_{0x} + v_0u_{0y} + w_0u_{0z}) &= u_{0zz}, \\ \varepsilon^2\text{Re}(v_{0t} + u_0v_{0x} + v_0v_{0y} + w_0v_{0z}) &= v_{0zz}, \\ \varepsilon^2\text{Re}(w_{0t} + u_0w_{0x} + v_0w_{0y} + w_0w_{0z}) &= -p_{0z} + w_{0zz},\end{aligned}$$

with boundary conditions:

$$\begin{aligned} w_0 &= \pm \frac{1}{2} h_{0t} \pm \frac{1}{2} u_0 h_{0x} \pm \frac{1}{2} v_0 h_{0y}, \\ \frac{\varepsilon}{2\text{Ca}}(h_{0xx} + h_{0yy}) &= -p_0 \mp u_{0z} h_{0x} \mp v_{0z} h_{0y} + 2w_{0z}, \\ \pm \varepsilon \text{Ma} \sigma_{0x}^\pm &= u_{0z}, \\ \pm \varepsilon \text{Ma} \sigma_{0y}^\pm &= v_{0z}. \end{aligned}$$

There are two possible scenarios:

1. Marangoni and capillary forces are negligible, and the tangential velocities  $u$  and  $v$  are constant across the film. Then we obtain the following hyperbolic system:

$$\begin{aligned} h_t + (uh)_x + (vh)_y &= 0, \\ u_t + uu_x + vv_y &= 0, \\ v_t + uv_x + vv_y &= 0, \end{aligned}$$

i.e. the flow is completely inertia-dominated.

2. Marangoni and capillary forces enter at leading order; then  $u$  and  $v$  are not constant across the film. In this case, we are not able to simplify the system further. If the velocity scaling is very fast, Marangoni and capillary forces only appear in leading order if  $\varepsilon$  is large. Hence, this model describes a relatively thick film for which the thin film approximations do not hold and the full problem has to be solved.

Both of these cases will not be studied any further in this thesis. The first case describes a film which thins very quickly due to the high velocity of the flow, such that it is very unstable and therefore not interesting for our application. Moreover, since we explicitly deal with thin films in this work, we will not consider the second model in more detail.

## 2.2 Surfactant

### 2.2.1 Physical model

In the case of a foam stabilized by the effect of a surfactant on the surface tension, we need a model describing the behaviour of that surfactant. We denote its bulk



concentration by  $C^s$  and assume that it is governed by convection and diffusion. Thus, we obtain the following equation for  $C^s$ :

$$C_t^s + uC_x^s + vC_y^s + wC_z^s = D_s(C_{xx}^s + C_{yy}^s + C_{zz}^s) \quad (2.42)$$

The diffusivity  $D_s$  is a material parameter which we assume to be independent of space and time.

### 2.2.2 Conditions at the free interfaces

As already mentioned before, surfactants tend to assemble at the surface of the liquid. Therefore, it is not sufficient to consider the concentration at the surface as the trace of the bulk concentration, but a new quantity is introduced, the surface concentration  $\Gamma$ . We assume that  $\Gamma$  is governed by convection, diffusion and a flux of surfactant from the bulk onto the surface, thus it is described by

$$\Gamma_t + \nabla_\Gamma \cdot (\mathbf{u}_\Gamma \Gamma) = \nabla_\Gamma \cdot (D_\Gamma \nabla_\Gamma) \Gamma + j. \quad (2.43)$$

The index  $\Gamma$  stands for the surface, i.e. the directions spanned by the tangential vectors defined in Section 2.1.2. The material parameter  $D_\Gamma$  is the surface diffusivity which is assumed to be constant, and  $j$  is the flux of surfactant from the bulk.

We have to close the system by adding some more equations for the newly introduced unknowns  $\Gamma$  and  $j$ , as well as for the surface tension  $\sigma$ . We need a relation between  $\Gamma$  and  $C^s$ , which is introduced by a constitutive equation for the flux  $j$ ,

$$j = j(C^s, \Gamma).$$

There are several such models in chemical literature, and we apply one of the most common ones, the *Langmuir-Hinshelwood* equation (see [13])

$$j = k_1(C^s(\Gamma_\infty - \Gamma) - k_2\Gamma). \quad (2.44)$$

In this model, the flux is assumed to be the difference between adsorption and desorption of surfactant at the surface. The adsorption is proportional to

- the bulk concentration  $C^s$ , i.e. the “reservoir” of surfactant in the bulk;
- the difference of the saturation concentration  $\Gamma_\infty$  and the concentration of surfactant at the surface  $\Gamma$ , i.e. the “space” that is left at the surface.

For the desorption we have a similar model, i.e. it is proportional to

- the concentration of surfactant at the surface (the reservoir);
- a constant material parameter  $k_2$ . This parameter models the space as in the adsorption. However, for the desorption it is assumed that the variation in the bulk surfactant concentration is small compared to the saturation concentration in the bulk, such that it can be approximated by a constant.

The material parameters  $k_1$  and  $k_2$  also determine the relative magnitudes of adsorption and desorption.

It is often assumed (see [13]) that the adsorption process happens on a much faster time scale than the other effects. In this case, (2.44) reduces to a relation for the thermodynamic equilibrium called the *Langmuir isotherm*,

$$\Gamma = \frac{\Gamma_\infty C^s}{k_2 + C^s}. \quad (2.45)$$

Another relation between the flux  $j$  and the bulk concentration  $C^s$  can be derived under the assumption that the flux onto the surface in the bulk is controlled by diffusion and therefore given by

$$\begin{aligned} j &= -D_s \frac{\partial C^s}{\partial n} \\ &= \frac{D_s}{\sqrt{1 + (h_x^\pm)^2 + (h_y^\pm)^2}} (\mp C_z^s \pm h_x^\pm C_x^s \pm h_y^\pm C_y^s). \end{aligned} \quad (2.46)$$

In contrast to Equation (2.44), this describes the behaviour in the bulk and not at the interface. However, due to continuity reasons, the two expressions are equal at the interface. Therefore, we can eliminate  $j$  and obtain two equations by equating (2.46) and (2.43) on the one hand and (2.46) and (2.44) on the other hand. Using (2.6) and (2.7) we get

$$k_1(C^s(\Gamma_\infty - \Gamma) - k_2\Gamma) = \frac{D_s}{\sqrt{4 + h_x^2 + h_y^2}} (\mp 2C_z^s + h_x C_x^s + h_y C_y^s) \quad (2.47)$$

and

$$\begin{aligned}
0 = & \Gamma_t^\pm + \frac{1}{\sqrt{4+h_x^2}} \left[ \left( \frac{4u\Gamma^\pm \pm 2h_x w\Gamma^\pm}{\sqrt{4+h_x^2}} \right)_x \pm h_x \left( \frac{2u\Gamma^\pm \pm h_x w\Gamma^\pm}{\sqrt{4+h_x^2}} \right)_z \right] \\
& + \frac{1}{\sqrt{(4+h_x^2)(4+h_x^2+h_y^2)}} \cdot \\
& \left[ -h_x h_y \left( \frac{-h_x h_y u\Gamma^\pm + (4+h_x^2)v\Gamma^\pm \pm 2h_y w\Gamma^\pm}{\sqrt{(4+h_x^2)(4+h_x^2+h_y^2)}} \right)_x \right. \\
& + (4+h_x^2) \left( \frac{-h_x h_y u\Gamma^\pm + (4+h_x^2)v\Gamma^\pm \pm 2h_y w\Gamma^\pm}{\sqrt{(4+h_x^2)(4+h_x^2+h_y^2)}} \right)_y \\
& \left. \pm 2h_y \left( \frac{-h_x h_y u\Gamma^\pm + (4+h_x^2)v\Gamma^\pm \pm 2h_y w\Gamma^\pm}{\sqrt{(4+h_x^2)(4+h_x^2+h_y^2)}} \right)_z \right] \\
& + \frac{D_\Gamma^\pm}{\sqrt{4+h_x^2+h_y^2}} \left[ h_x \left( \frac{h_x \Gamma_x^\pm + h_y \Gamma_y^\pm \mp 2\Gamma_z^\pm}{\sqrt{4+h_x^2+h_y^2}} \right)_x \right. \\
& + h_y \left( \frac{h_x \Gamma_x^\pm + h_y \Gamma_y^\pm \mp 2\Gamma_z^\pm}{\sqrt{4+h_x^2+h_y^2}} \right)_y \mp 2 \left( \frac{h_x \Gamma_x^\pm + h_y \Gamma_y^\pm \mp 2\Gamma_z^\pm}{\sqrt{4+h_x^2+h_y^2}} \right)_z \left. \right] \\
& - D_\Gamma^\pm (\Gamma_{xx}^\pm + \Gamma_{yy}^\pm + \Gamma_{zz}^\pm) - \frac{D_s}{\sqrt{4+h_x^2+h_y^2}} (\mp 2C_z^s + h_x C_x^s + h_y C_y^s).
\end{aligned} \tag{2.48}$$

### 2.2.3 Influence on the surface tension

Finally, we need a relation between the surface tension and the surfactant concentration. Therefore, we apply the *Frumkin equation* (or *von Szyckowski equation*, see [13])

$$\sigma^* - \sigma = -R\Theta\Gamma_\infty \ln \left( 1 - \frac{\Gamma}{\Gamma_\infty} \right). \tag{2.49}$$

which models that relation for a wide range of surfactants. Here  $R$  denotes the gas constant,  $\Theta$  the temperature and  $\sigma^*$  the surface tension of the pure liquid without surfactant. Note that this equation has a singularity for  $\Gamma = \Gamma_\infty$  and therefore becomes invalid in this limit. However, we will only consider relatively small concentrations in which this model is a good approximation of the real behaviour.

In thermodynamic equilibrium, we can plug (2.45) into (2.49) and obtain after differentiation:

$$\sigma_x = -R\Theta\Gamma_\infty \frac{C_x^s}{C^s + k_2}, \quad (2.50)$$

$$\sigma_y = -R\Theta\Gamma_\infty \frac{C_y^s}{C^s + k_2}, \quad (2.51)$$

$$\sigma_z = -R\Theta\Gamma_\infty \frac{C_z^s}{C^s + k_2}. \quad (2.52)$$

**Remark** *For the thin film model (2.31) – (2.33), only the spatial derivatives of the surface tension are needed.*

For small concentrations  $C^s \ll k_2$ , we can simplify (2.45) and (2.50) – (2.52) even further to obtain the linear relations

$$\Gamma = \frac{\Gamma_\infty}{k_2} C^s,$$

$$\begin{aligned} \sigma_x &= -\frac{R\Theta\Gamma_\infty}{k_2} C_x^s, \\ \sigma_y &= -\frac{R\Theta\Gamma_\infty}{k_2} C_y^s, \\ \sigma_z &= -\frac{R\Theta\Gamma_\infty}{k_2} C_z^s. \end{aligned}$$

## 2.2.4 Nondimensionalization

Additionally to the dimensionless variables introduced in (2.13), we nondimensionalize  $C^s$  and  $\Gamma$  by:

$$\begin{aligned} C^s &= C^* C^{s'}, \\ \Gamma^\pm &= \Gamma^* \Gamma^{\pm'}. \end{aligned}$$

We also introduce some similarity parameters:

- The Péclet number  $\text{Pe} = \frac{UL}{D_s}$ , which characterizes the relation of convection and diffusion in the bulk.
- The interface Péclet number  $\text{Pe}_\Gamma = \frac{UL}{D_\Gamma}$ , which does the same at the liquid-air interface.

- The replenishment number  $S = \frac{D_s C^*}{U \Gamma^*}$ , which is the relation of diffusion from the bulk onto the surface and convection at the surface.
- Moreover, we introduce  $\Lambda = \frac{\Gamma^*}{\Gamma_\infty}$  and  $\Pi = \frac{C^*}{k_2}$  which describe the order of magnitude of the concentrations compared to the saturation concentrations.

With these, the convection-diffusion equation (2.42) for the bulk concentration of the surfactant becomes (we drop the primes again):

$$\varepsilon^2 \text{Pe}(C_t^s + uC_x^s + vC_y^s + wC_z^s) = \varepsilon^2 C_{xx}^s + \varepsilon^2 C_{yy}^s + C_{zz}^s. \quad (2.53)$$

At the interfaces  $z = \pm \frac{h}{2}$ , we consider (2.48) to obtain:

$$\begin{aligned} 0 = & \Gamma_t^\pm + \frac{1}{2} [(2u\Gamma^\pm)_x \pm h_x(u\Gamma^\pm)_z] + \frac{1}{2} [2(v\Gamma^\pm)_y \pm h_y(v\Gamma^\pm)_z] \\ & - \frac{1}{\text{Pe}_\Gamma} (\Gamma_{xx}^\pm + \Gamma_{yy}^\pm + \Gamma_{zz}^\pm) + \frac{1}{4\text{Pe}_\Gamma} [\mp 2h_x\Gamma_{xz}^\pm \mp 2h_y\Gamma_{yz}^\pm \mp 2(h_x\Gamma_x^\pm)_z \\ & \mp 2(h_y\Gamma_y^\pm)_z + \frac{4}{\varepsilon^2}\Gamma_{zz}^\pm - (h_x^2 + h_y^2)\Gamma_{zz}^\pm] \\ & \pm \frac{\varepsilon S}{2} \left( \frac{2}{\varepsilon^2}C_z^s \mp h_x C_x^s \mp h_y C_y^s - \frac{1}{8}(h_x^2 + h_y^2)C_z^s \right) + \mathcal{O}(\varepsilon^2) \end{aligned} \quad (2.54)$$

Equation (2.47) becomes:

$$\frac{D_s}{\varepsilon k_1 L \Gamma^* \sqrt{4 + \varepsilon^2 h_x^2 + \varepsilon^2 h_y^2}} (\mp 2C_z^s + \varepsilon^2 h_x C_x^s + \varepsilon^2 h_y C_y^s) = \frac{C^s}{\Lambda} - C^s \Gamma - \frac{\Gamma}{\Pi}. \quad (2.55)$$

Finally, we have the Frumkin equation (2.49) for the relation of surface tension and surfactant concentration,

$$\sigma^* - \gamma - \Delta\gamma\sigma = -R\Theta\Gamma_\infty \ln(1 - \Lambda\Gamma). \quad (2.56)$$

### 2.2.5 Asymptotic expansion

We assume that the film is in thermodynamic equilibrium, that is  $\frac{D_s}{\varepsilon k_1 L \Gamma^*} \ll 1$ , such that Equation (2.55) reduces to the Langmuir isotherm

$$\Gamma_0 = \frac{\Pi}{\Lambda} \frac{C_0^s}{1 + \Pi C_0^s}. \quad (2.57)$$

The first and second derivatives of this expression with respect to  $x$  are

$$\Gamma_{0x} = \frac{\Pi}{\Lambda} \frac{C_{0x}^s}{(1 + \Pi C_0^s)^2}$$

and

$$\Gamma_{0xx} = \frac{\Pi}{\Lambda} \frac{C_{0xx}^s}{(1 + \Pi C_0^s)^2} - \frac{2\Pi^2}{\Lambda} \frac{(C_{0x}^s)^2}{(1 + \Pi C_0^s)^3}.$$

The derivatives with respect to  $y$  and  $z$  are computed analogously. Thus, we can replace all occurrences of  $\Gamma$  with the above expressions. We make the following assumptions:

- $\varepsilon^2 \text{Pe} \ll 1$ ,
- $\varepsilon^2 \text{Pe}_\Gamma \ll 1$  or  $\frac{\varepsilon}{S} \ll 1$ .

The first condition is the equivalent to  $\varepsilon^2 \text{Re} \ll 1$  from Section 2.1.5. The second one is related to the first via the velocity scaling  $U$  and ensures that the interface conditions are consistent.

We obtain for the bulk in leading order:

$$C_{0zz}^s = 0. \tag{2.58}$$

The interface condition (2.54) becomes

$$\mp \varepsilon S \text{Pe}_\Gamma C_{0z}^s = \frac{\Pi}{\Lambda} \frac{C_{0zz}^s}{(1 + \Pi C_0^s)^2} - \frac{2\Pi^2}{\Lambda} \frac{(C_{0z}^s)^2}{(1 + \Pi C_0^s)^3}.$$

Assuming continuity of  $C_{0zz}^s$ , this simplifies to

$$\pm \varepsilon S \text{Pe}_\Gamma C_{0z}^s = \frac{2\Pi^2}{\Lambda} \frac{(C_{0z}^s)^2}{(1 + \Pi C_0^s)^3}$$

This yields

$$C_{0z}^s = 0$$

at the interfaces and hence together with (2.58)

$$C_{0z}^s = 0$$

everywhere.

In order to obtain an evolution equation for the concentration  $C^s$ , we have to proceed to the next order, getting:

$$\text{Pe}(C_{0t}^s + u_0 C_{0x}^s + v_0 C_{0y}^s) = C_{0xx}^s + C_{0yy}^s + C_{1zz}^s$$

with interface condition

$$\begin{aligned} 0 = & (C_{0t}^s + u_0 C_{0x}^s + v_0 C_{0y}^s) + (1 + \Pi C_0^s)(u_{0x} C_0^s + u_{0y} C_0^s) \\ & + \frac{2\Pi}{\text{Pe}_\Gamma(1 + \Pi C_0^s)} ((C_{0x}^s)^2 + (C_{0y}^s)^2) - \frac{1}{\text{Pe}_\Gamma} (C_{0xx}^s + C_{0yy}^s) \\ & - \frac{\varepsilon S \Lambda (1 + \Pi C_0^s)^2}{2\Pi} (h_{0x} C_{0x}^s + h_{0y} C_{0y}^s \mp 2C_{1z}^s). \end{aligned}$$

Integration across the film yields (dropping zeros)

$$\begin{aligned}
0 &= \left( \frac{2\Pi}{\varepsilon S\Lambda(1 + \Pi C_0^s)^2} + \text{Pe} h \right) (C_t^s + uC_x^s + vC_y^s) \\
&+ \frac{2\Pi}{\varepsilon S\Lambda(1 + \Pi C^s)} (u_x C^s + u_y C^s) + \frac{4\Pi^2}{\varepsilon S \text{Pe}_\Gamma \Lambda (1 + \Pi C^s)^3} (C_x^{s2} + C_y^{s2}) \\
&- \frac{2\Pi}{\varepsilon S \text{Pe}_\Gamma \Lambda (1 + \Pi C_0^s)^2} (C_{xx}^s + C_{yy}^s) - (hC_x^s)_x - (hC_y^s)_y.
\end{aligned}$$

In the following, we will make in accordance to [9] the assumption that surface diffusion can be neglected, i.e.  $\text{Pe}_\Gamma$  is large. Then this equation simplifies to

$$\begin{aligned}
0 &= \left( \frac{2\Pi}{\varepsilon S\Lambda(1 + \Pi C_0^s)^2} + \text{Pe} h \right) (C_t^s + uC_x^s + vC_y^s) \\
&+ \frac{2\Pi}{\varepsilon S\Lambda(1 + \Pi C^s)} (u_x C^s + u_y C^s) - (hC_x^s)_x - (hC_y^s)_y. \quad (2.59)
\end{aligned}$$

## 2.2.6 Surface tension

Plugging (2.57) into the Frumkin equation (2.56), we obtain the following relations:

$$\begin{aligned}
\sigma_x &= -\frac{R\Theta\Gamma_\infty}{\Delta\gamma} \frac{C_x^s}{1 + \Pi C^s}, \\
\sigma_y &= -\frac{R\Theta\Gamma_\infty}{\Delta\gamma} \frac{C_y^s}{1 + \Pi C^s}, \\
\sigma_z &= -\frac{R\Theta\Gamma_\infty}{\Delta\gamma} \frac{C_z^s}{1 + \Pi C^s} = 0.
\end{aligned}$$

Note that in the equations derived in the Section 2.1.5 only these derivatives occur. Moreover, this validates the assumption  $\sigma_z = 0$ .

## 2.3 Volatile component

### 2.3.1 Physical model

Real gas or Diesel fuel is a mixture of a variety of different components with different physical properties such as surface tension and boiling point. We consider

a simple model of a mixture of two liquid components, one of which is volatile at the given temperature.

As in the case of a surfactant, the volatile component is assumed to be governed by convection and diffusion. We denote its concentration in the mixture by  $C^v$  and obtain a similar equation as before:

$$C_t^v + uC_x^v + vC_y^v + wC_z^v = D_v(C_{xx}^v + C_{yy}^v + C_{zz}^v) \quad (2.60)$$

with constant diffusivity  $D_v$ .

### 2.3.2 Interface conditions

In order to find the correct interface condition for the concentration of the volatile component, we consider an (infinitesimal) control volume  $\Omega$  at the interface  $h^+$  as in Figure 2.4. Let the velocity of the interface be  $\mathbf{v}_I$  and recall that the velocity

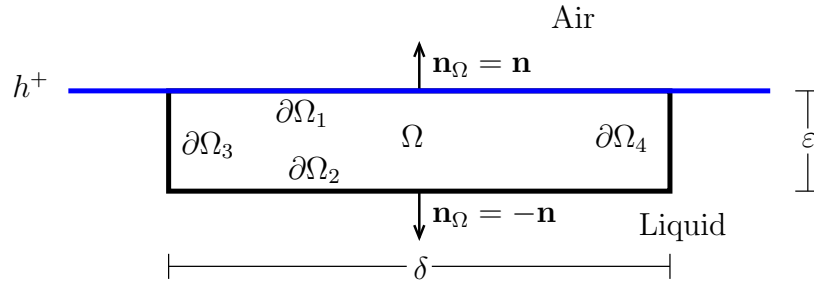


Figure 2.4: Derivation of the boundary conditions

of the fluid is  $\mathbf{u}_F$ . Since we consider an infinitesimally small control volume we can assume that  $\mathbf{v}_I \approx \text{const}$  on  $\Omega$ . The vector  $\mathbf{n}_\Omega$  denotes the normal on the boundaries of  $\Omega$  while  $\mathbf{n}$  is the normal on the interface  $h^+$ . The parameters  $\varepsilon$  and  $\delta$  are small.

Integrating Equation (2.60) over the control volume, and applying Stokes' theorem, we obtain

$$\begin{aligned} \int_{\Omega} C_t^v &= - \int_{\Omega} (\mathbf{u} - \mathbf{v}_I) \cdot \nabla C^v + D_v \int_{\Omega} \Delta C^v \\ &= \int_{\partial\Omega} (\mathbf{u} \cdot \mathbf{n}_\Omega - \mathbf{v}_I \cdot \mathbf{n}_\Omega) C^v - D_v \int_{\partial\Omega} \mathbf{n}_\Omega \cdot \nabla C^v, \end{aligned}$$

If we let  $\varepsilon$  tend to zero, this becomes

$$\int_{\partial\Omega_1} ((\mathbf{u} \cdot \mathbf{n} - \mathbf{v}_I \cdot \mathbf{n}) C^v - D_v \mathbf{n} \cdot \nabla C^v) = \int_{\partial\Omega_2} ((\mathbf{u} \cdot \mathbf{n} - \mathbf{v}_I \cdot \mathbf{n}) C^v - D_v \mathbf{n} \cdot \nabla C^v)$$



since the contribution from the boundaries  $\partial\Omega_3$  and  $\partial\Omega_4$  vanishes.

The left hand side of this equation describes the flux of the volatile component through the interface  $h^+$ . Liquid only leaves  $\Omega$  through this part of the boundary by evaporation, hence we equate this term to the amount of volatile component evaporating per surface area,  $e$ . Letting  $\delta$  tend to zero we obtain :

$$-D_v \mathbf{n} \cdot \nabla C^v + C^v (\mathbf{u}_F \cdot \mathbf{n} - \mathbf{v}_I \cdot \mathbf{n}) = e.$$

The same holds for the non-volatile component, with the difference that the evaporation is zero:

$$D_v \mathbf{n} \cdot \nabla C^v + (1 - C^v) (\mathbf{u}_F \cdot \mathbf{n} - \mathbf{v}_I \cdot \mathbf{n}) = 0.$$

Combining these two equations yields

$$-D_v \mathbf{n} \cdot \nabla C^v = (1 - C^v) e$$

and

$$\mathbf{u}_F \cdot \mathbf{n} - \mathbf{v}_I \cdot \mathbf{n} = e.$$

The same considerations can be done for the interface  $h^-$ , and the results may be rewritten as

$$\mp D_v (C_z^v - h_x^\pm C_x^v - h_y^\pm C_y^v) = (1 - C^v) e \sqrt{1 + (h_x^\pm)^2 + (h_y^\pm)^2} \quad (2.61)$$

and

$$w = h_t^\pm + u h_x^\pm + v h_y^\pm + e \sqrt{1 + (h_x^\pm)^2 + (h_y^\pm)^2}. \quad (2.62)$$

**Remark** *The equation describing the evolution of the interface (2.9) must be modified in the case of evaporation and replaced by (2.62).*

### 2.3.3 Determination of the evaporation rate

This leaves us with the determination of the evaporation rate  $e$ , for which we use a simplified evaporation model as given in [11]. We assume that the interface is in thermodynamic equilibrium, i.e. the vapour pressure  $p^v$  at the interface is equal to the saturation pressure  $p_{sat}$ . From this condition, the density of the vapour can be determined. The evaporation rate is equal to the negative density gradient of the vapour at the interface,

$$e = -\mathbf{n} \cdot \nabla \rho^v,$$

where  $\rho^v$  denotes the density of the vapour. In order to compute this quantity, we assume that the vapour in the bubble is only transported due to diffusion and

neglect convection effects. Note that we also assume a constant temperature such that we do not consider the energy equation.

We make a further simplification and assume that the total density of the gas (air + vapour) is constant in space such that we obtain

$$\rho_t^v = D_v \Delta \rho^v$$

in the bubble  $\Omega_B$ . Here  $D^v$  is the diffusivity of the vapour in air. From the condition

$$p^v = p_{sat}$$

we obtain

$$\rho^v = \rho(p_{sat})$$

as boundary condition on  $\partial\Omega_B$ . For more details we refer to [11].

### 2.3.4 Influence on the surface tension

As for the surfactant, we still need a relation between the concentration  $C^v$  and the surface tension. For the surface tension  $\sigma$ , we assume the simple relation

$$\sigma = C^v \gamma_v + (1 - C^v) \gamma_l, \quad (2.63)$$

where  $\gamma_v$  is the surface tension of the volatile component and  $\gamma_l$  that of the basic liquid.

### 2.3.5 Nondimensionalization

We introduce two more dimensionless variables,

$$\begin{aligned} C^v &= \tilde{C}^* C^{v'}, \\ e &= e^* e', \end{aligned}$$

and define the following quantities:

- The Péclet number  $\widetilde{\text{Pe}} = \frac{UL}{D_v}$  for the volatile component. This is exactly the same as for the surfactant and characterizes the relation of convection and diffusion.
- The parameter  $\mathcal{S} = \frac{Le^*}{D_v \tilde{C}^*}$  relates evaporation and diffusion.
- The parameter  $\mathcal{E} = \frac{e^*}{U}$  characterizes the relation between evaporation and convection.

The bulk equations are the same as for the surfactant, in particular

$$\varepsilon^2 \widetilde{\text{Pe}}(C_t^v + uC_x^v + vC_y^v + wC_z^v) = \varepsilon^2 C_{xx}^v + \varepsilon^2 C_{yy}^v + C_{zz}^v. \quad (2.64)$$

At the interfaces we have

$$\mp \frac{1}{\varepsilon \mathcal{S}} (2C_z^v \mp \varepsilon^2 h_x C_x^v \mp \varepsilon^2 h_y C_y^v) = (1 - \tilde{C}^* C^v) e \sqrt{4 + \varepsilon^2 h_x^2 + \varepsilon^2 h_y^2} \quad (2.65)$$

and

$$2w = \pm h_t \pm u h_x \pm v h_y \pm \frac{\mathcal{E}}{\varepsilon} e \sqrt{4 + \varepsilon^2 h_x^2 + \varepsilon^2 h_y^2} \quad (2.66)$$

The latter equation replaces (2.14).

### 2.3.6 Asymptotic analysis

As in the previous cases, we make some assumptions:

- $\varepsilon^2 \widetilde{\text{Pe}} \ll 1$ ,
- $\mathcal{S} \lesssim \mathcal{O}(\varepsilon)$ ,
- $\mathcal{E} \lesssim \mathcal{O}(\varepsilon)$ .

The first condition is the same as for the surfactant case (see Section 2.2.5). If the other two conditions do not hold, evaporation is dominant and the film thins mainly due to this effect. In this case, the scaling we have assumed is incorrect and the equations need to be rescaled.

The leading order system reads

$$C_{0zz}^v = 0$$

with interface condition

$$C_{0z}^v = 0$$

at both sides of the film, leading to

$$C_{0z}^v = 0$$

also in the bulk.

In order to get a closed system, we proceed again to order  $\mathcal{O}(\varepsilon^2)$ :

$$\widetilde{\text{Pe}}(C_{0t}^v + u_0 C_{0x}^v + v_0 C_{0y}^v) = C_{0xx}^v + C_{0yy}^v + C_{1zz}^v. \quad (2.67)$$

At the interfaces, the following condition holds:

$$\mp \frac{\varepsilon}{\mathcal{S}}(2C_{1z}^v \mp h_{0x}C_{0x}^v \mp h_{0y}C_{0y}^v) = 2(1 - \tilde{C}^*C^v)e_0. \quad (2.68)$$

Integration of (2.67) together with (2.68) leads to the model for a liquid containing a volatile component:

$$0 = h_0 \widetilde{\text{Pe}}(C_{0t}^v + u_0C_{0x}^v + v_0C_{0y}^v) + \frac{2\mathcal{S}}{\varepsilon}(1 - \tilde{C}^*C^v)e_0 - (h_0C_{0x})_x + (h_0C_{0y})_y. \quad (2.69)$$

Moreover, Equation (2.19) is replaced by

$$w_0 = \pm \frac{1}{2}h_{0t} \pm \frac{1}{2}u_0h_{0x} \pm \frac{1}{2}v_0h_{0y} \pm \frac{\mathcal{E}}{\varepsilon}e_0,$$

which leads to a modified equation for the mass conservation (2.23):

$$h_{0t} + (u_0h_0)_x + (v_0h_0)_y + \frac{2\mathcal{E}}{\varepsilon}e_0 = 0. \quad (2.70)$$

### 2.3.7 Surface tension and evaporation rate

We need to determine the influence of the concentration  $C^v$  on the surface tension  $\sigma$ . Equation (2.63) yields

$$\sigma_{0x} = \frac{\tilde{C}^*(\gamma_v - \gamma_l)}{\Delta\gamma}C_{0x}^v.$$

We will in the following assume that  $(\gamma_v - \gamma_l) \sim \Delta\gamma$ , such that the concentration of the volatile component is of order one, i.e.  $\tilde{C}^* = 1$ . If the concentration is of a smaller order, the variation of the surface tension is too small to influence the flow of liquid in a noticeable way. Note that this means we have the relation  $\mathcal{S} = \widetilde{\text{Pe}}\mathcal{E}$ .

Finally, we need to determine the evaporation rate  $e_0$ . We will in the following assume that evaporation has only a small influence on the vapour concentration in the bubble, such that  $e_0$  is approximately constant.

## 2.4 Summary

In this chapter, we have derived equations describing the evolution of thin films under the effects of inertia, viscosity, capillarity, gravity, surfactants and volatile components. In the following, we will present the equations derived in the previous sections once more in compact form for the three different cases.

### 2.4.1 Pure liquid

This is the model we derived for a pure liquid without the presence of a surfactant or a volatile component.

$$0 = h_t + (uh)_x + (vh)_y, \quad (2.71)$$

$$0 = \frac{\varepsilon}{2\text{Ca}} h(h_{xx} + h_{yy})_x - \text{Re} \cdot h(u_t + uu_x + vv_y) + h \frac{g \cdot \text{Re}}{\text{Fr}} e_{gx} + 4(hu_x)_x + 2(hv_y)_x + (hv_x)_y + (hu_y)_y, \quad (2.72)$$

$$0 = \frac{\varepsilon}{2\text{Ca}} h(h_{xx} + h_{yy})_y - \text{Re} \cdot h(v_t + uv_x + vv_y) + h \frac{g \cdot \text{Re}}{\text{Fr}} e_{gy} + 4(hv_y)_y + 2(hu_x)_y + (hu_y)_x + (hv_x)_x. \quad (2.73)$$

### 2.4.2 Presence of a surfactant

This system describes the case of a liquid with the presence of a surfactant. Abbreviating

$$\Sigma = \frac{R\Theta\Gamma_\infty}{\Delta\gamma},$$

we obtain:

$$0 = h_t + (uh)_x + (vh)_y, \quad (2.74)$$

$$0 = -\frac{2\text{Ma}\Sigma}{\varepsilon} \frac{C_x^s}{1 + \Pi C^s} + \frac{\varepsilon}{2\text{Ca}} h(h_{xx} + h_{yy})_x - \text{Re} h(u_t + uu_x + vv_y) + h \frac{g \cdot \text{Re}}{\text{Fr}} e_{gx} + 4(hu_x)_x + 2(hv_y)_x + (hv_x)_y + (hu_y)_y, \quad (2.75)$$

$$\begin{aligned}
 0 &= -\frac{2\text{Ma}\Sigma}{\varepsilon} \frac{C_y^s}{1 + \Pi C^s} + \frac{\varepsilon}{2\text{Ca}} h(h_{xx} + h_{yy})_y \\
 &\quad - \text{Re } h(v_t + uv_x + vv_y) + h \frac{g \text{Re}}{\text{Fr}} e_{gy} \\
 &\quad + 4(hv_y)_y + 2(hu_x)_y + (hu_y)_x + (hv_x)_x, \tag{2.76}
 \end{aligned}$$

$$\begin{aligned}
 0 &= \left( \frac{2\Pi}{\varepsilon S\Lambda(1 + \Pi C_0^s)^2} + \text{Pe } h \right) (C_t^s + uC_x^s + vC_y^s) \\
 &\quad + \frac{2\Pi}{\varepsilon S\Lambda(1 + \Pi C^s)} (u_x C^s + v_y C^s) - (hC_x^s)_x - (hC_y^s)_y. \tag{2.77}
 \end{aligned}$$

### 2.4.3 Presence of a volatile component

Finally, this is the model for a mixture of two liquid components one of which is volatile. With

$$\tilde{\Sigma} = \frac{\gamma_l - \gamma_v}{\Delta\gamma}$$

we obtain

$$0 = h_t + (uh)_x + (vh)_y + \frac{2\mathcal{E}}{\varepsilon} e, \tag{2.78}$$

$$\begin{aligned}
 0 &= -\frac{2\text{Ma}\tilde{\Sigma}}{\varepsilon} C_x^v + \frac{\varepsilon}{2\text{Ca}} h(h_{xx} + h_{yy})_x - \text{Re } h(u_t + uu_x + vu_y) \\
 &\quad + h \frac{g \text{Re}}{\text{Fr}} e_{gx} + 4(hu_x)_x + 2(hv_y)_x + (hv_x)_y + (hu_y)_y, \tag{2.79}
 \end{aligned}$$

$$\begin{aligned}
 0 &= -\frac{2\text{Ma}\tilde{\Sigma}}{\varepsilon} C_y^v + \frac{\varepsilon}{2\text{Ca}} h(h_{xx} + h_{yy})_y - \text{Re } h(v_t + uv_x + vv_y) \\
 &\quad + h \frac{g \text{Re}}{\text{Fr}} e_{gy} + 4(hv_y)_y + 2(hu_x)_y + (hu_y)_x + (hv_x)_x, \tag{2.80}
 \end{aligned}$$

$$0 = h\tilde{\text{Pe}}(C_t^v + uC_x^v + vC_y^v) + \frac{2\tilde{\text{Pe}}\mathcal{E}}{\varepsilon} (1 - C^v)e - (hC_x^v)_x - (hC_y^v)_y. \tag{2.81}$$

**Remark** The parameter  $\tilde{\Sigma}$  can be either positive or negative depending on the values of the surface tension for the two components. If it is positive (i.e. if  $\sigma_l > \sigma_v$ ), we have a Marangoni positive fluid and the film is stabilized. Otherwise, the fluid is Marangoni negative and the decay is accelerated.

## Chapter 3

# Analysis of a foam film in fuel

In the previous chapter, we have derived a system of equations for the description of a thin film between two free surfaces. We have considered all the phenomena that we assume to play an important role in the thinning process. In particular, these are inertia, viscosity, capillarity, gravity, and Marangoni forces due to the presence of surfactants or a volatile component. Moreover, we have derived equations modelling the surfactant and volatile component.

In the following, we will consider the original problem, i.e. the thinning of a real foam lamella occurring in gasoline or diesel. We will analyze under which circumstances and in which parts of the foam we can apply the thin film equations (2.71) – (2.81) and formulate a model for the description of the behaviour of a foam film.

At first, we will discuss the computational domain in Section 3.1 and the initial and boundary conditions in Section 3.2. Moreover, the relevant physical parameters will be determined in Section 3.3. When the complete model has been formulated in Section 3.4, we will discuss its analytical properties (Section 3.5) and then develop a scheme for its numerical solution (Section 3.6). The chapter is closed with an error analysis in Section 3.7.

### 3.1 Setting of the problem

We deal with the foam arising in a car tank during the filling process. In order to gain knowledge about its decay rate, we study the thinning of single foam films. Therefore, we have to study the environment of the given process and the general behaviour of fuel and foam in the process.

When we develop the model for a lamella, we have to take the circumstances of its formation into account. There are two main reasons for the presence of foam during the filling of a car tank. On the one hand, a typical tank has a very complex geometry, since it is among the last components to be designed in a car and is literally squeezed into the remaining space. The flow of fuel in such a geometry is therefore confronted with obstacles and turnings which lead to disturbances and turbulences at the surface of the fluid. This causes the creation of foam just like the stirring of soapy water.

On the other hand, the fluid entering the tank through the fuel nozzle is already an emulsion of fuel and air. The reason for this is that during the filling of the tank, benzene and air are sucked out and mixed with the fuel.

In the following, we assume on this basis that we can consider a foam starting as a sphere packing and drying due to drainage. The computation starts at the time when the film is thin enough such that the thin film approximations can be applied. We will discuss in Section 3.2 which initial conditions can be used.

### Computational domain

In Chapter 2, we have not taken any boundary conditions into account (only interfaces), but considered the Riemann problem in one and two dimensions. However, a real lamella obviously has a finite extension. In order to simulate its behaviour, we therefore need to determine a suitable computational domain.

Let us first consider the case of a two-dimensional lamella as in Figure 3.1. We assume that it is symmetric with respect to the axis  $x = 0$ . We need to pay atten-

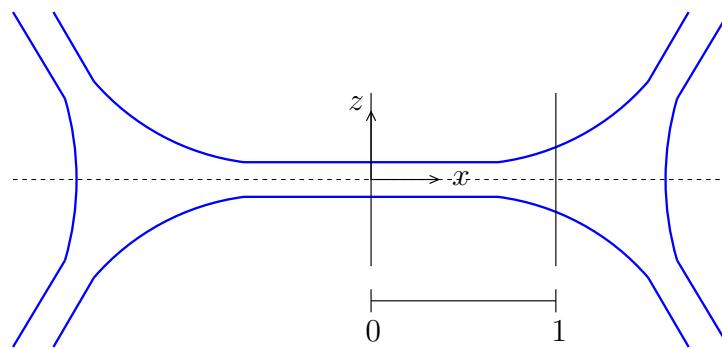


Figure 3.1: Computational domain for a 2D lamella

tion to two aspects when defining the (one-dimensional) computational domain. On the one hand, the error made in the thin film approximations depends on the



ratio  $\varepsilon$  of thickness and length of the lamella. Hence, the approximation becomes worse in the transition region. On the other hand, we will show in Section 3.2 that the boundary conditions are best prescribed in the center of the Plateau border. A compromise between these two conflicting criteria will be found depending on the magnitude of  $\varepsilon$ .

Let us next consider a three-dimensional lamella as shown in Figure 3.2. As we

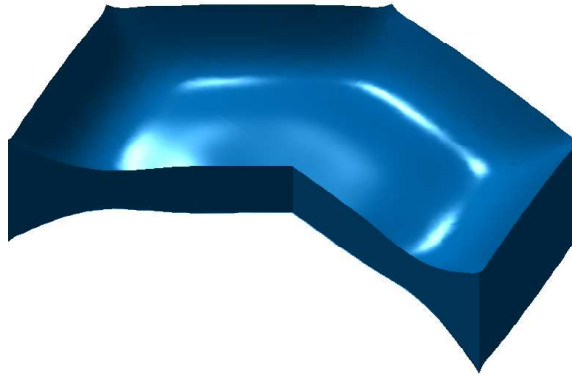


Figure 3.2: Shape of a 3D lamella

have seen in Chapter 1, a foam bubble is approximately a polyhedron, hence the lamella is a polygon (one face of a polyhedron). For the computations, we will restrict ourselves to pentagonal lamellae, since these are dominant in real foams (see [16]).

**Remark** *The reason for this is Plateau's law which demands an angle of approximately  $109.5^\circ$  between two Plateau borders. This condition can only be fulfilled if Plateau borders are curved. This curvature can have the smallest values in a pentagon, since the mean inner angle is with  $108^\circ$  very close to the required value of  $109.5^\circ$ . The next closer shape is the hexagon with a mean angle of  $120^\circ$ , while for all other polygons these values differ much more from  $109.5^\circ$ , which leads to a higher curvature of the Plateau borders. Therefore, 5-sided polygons are energetically favourable due to their smallest surface per unit volume compared to other lamella shapes.*

Moreover, we consider a regular polyhedron and assume a symmetric problem, such that the computational domain may be reduced to a triangle as shown in Figure 3.3.

**Remark** *If gravity is considered in the equations, the assumption of symmetry does not hold in general and the full lamella has to be taken into account in the computations.*

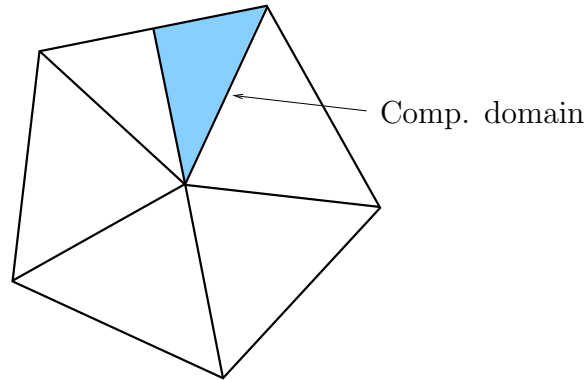


Figure 3.3: Computational domain for polygonal lamella

### Further assumptions

The following assumptions are made about the model:

- Exterior forces acting on the lamella due to the foam flow are negligible.
- The geometry of the computational domain is considered to be constant in time.
- The curvature of the Plateau borders can be neglected.

### Convention

Due to the thin film approximation, the spatial dimension of the problem has been reduced by one. The 1D problem corresponds to a 2D lamella, while the 2D problem corresponds to a 3D lamella. In the following, we will refer to the different cases by the spatial dimension of the problem, not that of the lamella.

## 3.2 Initial and boundary conditions

As we have already mentioned in the previous section, no boundary conditions at the ends of the thin film have been considered in Chapter 2. In this chapter however, we are dealing with real foam lamella. Therefore, we discuss conditions at the boundaries of the computational domain. Moreover, the challenge of finding initial values for the lamella problem is addressed.

### 3.2.1 One-dimensional problem

We first consider the simpler case of a two-dimensional foam as in Figure 3.1. Apart from the initial solution, which will be discussed in Section 3.2.3, we need conditions at the boundaries  $x = 0$  and  $x = 1$ .

#### Symmetry conditions at $x = 0$

We have no difficulties in defining boundary conditions here since we assume symmetry of the solution with respect to  $x = 0$ . In particular this means that for the film thickness  $h$ , the velocity  $u$  and the concentrations  $C^s$  and  $C^v$ , respectively, we have

$$h_x = 0, \quad (3.1)$$

$$u = 0, \quad (3.2)$$

$$C_x^{s/v} = 0. \quad (3.3)$$

In Section 3.4, we will introduce a fourth order regularization term for the thickness  $h$ . Therefore, we obtain another symmetry condition, namely

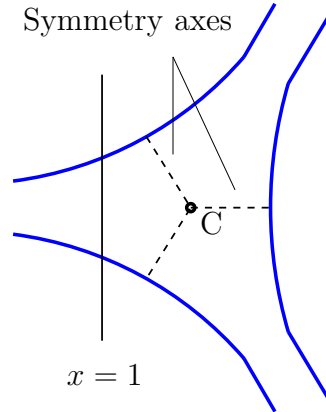
$$h_{xxx} = 0. \quad (3.4)$$

#### Conditions at the Plateau border ( $x = 1$ )

The task of finding conditions at the Plateau border end of the lamella is less trivial. Although there are symmetries in the Plateau border (see Figure 3.4), these are outside of the computational domain and therefore not directly utilizable.

We begin with the discussion of conditions for  $h$ . For a thin film, the curvature of the interface is much larger in the Plateau border than in the lamella part. Hence, the Plateau border is dominated by capillary pressure, and the curvature is approximately constant there. We denote this (dimensional) curvature by  $\kappa'$  and find that its order of magnitude is between  $L^{-1}$  and  $(\varepsilon L)^{-1}$ , i.e. the radius of curvature is somewhere between the length of the lamella and its thickness, depending on the liquid content and the history of the foam.

Since the curvature of the Plateau border is the main reason for film thinning, we will prescribe it as boundary condition for the thin film equations. Recall that in the thin film approximation, the curvature of the interface is given by  $\Delta h$  ( $\Delta$  denotes the Laplace operator) and for a capillarity-dominated film, the momentum equation reduces to  $h_{xxx} = 0$  in 1D. In dimensionless variables, the curvature of the Plateau border is therefore given by  $\kappa = \varepsilon^{-1}\kappa'$ .

Figure 3.4: Boundary at  $x = 1$ 

The first boundary condition for the thickness  $h$  at the Plateau border is therefore

$$h_{xx} = \kappa. \quad (3.5)$$

There are several possibilities to define the second condition for  $h$ :

1. One approach is to assume that the liquid, which is draining out of the lamella into the Plateau border, is completely transported away due to foam drainage. In this case, the thickness  $h$  at the boundary can be assumed to be constant.

More generally one may couple the thin film model with a foam drainage model, such that the flow into the Plateau border acts as a source in the foam drainage equations. In this case the thickness and curvature at the boundary  $x = 1$  may be obtained at each time-step from the drainage model, that is

$$h(1, t) = h_{PB}(t). \quad (3.6)$$

2. We can directly use the reduced momentum equation and set

$$h_{xxx} = 0. \quad (3.7)$$

If  $h_{PB}$  is given or can be obtained, the first approach is to be preferred. However, in general we do not have this information such that we will use the second alternative, although it is a less exact approximation.

Next, consider the velocity  $u$ , for which one more condition at  $x = 1$  is needed. There are several possibilities for this, and in the following, we will discuss their advantages and disadvantages.

1. The velocity of the flow is zero at center C of the Plateau border due to symmetry reasons (see Figure 3.4). Therefore, we assume that it is small close to the center and one possibility is to set

$$u(1) = 0.$$

However, this approach only works if the computational domain includes a large part of the Plateau border.

2. Another possible condition is to set  $u_x(1) = 0$ , but as in the first case, this is only a good approximation close to the center of the Plateau border.
3. A third approach is to set constant flux at  $x = 1$ , that is

$$(uh)_x = 0. \quad (3.8)$$

Plugging this into the mass equation, we observe that this results in  $h_t(1) = 0$ , such that the thickness of the lamella at the boundary remains constant. If the behaviour of the thickness of the Plateau border is known (for example from a coupling with a foam drainage equation), this condition can be improved to

$$(uh)_x = -h_t(1)$$

at the boundary  $x = 1$ .

In the following, we will use the third approach.

Finally the concentrations  $C^s$  and  $C^v$ , respectively, are considered. Two possibilities suggest themselves. On the one hand we may assume that the Plateau border acts as a kind of large container in which the concentration is approximately constant due to the fact that the influence from the lamella is small. In this case, we set the boundary concentration equal to this constant value, that is

$$C^{s/v} = C_{PB}^{s/v}. \quad (3.9)$$

However, this is not adequate if we assume a thicker film in which case the influence from the lamella can no longer be neglected. In that case, we still assume that the concentration is approximately constant in the Plateau border but varies with time. Then we prescribe a homogeneous Neumann condition,

$$C_x^{s/v} = 0. \quad (3.10)$$

We will consider both of these alternatives in the computations.

### 3.2.2 Two-dimensional problem

We consider a triangular domain as in Figure 3.5, where we have two boundaries at which we prescribe symmetry conditions ( $\partial\Omega_1$ ) and one boundary situated at the Plateau border ( $\partial\Omega_2$ ). We will see that most of the conditions derived in the previous section can be transferred to the three-dimensional case.

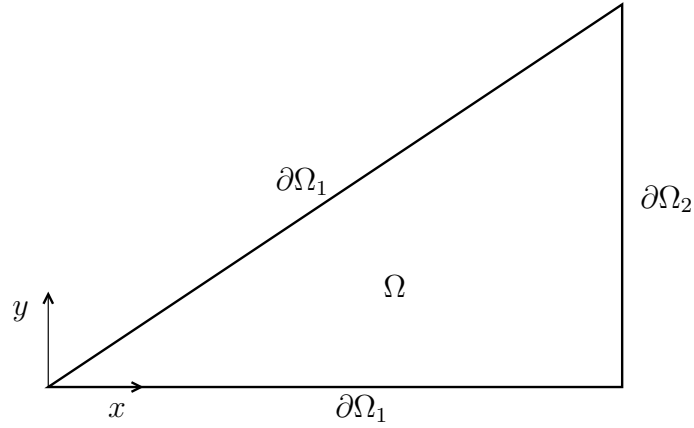


Figure 3.5: Computational domain

#### Symmetry conditions at $\partial\Omega_1$

We have homogeneous Neumann conditions for  $h$  and  $C^{s/v}$ , as well as for the tangential component of the velocity. The normal velocity needs to be zero at the boundary. If we denote the velocity by  $\mathbf{U} = \begin{pmatrix} u \\ v \end{pmatrix}$  and its tangential component by  $U^t = \mathbf{t} \cdot \mathbf{U}$ , this gives

$$0 = (\mathbf{n} \cdot \nabla)h, \quad (3.11)$$

$$0 = (\mathbf{n} \cdot \nabla)(h_{xx} + h_{yy}), \quad (3.12)$$

$$0 = \mathbf{n} \cdot \mathbf{U}, \quad (3.13)$$

$$0 = (\mathbf{n} \cdot \nabla)U^t, \quad (3.14)$$

$$0 = (\mathbf{n} \cdot \nabla)C^{s/v}. \quad (3.15)$$

**Remark** Note that the normal and tangential unit vectors  $\mathbf{n}$  and  $\mathbf{t}$  are different from the ones used in Chapter 2. Here, they are vectors in the  $x$ - $y$ -plane normal and tangential to the computational domain  $\Omega$ .

### Conditions at the Plateau border boundary $\partial\Omega_2$

Transferring the considerations from Section 3.2.1, we obtain the following conditions for  $h$ . We prescribe the curvature at the boundary, i.e.

$$\Delta h = h_{xx} + h_{yy} = \kappa. \quad (3.16)$$

For the second condition we have two possibilities, in analogy to the one-dimensional case:

1. If we have a coupling with a model for the Plateau border, we can set

$$h = h_{\text{PB}}(t). \quad (3.17)$$

2. Otherwise, which is the case in the following, the normal derivative of the curvature is assumed to be zero, that is

$$0 = (\mathbf{n} \cdot \nabla)\Delta h.$$

There are several options to establish boundary conditions for the velocity components  $u$  and  $v$ . Setting the velocity or its normal derivative to zero at the boundary has the same disadvantages as discussed in Section 3.2.1. Therefore we consider two remaining options:

1. One possibility is to prescribe a condition for the flux  $h\mathbf{U}$ . Analogous to the one-dimensional case, we set the normal derivative of the normal flux  $U^n = \mathbf{n} \cdot \mathbf{U}$  equal to zero:

$$\mathbf{n} \cdot \nabla(hU^n) = 0. \quad (3.18)$$

However, we need a second condition, which can be either

$$\mathbf{t} \cdot \nabla(hU^n) = 0 \quad (3.19)$$

or

$$\mathbf{n} \cdot \nabla(hU^t) = 0. \quad (3.20)$$

Both of these alternatives have the drawback that they are not physically motivated.

2. An alternative approach is motivated by the viscosity in the momentum equations. We also prescribe homogeneous Neumann conditions for the flux, but this time corresponding to the directions in which the viscosity is acting. This yields

$$\mathbf{n} \cdot \begin{pmatrix} 4(uh)_x + 2(vh)_y \\ (vh)_x + (uh)_y \end{pmatrix} = 0, \quad (3.21)$$

$$\mathbf{n} \cdot \begin{pmatrix} (uh)_y + (vh)_x \\ 4(vh)_y + 2(uh)_x \end{pmatrix} = 0. \quad (3.22)$$

Numerical experiments indicate that this last approach produces the best results, such that we will use this in the remainder of this work.

Finally, we consider the concentrations of the surfactant and the volatile component, respectively. Here, we can transfer the conditions from Section 3.2.1 directly to the two-dimensional case, that is we use either

$$C^{s/v} = C_{PB}, \quad (3.23)$$

where  $C_{PB}$  is the constant concentration given in the Plateau border, or

$$0 = (\mathbf{n} \cdot \nabla) C^{s/v}. \quad (3.24)$$

### 3.2.3 Initial conditions

For the choice of initial conditions we have to keep the history of the foam in mind, i.e. in which way it has been created. As we have discussed in Section 3.1, we assume that we have initially an emulsion which becomes a foam due to drainage effects. In other words, we start the computation somewhere in the middle of the thinning process, which makes it difficult to prescribe correct initial conditions.

We leave this problem open for the moment. As we will see in Chapter 5, approximate solutions can be used as a guess for the initial conditions. This problem will be discussed in more detail there.

## 3.3 Discussion of parameter sizes

In order to solve the film-thinning problem for a real foam, we need to have some information about the physical parameters appearing in our model such that we can evaluate the occurring similarity numbers.

However, we face the problem that we do not have enough information about the fluid under consideration – i.e. fuel – to uniquely determine all of the parameters. Especially, the parameters describing the surfactant and the volatile component, respectively, are difficult to obtain. The reason for this is that due to the complex composition of fuels, we do not know which substances are responsible for the effects.

Moreover, fuel is not a uniquely defined liquid with definite parameters, but there are strong variations depending on its composition. However, in Tables 3.1, 3.2 and 3.3 we have listed all of the occurring physical parameters and given ranges for their values.



Parameter	Description	Range	Unit	Explanation
$L$	Typical length scale	$10^{-4} - 10^{-2}$	$m$	Typical bubble size, from observations
$T$	Time scale	$10^{-2} - 1$	$s$	Time in which typical bubbles in fuel burst
$U$	Typical velocity	$10^{-4} - 1$	$\frac{m}{s}$	Typical length scale divided by time scale
$\varepsilon$	Thickness-length ratio	$\leq 10^{-1}$		For larger values error in TFE becomes too large
$\rho$	Density	$\approx 8 \cdot 10^2$	$\frac{kg}{m^3}$	Dependent on the composition of the fuel
$\mu$	Viscosity	$5 \cdot 10^{-4} - 4 \cdot 10^{-3}$	$\frac{kg}{ms}$	Dependent on the composition of the fuel
$\gamma$	Surface tension	$2 \cdot 10^{-2} - 3 \cdot 10^{-2}$	$\frac{N}{m}$	Dependent on the composition of the fuel
$\Delta\gamma$	Surface tension variation	$10^{-3}$	$\frac{N}{m}$	If surfactant or volatile component is present
$g$	Gravitational acceleration	10	$\frac{m}{s^2}$	On earth
$\kappa$	Plateau border curvature	$\mathcal{O}(\varepsilon^{-1}) - \mathcal{O}(\varepsilon^{-2})$		See Section 3.2

Table 3.1: Parameters for the pure liquid

Parameter	Description	Range	Unit	Explanation
$D_s$	Diffusivity	$10^{-10} - 10^{-5}$	$\frac{m^2}{s}$	Unknown, therefore broad span is given
$D_\Gamma$	Surface diffusivity	$10^{-10} - 10^{-5}$	$\frac{m^2}{s}$	Assumed to be equal to $D_s$
$C^*$	Typical bulk concentration	$\approx 10^{-4}$	$\frac{mol}{m^3}$	Guess (no information about surfactant)
$\Gamma_\infty$	Surface saturation concentration	$\leq 10^{-6} - \leq 10^{-5}$	$\frac{mol}{m^2}$	Based on [9]
$\Gamma^*$	Typical surface concentration	$\leq 10^{-6} - \leq 10^{-5}$	$\frac{mol}{m^2}$	Must be lower than $\Gamma_\infty$
$k_2$	Langmuir parameter	$10^{-2} - 1$	$\frac{mol}{m^3}$	Larger than $C^*$ , guess
$R$	Universal gas constant	$\approx 8$	$\frac{J}{molK}$	
$\Theta$	Temperature	$\approx 300$	$K$	Outside temperature

Table 3.2: Parameters for the surfactant

Parameter	Description	Range	Unit	Explanation
$D_v$	Diffusivity	$10^{-10} - 10^{-5}$	$\frac{m^2}{s}$	Similar to $D_s$
$e^*$	Evaporation rate	$10^{-5} - 10^{-4}$	$\frac{m}{s}$	[9]

Table 3.3: Parameters for the volatile component

### 3.4 Resulting model for fuel foam

In the previous section we have compiled all the necessary parameters to compute the similarity numbers appearing in the TFE (2.71) – (2.81). Together with the boundary and initial conditions derived in Section 3.2, we are now able to formulate the complete model for the thinning of a lamella with respect to a specific problem of interest.

Let us consider some special cases for the parameters determined in the previous section in order to gain an impression of the resulting models. The relevant similarity numbers associated to these examples are listed in Table 3.4.

**Example 1.** In the first case, we assume a bubble size of  $10^{-3}m$  and a velocity scale of  $10^{-3}m/s$ , which corresponds to a time scale of  $1s$ . We consider a thin film with a ratio of thickness and length of  $\varepsilon = 10^{-2}$ . We set the diffusivity to  $10^{-6}m^2/s$  for both surfactant and volatile component. The typical concentrations for the surfactant are assumed to be  $C^* = 10^{-4}mol/m^3$ ,  $\Gamma^* = 10^{-7}mol/m^2$ ,  $\Gamma_\infty = 10^{-6}mol/m^2$  and  $k_2 = 10^{-2}mol/m^3$ . For the evaporation, we assume  $e^* = 10^{-5}m/s$ .

Since we are only interested in ballpark figures at the moment, we consider a density of  $\rho = 10^3m/s$ , a viscosity of  $\mu = 10^{-3}kg/ms$  and surface tension of  $\gamma = 2 \cdot 10^{-2}N/m$ . The remaining parameters are uniquely determined in Section 3.3.

**Example 2.** Next, we consider the same parameter values, but a faster velocity scale of  $10^{-2}m/s$ .

**Example 3.** Finally, we use the same values as in the second example but with  $\varepsilon = 10^{-1}$ , i.e. a relatively thick film.

We notice from Table 3.4 that we cannot generally neglect any of the considered effects. Therefore, we will in the following consider the full set of equations (2.71) – (2.81) derived in Chapter 2. However, under certain circumstances simplified models can be applied, depending on the parameters. In the limit of a very thin film for example, that is  $\varepsilon \rightarrow 0$ , some simplifications can be made. We will consider this case in more detail in Chapter 4.

We are now in the position to formulate the full mathematical problem, where we restrict ourselves at the moment to the case of a surfactant stabilizing the foam. The case of a volatile component can be treated analogously with minor changes. Hereby, we regularize the mass equation with a fourth order term for  $h$  weighted by a parameter  $\delta$ . This is done in order to control the third order derivative appearing in the momentum equation. Moreover, it allows us to impose boundary conditions for the third derivatives of  $h$ , as discussed in Section 3.2.

Similarity number	calculated by	Example 1	Example 2	Example 3
Re	$\frac{\rho LU}{\mu}$	1	10	10
$\frac{\text{Re} \cdot g}{\text{Fr}}$	$\text{Re} \frac{Lg}{U^2}$	$10^4$	$10^3$	$10^3$
$\frac{\varepsilon}{2\text{Ca}}$	$\frac{\varepsilon \gamma}{2\mu U}$	100	10	100
$\frac{\text{Ma}}{\varepsilon}$	$\frac{\Delta \gamma}{\varepsilon \mu U}$	$10^5$	$10^4$	$10^3$
$\Lambda$	$\frac{\Gamma^*}{\Gamma_\infty}$	$10^{-1}$	$10^{-1}$	$10^{-1}$
$\Pi$	$\frac{C^*}{k_2}$	$10^{-2}$	$10^{-2}$	$10^{-2}$
$\Sigma$	$\frac{RT\Gamma_\infty}{\Delta \gamma}$	3	3	3
Pe	$\frac{UL}{D_s}$	1	10	10
$\frac{\Pi}{\varepsilon S \Lambda}$	$\frac{U\Gamma^*\Pi}{\varepsilon D_s C^* \Lambda}$	10	$10^2$	10
$\widetilde{\text{Pe}}$	$\frac{UL}{D_v}$	1	10	10
$\frac{\varepsilon}{\varepsilon}$	$\frac{e^*}{\varepsilon U}$	1	$10^{-1}$	$10^{-2}$
$\widetilde{\Sigma}$	$\frac{\sigma_l - \sigma_v}{\Delta \gamma}$	1	1	1

Table 3.4: Approximate similarity numbers

**Problem 1** Let  $\Omega \subset \mathbb{R}^2$  be the computational domain as in Figure 3.5, where  $\partial\Omega_1$  is the symmetry boundary and  $\partial\Omega_2$  the boundary located at the Plateau border.

Find  $h, u, v, C^s : [0, T] \times \Omega \rightarrow \mathbb{R}$ , such that

$$0 = h_t + (uh)_x + (vh)_y + \delta \Delta \Delta h, \quad (3.25)$$

$$\begin{aligned} 0 = & -\frac{2\text{Ma}\Sigma}{\varepsilon} \frac{C_x^s}{1 + \Pi C^s} + \frac{\varepsilon}{2\text{Ca}} h(h_{xx} + h_{yy})_x \\ & - \text{Re} \cdot h(u_t + uu_x + vu_y) + h \frac{g \cdot \text{Re}}{\text{Fr}} e_{gx} \\ & + 4(hu_x)_x + 2(hv_y)_x + (hv_x)_y + (hu_y)_y, \end{aligned} \quad (3.26)$$

$$\begin{aligned} 0 = & -\frac{2\text{Ma}\Sigma}{\varepsilon} \frac{C_y^s}{1 + \Pi C^s} + \frac{\varepsilon}{2\text{Ca}} h(h_{xx} + h_{yy})_y \\ & - \text{Re} \cdot h(v_t + uv_x + vv_y) + h \frac{g \cdot \text{Re}}{\text{Fr}} e_{gy} \\ & + 4(hv_y)_y + 2(hu_x)_y + (hu_y)_x + (hv_x)_x, \end{aligned} \quad (3.27)$$

$$\begin{aligned}
0 &= \left( \frac{2\Pi}{\varepsilon S \Lambda (1 + \Pi C_0^s)^2} + \text{Pe } h \right) (C_t^s + u C_x^s + v C_y^s) \\
&\quad + \frac{2\Pi}{\varepsilon S \Lambda (1 + \Pi C^s)} (u_x C^s + u_y C^s) - (h C_x^s)_x - (h C_y^s)_y \quad (3.28)
\end{aligned}$$

holds in  $[0, T] \times \Omega$ . Moreover, the initial conditions

$$\begin{aligned}
h &= h_0, \\
u &= u_0, \\
v &= v_0, \\
C^s &= C_0^s
\end{aligned}$$

are fulfilled on  $\{0\} \times \Omega$ , and

$$\begin{aligned}
0 &= (\mathbf{n} \cdot \nabla) h, \\
0 &= (\mathbf{n} \cdot \nabla)(\Delta h), \\
0 &= \mathbf{n} \cdot \mathbf{U}, \\
0 &= (\mathbf{n} \cdot \nabla) U^t, \\
0 &= (\mathbf{n} \cdot \nabla) C^s,
\end{aligned}$$

holds at the symmetry boundary  $\partial\Omega_1$ , and

$$\begin{aligned}
\kappa &= \Delta h, \\
0 &= (\mathbf{n} \cdot \nabla)(\Delta h), \\
0 &= \mathbf{n} \cdot \begin{pmatrix} 4(uh)_x + 2(vh)_y \\ (vh)_x + (uh)_y \end{pmatrix}, \\
0 &= \mathbf{n} \cdot \begin{pmatrix} (uh)_y + (vh)_x \\ 4(vh)_y + 2(uh)_x \end{pmatrix}, \\
0 &= (\mathbf{n} \cdot \nabla) C^s
\end{aligned}$$

at  $\partial\Omega_2$ . Hereby  $\mathbf{U} = \begin{pmatrix} u \\ v \end{pmatrix}$  and  $U^n$  and  $U^t$  are the normal and tangential component of  $\mathbf{U}$ , respectively.

For different boundary conditions the problem needs to be modified accordingly.

Given the physical parameters and a suitable initial condition, we have developed a model that only depends on one outer parameter, namely the curvature  $\kappa$  of the Plateau border. This quantity has to be provided by a global foam model. In turn, the model provides a time  $t_{crit}$  at which a given critical value for the thickness  $h$  is reached. This time determines the mean lifetime of a foam film with the given properties.

### 3.5 Analytical discussion of the problem

In the previous section, we have formulated the model for the evolution of a foam lamella. Before we are going to solve this model numerically, the question of existence and uniqueness for this problem must be addressed at first. We will clear this question for the linearized problem and afterwards discuss the nonlinear problem.

#### 3.5.1 Classification of the PDE

Firstly, we will determine the type of the system of partial differential equations in Problem 1. Since we are dealing with a fourth order equation, we cannot directly use the standard approaches for the classification of PDE's, since they require the highest derivative to be of first or second order.

Therefore, we transform our system into a system of first order equations in the dependent variables  $\mathbf{Y} = (h, h_x, h_{xx}, h_{xxx}, u, u_x, C, C_x)^\top$ . (We consider wlog the one-dimensional problem.) It can be written as

$$A\mathbf{Y}_t + B\mathbf{Y}_x = \mathbf{C}, \quad (3.29)$$

where

$$A = \begin{pmatrix} 1 & 0 & 0 & 0 & 0 & 0 & 0 & 0 \\ 0 & 0 & 0 & 0 & 0 & 0 & 0 & 0 \\ 0 & 0 & 0 & 0 & 0 & 0 & 0 & 0 \\ 0 & 0 & 0 & 0 & 0 & 0 & 0 & 0 \\ 0 & 0 & 0 & 0 & \text{Re } h & 0 & 0 & 0 \\ 0 & 0 & 0 & 0 & 0 & 0 & 0 & 0 \\ 0 & 0 & 0 & 0 & 0 & 0 & \frac{2\Pi}{\varepsilon S\Lambda} + \text{Pe } h & 0 \\ 0 & 0 & 0 & 0 & 0 & 0 & 0 & 0 \end{pmatrix}$$

and

$$B = \begin{pmatrix} u & 0 & 0 & \delta & h & 0 & 0 & 0 \\ 1 & 0 & 0 & 0 & 0 & 0 & 0 & 0 \\ 0 & 1 & 0 & 0 & 0 & 0 & 0 & 0 \\ 0 & 0 & 1 & 0 & 0 & 0 & 0 & 0 \\ \text{Re } hu & 0 & -\frac{\varepsilon}{2\text{Ca}}h & 0 & 0 & -4h & \frac{2\text{Ma}\Sigma}{\varepsilon} & 0 \\ 0 & 0 & 0 & 0 & 1 & 0 & 0 & 0 \\ 0 & 0 & 0 & 0 & \frac{2\Pi}{\varepsilon S\Lambda}C & 0 & (\frac{2\Pi}{\varepsilon S\Lambda} + \text{Pe } h)u & -h \\ 0 & 0 & 0 & 0 & 0 & 0 & 1 & 0 \end{pmatrix}.$$

The vector  $\mathbf{C}$  contains all the remaining derivative-free terms.

In order to classify this system, we apply an approach based on the method of characteristics (ref. [33]). A nontrivial solution of (3.29) requires that the determinant

$$\det(\dot{x}A^\top + tB^\top) \stackrel{!}{=} 0.$$

The  $\dot{\cdot}$  denotes the derivative along a characteristic.

In this case, we obtain

$$\det(\dot{x}A^\top + tB^\top) = -4\delta h^2 t^8.$$

Hence, the system has one repeated real root  $t = 0$  and is therefore parabolic. It can also be observed that the domain of influence of each point is the complete computational domain.

**Remark** *If we consider the non-regularized system ( $\delta = 0$ ), we obtain a seventh-order system for which the determinant is always zero. Hence, we are not able to classify the system without regularization.*

### 3.5.2 An existence and uniqueness result for the linearized problem

We consider a one-dimensional problem in the presence of a surfactant, in which the constant parameters are set to 1. Moreover, we do not regard any boundary conditions, but assume a Riemann problem on  $\mathbb{R}$ . In this case, Problem 1 becomes:

**Riemann problem** *Find  $h, u, C^s : [0, T] \times \mathbb{R} \rightarrow \mathbb{R}$ , such that*

$$\begin{aligned} 0 &= h_t + (hu)_x + \delta h_{xxxx}, \\ 0 &= u_t + uu_x - h_{xxx} - u_{xx} - \frac{h_x}{h}u_x + \frac{C_x^s}{h} - 1, \\ 0 &= C_t^s + uC_x^s + \frac{u_x C^s}{1+h} - \frac{hC_{xx}^s}{1+h} - \frac{h_x C_x^s}{1+h}, \end{aligned}$$

on  $[0, T] \times \mathbb{R}$  and

$$\begin{aligned} h &= h_0, \\ u &= u_0, \\ C^s &= C_0^s. \end{aligned}$$

on  $\{0\} \times \mathbb{R}$ .

We linearize this problem with respect to the initial values  $h_0, u_0$  and  $C_0^s$ , yielding the

**Linearized problem** Find  $h, u, C^s : [0, T] \times \mathbb{R} \rightarrow \mathbb{R}$ , such that

$$\begin{aligned}
0 &= h_t + (hu_0)_x + (h_0u)_x - (h_0u_0)_x + \delta h_{xxx}, \\
0 &= u_t + (u_0u)_x - h_{xxx} - u_{xx} - \frac{h_{0x}}{h_0}u_x - \frac{u_{0x}}{h_0}h_x + \frac{u_{0x}h_{0x}}{h_0^2}h \\
&\quad + \frac{C_x^s}{h_0} - \frac{C_{0x}^s}{h_0^2}h - 1 - u_0u_{0x} + \frac{C_{0x}^s}{h_0}, \\
0 &= C_t^s + u_0C_x^s + C_{0x}^s u + \frac{C_0^s}{1+h_0}u_x + \frac{u_{0x}}{1+h_0}C^s - \frac{u_{0x}C_0^s}{(1+h_0)^2}h \\
&\quad - \frac{h_0}{1+h_0}C_{xx}^s - \frac{C_{0xx}^s}{1+h_0}h + \frac{h_0C_{0xx}^s}{(1+h_0)^2}h \\
&\quad - \frac{h_{0x}}{1+h_0}C_x^s - \frac{C_{0x}^s}{1+h_0}h_x + \frac{h_{0x}C_{0x}^s}{(1+h_0)^2}h \\
&\quad - u_0C_{0x}^s - \frac{u_{0x}C_0^s}{(1+h_0)^2} + \frac{h_0C_{0xx}^s}{(1+h_0)^2} + \frac{h_{0x}C_{0x}^s}{(1+h_0)^2}
\end{aligned}$$

on  $[0, T] \times \mathbb{R}$  and

$$\begin{aligned}
h &= h_0, \\
u &= u_0, \\
C^s &= C_0^s.
\end{aligned}$$

on  $\{0\} \times \mathbb{R}$ .

For the weak formulation of the linearized problem, the mathematical definitions of the respective spaces and norms are needed.

**Definition 5** Let

$$H^m(\mathbb{R}) = \{u \in L^2(\mathbb{R}) : D^\alpha u \in L^2(\mathbb{R}), |\alpha| \leq m\}$$

be a Sobolev space of order  $m$ . In particular  $H^0(\mathbb{R}) = L^2(\mathbb{R})$ .

Define the spaces  $V, H$  by

$$\begin{aligned}
V &:= H^2(\mathbb{R}) \times H^1(\mathbb{R}) \times H^1(\mathbb{R}), \\
H &:= L^2(\mathbb{R}) \times L^2(\mathbb{R}) \times L^2(\mathbb{R}),
\end{aligned}$$

and the corresponding scalar products by

$$\begin{aligned}
((u, v)) &:= (u, v)_V = (u_1, v_1)_{H^2} + (u_2, v_2)_{H^1} + (u_3, v_3)_{H^1}, \\
(\phi, \psi) &:= (\phi, \psi)_H = (\phi_1, \psi_1)_{L^2} + (\phi_2, \psi_2)_{L^2} + (\phi_3, \psi_3)_{L^2},
\end{aligned}$$



where  $(\cdot, \cdot)_{H^m}$  and  $(\cdot, \cdot)_{L^2}$  are the standard norms defined on the spaces  $H^m$  and  $L^2$ . Moreover, let the norms induced by these scalar products be denoted by  $\|\cdot\|$  and  $|\cdot|$ , respectively. Note that  $V$  and  $H$  are Hilbert spaces with respect to  $((\cdot, \cdot))$  and  $(\cdot, \cdot)$ , respectively.

**Definition 6** Let  $V, H$  be a pair of real, separable Hilbert spaces with corresponding scalar products  $((\cdot, \cdot))$  and  $(\cdot, \cdot)$ , and norms  $\|\cdot\|$  and  $|\cdot|$ .

Let  $T \in \mathbb{R} \cup \{\infty\}$ ,  $B$  be a Banach space.  $L^2(B) := L^2(0, T; B)$  denotes the space of functions  $(t \rightarrow f(t)) : (0, T) \rightarrow B$  such that

1.  $f$  is measurable for  $dt$ ,
2.  $\|f\|_{L^2(B)} = \left( \int_0^T \|f(t)\|_B^2 dt \right)^{1/2} < \infty$ .

Moreover, we define the space

$$W(V) := W(0, T; V, V') := \{u : u \in L^2(V), u' \in L^2(V')\},$$

where  $V'$  denotes the dual space of  $V$ .

Using Definition 5, we can state the weak formulation of the linearized problem,

**Problem 2 (Weak problem)** Find

$$\mathbf{X} = \begin{pmatrix} h \\ u \\ C^s \end{pmatrix} : [0, T] \rightarrow V$$

fulfilling

$$\mathbf{X}(t=0) = \mathbf{X}_0 \in V, \tag{3.30}$$

such that

$$\frac{d}{dt}((\mathbf{X}(\cdot), \Phi)) + a(\mathbf{X}(\cdot), \Phi) = ((\mathbf{f}, \Phi)), \tag{3.31}$$

holds for all test functions  $\Phi = (\phi_1, \phi_2, \phi_3)^\top \in V$ , where  $a$  and  $\mathbf{f}$  are defined by

$$\begin{aligned}
a(\mathbf{X}, \Phi) = & - \int u_0 h \phi_{1x} - \int h_0 u \phi_{1x} + \int \delta h_{xx} \phi_{1xx} - \int u_0 u \phi_{2x} + \int h_{xx} \phi_{2x} \\
& + \int u_x \phi_{2x} - \int \frac{h_{0x}}{h_0} u_x \phi_2 - \int \frac{u_{0x}}{h_0} h_x \phi_2 + \int \frac{u_{0x} h_{0x}}{h_0^2} h \phi_2 \\
& + \int \frac{C_x^s}{h_0} \phi_2 - \int \frac{C_{0x}^s}{h_0^2} h \phi_2 + \int u_0 C_x^s \phi_3 + \int C_{0x}^s u \phi_3 + \int \frac{C_0^s}{1+h_0} u_x \phi_3 \\
& + \int \frac{u_{0x}}{1+h_0} C_x^s \phi_3 - \int \frac{u_{0x} C_0^s}{(1+h_0)^2} h \phi_3 + \int \frac{h_0}{1+h_0} C_x^s \phi_{3x} \\
& - \int \frac{h_0 h_{0x}}{(1+h_0)^2} C_x^s \phi_3 + \int \frac{C_{0x}^s}{1+h_0} h \phi_{3x} - \int \frac{C_{0x}^s h_{0x}}{(1+h_0)^2} h \phi_3 \\
& - \int \frac{h_0 C_{0x}^s}{(1+h_0)^2} h_x \phi_3 - \int \frac{h_0 C_{0x}^s}{(1+h_0)^2} h \phi_{3x} + \int \frac{2h_0 h_{0x} C_{0x}^s}{(1+h_0)^3} h \phi_3 \quad (3.32)
\end{aligned}$$

$$\begin{aligned}
((f, \Phi)) = & - \int h_0 u_0 \phi_{1x} + \int \phi_2 - \frac{1}{2} \int u_0^2 \phi_{2x} - \int \frac{C_{0x}^s}{h_0} \phi_2 + \int u_0 C_{0x}^s \phi_3 \\
& + \int \frac{u_{0x} C_0^s}{(1+h_0)^2} \phi_3 + \int \frac{h_0 C_{0x}^s}{(1+h_0)^2} \phi_{3x} - \int \frac{2h_0 h_{0x} C_{0x}^s}{(1+h_0)^3} \phi_3 \quad (3.33)
\end{aligned}$$

All the integrations are performed over  $\mathbb{R}$ .

We will now formulate the main theorem of this section.

**Theorem 1** *Let  $h_0, u_0, C_0^s$  and their respective spatial derivatives be bounded by some  $\tilde{M}$  and let  $h_0(x) \geq H_0 > 0$  for all  $x \in \mathbb{R}$ . Let  $\delta > \frac{1}{4}$ .*

*Then there exists a unique solution  $\mathbf{X}$  of Problem 2 and the solution fulfills*

$$\mathbf{X} \in W(0, T; V, V').$$

In order to prove Theorem 1, we will apply results from [12], specifically Chapter XVIII (Variational methods), §3, Theorems 1 and 2. We will state the main results here, for a complete derivation and proofs we refer to the original.

Consider the following four conditions:

**Condition 1** *Let  $V, H$  be defined as in Definition 6.  $V$  is dense in  $H$ , such that we have (by identifying  $H$  and its dual  $H'$ )*

$$V \hookrightarrow H \hookrightarrow V',$$

where  $\hookrightarrow$  denotes continuous injection.

**Condition 2** For each  $t \in [0, T]$  we are given a continuous bilinear form  $a$  on  $V \times V$  with the following properties: For each  $u, v \in V$ , the function  $t \rightarrow a(t; u, v)$  is measurable and there exists a constant  $M = M(t) > 0$  such that

$$|a(t; u, v)| \leq M \|u\| \cdot \|v\| \quad \text{for all } u, v \in V.$$

**Condition 3** The bilinear form  $a$  is coercive over  $V$  with respect to  $H$ , i.e. there exist constants  $\lambda, \alpha$  with  $\alpha > 0$  such that

$$a(t; u, u) + \lambda |u|^2 \geq \alpha \|u\|^2 \quad \forall t \in [0, T], \forall u \in V.$$

**Condition 4** The initial conditions and sources satisfy

$$u_0 \in H, \quad f \in L^2(V').$$

Using these, the following theorem can be stated:

**Theorem 2** Consider the following problem:

Find  $u$  satisfying

$$u \in W(V)$$

and

$$\frac{d}{dt}((u(\cdot), v)) + a(\cdot; u(\cdot), v) = ((f(\cdot), v))$$

in the sense of distributions for all  $v \in V$ ; moreover,

$$u(0) = u_0.$$

Suppose the spaces  $V, H$  are given and satisfy Condition 1,  $a(t; u, v)$  satisfies Conditions 2 and 3, and  $u_0, f$  satisfy Condition 4.

Then the problem has a unique solution  $u$  fulfilling

$$u \in W(0, T; V, V').$$

For the proof we refer to [12].

In order to prove Theorem 1, we also need the following two lemmata:

**Lemma 1** (Hölder's inequality)

Let  $1 < p < \infty$  and  $p'$  such that  $\frac{1}{p} + \frac{1}{p'} = 1$ . If  $u \in L^p(\mathbb{R})$  and  $v \in L^{p'}(\mathbb{R})$ , then  $uv \in L^1(\mathbb{R})$  and

$$\int_{\mathbb{R}} |u(x)v(x)| dx \leq \|u\|_p \|v\|_{p'}.$$

**Lemma 2** *Let  $\varepsilon_0$  be a finite, positive number. Then there exists a constant  $K(\varepsilon_0)$  such that*

$$|v_x| \leq K\varepsilon|v_{xx}| + K\varepsilon^{-1}|v|$$

for all  $\varepsilon \leq \varepsilon_0$  and any  $v \in H^2(\mathbb{R})$ .

Both of these and their respective proofs can be found in [1], pages 23 and 75.

Finally we can now proceed to the proof of the main theorem.

*Proof (of Theorem 1).* We have to show that Conditions 1 – 4 hold for Problem 2. Then the proof follows from Theorem 2.

**ad Condition 1.** Condition 1 is fulfilled for each of the two pairs of spaces  $H^1$  and  $L^2$ ,  $H^2$  and  $L^2$  (for a proof see for example [1]). But then it is also fulfilled for the product of the spaces, i.e for  $V$  and  $H$ .

**ad Condition 2.** We have to show that the bilinear functional  $a$  is bounded, i.e. for each  $\mathbf{X}, \Phi \in V$ ,  $t \rightarrow a(u, v)$  is measurable and there exists a constant  $M = M(t) > 0$  such that

$$|a(\mathbf{X}, \Phi)| \leq M\|\mathbf{X}\| \cdot \|\Phi\| \quad \forall u, v \in V$$

Since we assumed that  $h_0, h_{0x}, u_0, u_{0x}, C_0^s, C_{0x}^s \leq \tilde{M}$  are all bounded, we can drag them in front of the integrals in equation (3.32). Furthermore  $h_0^{-1}$  is bounded by  $H_0^{-1}$ . We denote the common bound of  $\tilde{M}$  and  $H_0^{-1}$  by  $M_0$  and

obtain from (3.32):

$$\begin{aligned}
|a(\mathbf{X}, \Phi)| &\leq M_0 \int |h\phi_{1x}| + M_0 \int |u\phi_{1x}| + \delta \int |h_{xx}\phi_{1xx}| \\
&\quad + M_0 \int |u\phi_{2x}| + \int |h_{xx}\phi_{2x}| + \int |u_x\phi_{2x}| \\
&\quad + M_0^2 \int |u_x\phi_2| + M_0^2 \int |h_x\phi_2| + M_0^4 \int |h\phi_2| \\
&\quad + M_0 \int |C_x^s\phi_2| + M_0^3 \int |h\phi_2| + M_0 \int |C_x^s\phi_3| \\
&\quad + M_0 \int |u\phi_3| + M_0^2 \int |u_x\phi_3| + M_0^2 \int |C^s\phi_3| \\
&\quad + M_0^4 \int |h\phi_3| + M_0^2 \int |C_x^s\phi_{3x}| + M_0^4 \int |C_x^s\phi_3| \\
&\quad + M_0^2 \int |h\phi_{3x}| + M_0^4 \int |h\phi_3| + M_0^4 \int |h_x\phi_3| \\
&\quad + M_0^4 \int |h\phi_{3x}| + M_0^6 \int |h\phi_3| \\
&\stackrel{\text{Lemma 1}}{\leq} M \cdot (|h|\phi_{1x}| + |u|\phi_{1x}| + |h_{xx}|\phi_{1xx}| + |u|\phi_{2x}| \\
&\quad + |h_{xx}|\phi_{2x}| + |u_x|\phi_{2x}| + |u_x|\phi_2| + |h_x|\phi_2| + |h|\phi_2| \\
&\quad + |C_x^s|\phi_2| + |h|\phi_2| + |C_x^s|\phi_3| + |u|\phi_3| + |u_x|\phi_3| \\
&\quad + |C^s|\phi_3| + |h|\phi_3| + |C_x^s|\phi_{3x}| + |C_x^s|\phi_3| + |h|\phi_{3x}| \\
&\quad + |h|\phi_3| + |h_x|\phi_3| + |h|\phi_{3x}| + |h|\phi_3|) \\
&\leq M \cdot (|h| + |h_x| + |h_{xx}| + |u| + |u_x| + |C^s| + |C_x^s|) \\
&\quad \cdot (|\phi_1| + |\phi_{1x}| + |\phi_{1xx}| + |\phi_2| + |\phi_{2x}| + |\phi_3| + |\phi_{3x}|) \\
&\leq M \cdot \|X\| \cdot \|\Phi\|.
\end{aligned}$$

Note that the notation for the integrals is an abbreviation, i.e.

$$\int |ab| = \int_{\mathbb{R}} |a(x)b(x)| dx,$$

such that  $|\cdot|$  denotes the absolute value, not the norm in  $H$ .

**ad Condition 3.** For coercivity of the bilinear form  $a$  over  $V$  with respect to  $H$ , we have to show that there exist constants  $\lambda, \alpha$  with  $\alpha > 0$  such that

$$a(\mathbf{X}, \mathbf{X}) + \lambda|\mathbf{X}|^2 \geq \alpha\|\mathbf{X}\|^2$$

is fulfilled for all  $t \in [0, \Delta T]$  and for all  $u \in V$ .

We assume wlog that  $\delta = 1$ , but the proof can be done analogously for any  $\delta > \frac{1}{4}$ .

Let  $\varepsilon_0$  be a finite, positive number,  $K(\varepsilon_0)$  be a constant such that Lemma 2 is fulfilled, and choose  $\varepsilon$  such that  $K\varepsilon \leq 1$ .

Moreover, choose constants  $\alpha > 0$ ,  $\lambda$  such that  $2\sqrt{\delta - 2\alpha}\sqrt{1 - \alpha} \geq 1$  and  $\lambda \geq \left(12 + \frac{9}{2\tilde{H}}\right)\bar{M}^2 + 2\bar{M}$ . In particular, for  $\delta = 1$  we set  $\alpha = \min\{\frac{1}{4}, \frac{\tilde{H}}{2}\}$ , where  $\tilde{H} := \frac{H_0}{1+H_0}$ .

We plug (3.32) into the ansatz and use Lemmata 1 and 2 in order to get

$$\begin{aligned}
& a(\mathbf{X}, \mathbf{X}) + \lambda|\mathbf{X}|^2 - \alpha\|\mathbf{X}\|^2 \\
&= - \int u_0 h h_x - \int h_0 u h_x + \int \delta h_{xx} h_{xx} - \int u_0 u u_x + \int h_{xx} u_x \\
&\quad + \int u_x u_x - \int \frac{h_{0x}}{h_0} u_x u - \int \frac{u_{0x}}{h_0} h_x u + \int \frac{u_{0x} h_{0x}}{h_0^2} h u \\
&\quad + \int \frac{C_x^s}{h_0} u - \int \frac{C_{0x}^s}{h_0^2} h u + \int u_0 C_x^s C^s + \int C_{0x}^s u C^s + \int \frac{C_0^s}{1+h_0} u_x C^s \\
&\quad + \int \frac{u_{0x}}{1+h_0} C^s C^s - \int \frac{u_{0x} C_0^s}{(1+h_0)^2} h C^s + \int \frac{h_0}{1+h_0} C_x^s C^s \\
&\quad - \int \frac{h_0 h_{0x}}{(1+h_0)^2} C_x^s C^s + \int \frac{C_{0x}^s}{1+h_0} h C_x^s - \int \frac{C_{0x}^s h_{0x}}{(1+h_0)^2} h C^s \\
&\quad - \int \frac{h_0 C_{0x}^s}{(1+h_0)^2} h_x C^s - \int \frac{h_0 C_{0x}^s}{(1+h_0)^2} h C_x^s + \int \frac{2h_0 h_{0x} C_{0x}^s}{(1+h_0)^3} h C^s \\
&\quad + \lambda|h|^2 + \lambda|u|^2 + \lambda|C^s|^2 - \alpha|h_{xx}|^2 - \alpha|h_x|^2 - \alpha|h|^2 \\
&\quad - \alpha|u_x|^2 - \alpha|u|^2 - \alpha|C_x^s|^2 - \alpha|C^s|^2 \\
&\geq (\delta - \alpha - \alpha K^2 \varepsilon^2) |h_{xx}|^2 + (1 - \alpha) |u_x|^2 + \left( \frac{H_0}{1+H_0} - \alpha \right) |C_x^s|^2 \\
&\quad + (\lambda - \alpha K^2 \varepsilon^{-2} - \alpha - MK\varepsilon^{-1}) |h|^2 + (\lambda - \alpha - M^2) |C^s|^2 \\
&\quad + (\lambda - \alpha) |u|^2 - (MK\varepsilon + 2\alpha K^2) |h| |h_{xx}| - 2M^2 K\varepsilon |u| |h_{xx}| \\
&\quad - (2M^2 K\varepsilon^{-1} + 2M^4) |u| |h| - 2M^2 |u| |u_x| - |h_{xx}| |u_x| \\
&\quad - M |C_x^s| |u| - M |u| |C^s| - M^2 |u_x| |C^s| - (3M^6 + M^4 K\varepsilon^{-1}) |h| |C^s| \\
&\quad - 2M^4 |C_x^s| |C^s| - 2M^4 |h| |C_x^s| - M^4 K\varepsilon |h_{xx}| |C^s| \\
&=: D
\end{aligned}$$

for some constant  $M \in \mathbb{R}$ .

We need to show that  $D \geq 0$ . This is done by converting the terms into expressions of the form  $(Ah_{xx} - Bh)^2$  and similar. Particularly interesting is the term  $-|h_{xx}||u_x|$ , which needs to be balanced by the expressions

including  $|h_{xx}|^2$  and  $|u_x|^2$ . We obtain:

$$\begin{aligned} (\delta - \alpha - \alpha K^2 \varepsilon^2) |h_{xx}|^2 + (1 - \alpha) |u_x|^2 - |h_{xx}| |u_x| &= \\ \left( \sqrt{\delta - \alpha - \alpha K^2 \varepsilon^2} |h_{xx}| - \sqrt{1 - \alpha} |u_x| \right)^2 & \\ - \left( 1 - 2\sqrt{\delta - \alpha - \alpha K^2 \varepsilon^2} \sqrt{1 - \alpha} \right) |h_{xx}| |u_x| &\geq 0 \end{aligned} \quad (3.34)$$

for the chosen  $\alpha$ .

Altogether, we obtain for some  $\bar{M} \in \mathbb{R}$ :

$$\begin{aligned} D &\geq (1 - 2\alpha) |h_{xx}|^2 + (1 - \alpha) |u_x|^2 + \frac{\tilde{H}}{2} |C_x^s|^2 \\ &\quad + (\lambda - \bar{M}) (|h|^2 + |C^s|^2 + |u|^2) - |h_{xx}| |u_x| \\ &\quad - \bar{M} \left( |h| |h_{xx}| + |u| |h_{xx}| + |u| |h| + |u| |u_x| + |C_x^s| |u| + |u| |C^s| \right. \\ &\quad \left. + |u_x| |C^s| + |h| |C^s| + |C_x^s| |C^s| + |h| |C_x^s| + |h_{xx}| |C^s| \right) \\ &\geq \left( \sqrt{\frac{3}{8}} |h_{xx}| - \sqrt{\frac{2}{3}} |u_x| \right)^2 + \left( \sqrt{6\bar{M}} |h| - \frac{1}{\sqrt{24}} |h_{xx}| \right)^2 \\ &\quad + \left( \sqrt{6\bar{M}} |u| - \frac{1}{\sqrt{24}} |h_{xx}| \right)^2 + \left( \sqrt{6\bar{M}} |C| - \frac{1}{\sqrt{24}} |h_{xx}| \right)^2 \\ &\quad + \left( \sqrt{6\bar{M}} |u| - \frac{1}{\sqrt{24}} |u_x| \right)^2 + \left( \sqrt{6\bar{M}} |C| - \frac{1}{\sqrt{24}} |u_x| \right)^2 \\ &\quad + \left( \sqrt{\frac{9}{2\tilde{H}}} \bar{M} |u| - \sqrt{\frac{\tilde{H}}{18}} |C_x| \right)^2 + \left( \sqrt{\frac{9}{2\tilde{H}}} \bar{M} |C| - \sqrt{\frac{\tilde{H}}{18}} |C_x| \right)^2 \\ &\quad + \left( \sqrt{\frac{9}{2\tilde{H}}} \bar{M} |h| - \sqrt{\frac{\tilde{H}}{18}} |C_x| \right)^2 + \left( \sqrt{\frac{\bar{M}}{2}} |h| - \sqrt{\frac{\bar{M}}{2}} |u| \right)^2 \\ &\quad + \left( \sqrt{\frac{\bar{M}}{2}} |u| - \sqrt{\frac{\bar{M}}{2}} |C| \right)^2 + \left( \sqrt{\frac{\bar{M}}{2}} |C| - \sqrt{\frac{\bar{M}}{2}} |h| \right)^2 \\ &\geq 0. \end{aligned}$$

Hence, Condition 3 is fulfilled.

**ad Condition 4.** The condition on  $\mathbf{X}_0$  follows immediately from the assumptions of the problem since  $V \subset H$ .

The condition on  $\mathbf{f}$  holds if  $((\mathbf{f}, \Phi)) < \infty$  for all  $\Phi \in V$ . This can easily be shown analogously to the proof of Condition 2.

This concludes the proof of Theorem 1.

□

**Remark** *A relatively strong regularization ( $\delta > \frac{1}{4}$ ) for  $h$  is needed in order to control the third-order term in the proof. However, this does not mean that there cannot exist a solution to the nonlinear problem if  $\delta \leq \frac{1}{4}$ , since regularizing effects may have vanished in the linearization.*

We have shown that there exists a unique solution  $\mathbf{X}$  of Problem 2 which fulfills

$$\mathbf{X} \in W(0, \Delta T; V, V').$$

Moreover, the following estimates hold:

**Theorem 3** *Let  $\mathbf{X}_0, \mathbf{X}_0^* \in H$ ,  $\mathbf{f}, \mathbf{f}^* \in L^2(V')$  and let  $\mathbf{X}$  and  $\mathbf{X}^*$  be the corresponding solutions of Problem 2. Then*

$$\|\mathbf{X} - \mathbf{X}^*\|_{L^1(H)} \leq \left( |\mathbf{X}_0 - \mathbf{X}_0^*|^2 + \frac{1}{\alpha} \|\mathbf{f} - \mathbf{f}^*\|_{L^2(V')}^2 \right)^{1/2}$$

and

$$\|\mathbf{X} - \mathbf{X}^*\|_{L^2(V)} \leq \frac{1}{\sqrt{\alpha}} \left( |\mathbf{X}_0 - \mathbf{X}_0^*|^2 + \frac{1}{\alpha} \|\mathbf{f} - \mathbf{f}^*\|_{L^2(V')}^2 \right)^{1/2}.$$

For the proof see [12].

**Remark** *Note that  $\alpha$  depends on the regularization parameter  $\delta$  as well as on the lower bound for the initial lamella thickness  $H_0$ .*

### 3.5.3 Discussion of the nonlinear problem

We have shown the existence and uniqueness of a solution to the linearized problem. In order to see in which way this may be used to obtain a similar result for the nonlinear problem, let us define the following

**Piecewise linearized problem** *Find*

$$\mathbf{X}_n = \begin{pmatrix} h_n \\ u_n \\ C_n^s \end{pmatrix} : [0, T] \rightarrow V$$

such that

$$\frac{d}{dt}((\mathbf{X}_n(\cdot), \Phi)) + a(\mathbf{X}_n(\cdot), \Phi) = ((\mathbf{f}, \Phi)),$$



holds on the interval  $[0, \frac{T}{n}]$  with

$$\mathbf{X}_n(t=0) = \mathbf{X}_0 \in V$$

for all test functions  $\Phi \in V$ , where  $a$  and  $\mathbf{f}$  are defined as in Equations (3.32) and (3.33), respectively. Moreover, on each interval  $[\frac{kT}{n}, \frac{(k+1)T}{n}]$ ,  $k = 1, \dots, n-1$ ,

$$\frac{d}{dt}((\mathbf{X}_n(\cdot), \Phi)) + a_k(\mathbf{X}_n(\cdot), \Phi) = ((\mathbf{f}_k, \Phi)),$$

holds with  $\mathbf{X}_n$  continuous in  $t = \frac{kT}{n}$ , where  $a_k$  and  $\mathbf{f}_k$  are defined similar to  $a$  and  $\mathbf{f}$  with the only difference that  $h_0$ ,  $u_0$  and  $C_0^s$  are replaced by  $h_n(\frac{kT}{n})$ ,  $u_n(\frac{kT}{n})$  and  $C_n^s(\frac{kT}{n})$ .

In other words, on each interval  $[\frac{kT}{n}, \frac{(k+1)T}{n}]$ , the linearized problem is considered, where the linearization is performed with respect to the solution of the problem on the previous interval  $[\frac{(k-1)T}{n}, \frac{kT}{n}]$  at the point  $\frac{kT}{n}$ .

A possible existence proof for the nonlinear problem could go along the following lines:

**Step 1.** Show that a solution  $\mathbf{X}_n$  of the piecewise linearized problem exists for all  $n \in \mathbb{N}$  and that  $\lim_{n \rightarrow \infty} \|\mathbf{X}_n\|$  is bounded.

**Step 2.** Show that the set of solutions  $\{\mathbf{X}_n(t), n \in \mathbb{N}\}$  is equicontinuous with respect to  $t$ . Then, using the theorem of Arzela and Ascoli (see [40]), there exists a subseries  $\mathbf{X}_{n_j}$  which converges uniformly in to some  $\mathbf{Y} \in V$ .

**Step 3.** Plug  $\mathbf{Y}$  into the nonlinear problem and show that it is a solution.

Step 1 requires certain estimates on the solution of piecewise linear problem. In this context, we state

**Proposition 1** *Let  $\mathbf{X}_0 \in H$ ,  $\mathbf{f} \in L^2(V')$  and let  $\mathbf{X}$  be the corresponding solution of Problem 2. Assume that*

$$\|\mathbf{X}(T)\| \leq (1 + C_1 T)\|\mathbf{X}_0\| + C_2 T$$

for some constants  $C_1, C_2 \in \mathbb{R}$  independent of  $\mathbf{X}$ ,  $\mathbf{X}_0$  and  $\mathbf{f}$ . Moreover, assume that if  $h_0$ ,  $u_0$ , etc. are bounded by  $\tilde{M}$ , then  $h(T)$ ,  $u(T)$ , etc. are bounded by  $\tilde{M}_2$ , where

$$\tilde{M}_2 \leq (1 + C_1 T)\tilde{M} + C_2 T.$$

Finally, assume that if  $|h_0^{-1}| < H_0^{-1}$ , then  $|h(T)^{-1}| < H_1^{-1}$  holds with

$$H_1^{-1} \leq (1 + C_1 T)H_0^{-1} + C_2 T.$$

Then for each  $n \in \mathbb{N}$ , a solution  $\mathbf{X}_n$  to the piecewise linearized problem exists, and  $\|\mathbf{X}_n\|$  is bounded for  $n \rightarrow \infty$ .

*Proof.* The result follows from the application of the discrete Gronwall lemma to  $\mathbf{X}(\frac{kT}{n})$ ,  $\tilde{M}$  and  $H_0^{-1}$ .

Unfortunately, the estimates of Theorem 3 do not satisfy the required assumptions of Proposition 1. Better estimates could not be achieved due to the difficulties arising from the third order term in connection with the nonlinearity of the problem.

## 3.6 A numerical scheme for the solution of the lamella problem

Finally, we want to solve the lamella problem numerically. In the following, we will define a numerical scheme for the solution of Problem 1. Since we are dealing with a parabolic system and assume that the flow is not convection-dominated, we will use a Galerkin finite element approach for the numerical scheme. For a detailed discussion of finite element methods and analytical results we refer to [7].

### 3.6.1 A Galerkin finite element approach

We consider wlog the one-dimensional case with  $\Pi \ll 1$ . The method can be formulated analogously for the two-dimensional problem. The problem reads:

Let  $\Omega = [0, 1]$ . Find  $\mathbf{X} = (h, u, C^s)^\top : [0, T] \times \Omega \rightarrow \mathbb{R}$ , such that

$$0 = h_t + (uh)_x + \delta h_{xxxx}, \quad (3.35)$$

$$0 = \text{Re } h(u_t + uu_x) - 4(hu_x)_x + \frac{2\text{Ma}\Sigma}{\varepsilon} C_x^s - \frac{\varepsilon}{2\text{Ca}} h h_{xxx} - h \frac{g \cdot \text{Re}}{\text{Fr}} e_{gx}, \quad (3.36)$$

$$0 = \left( \frac{2\Pi}{\varepsilon S\Lambda} + \text{Pe } h \right) (C_t^s + u C_x^s) + \frac{2\Pi}{\varepsilon S\Lambda} u_x C^s - (h C_x^s)_x \quad (3.37)$$

in  $[0, T] \times \Omega$  and

$$\mathbf{X} = \mathbf{X}_0 \quad (3.38)$$

on  $\{0\} \times \Omega$ . Moreover, the essential boundary conditions

$$0 = h_x, \quad (3.39)$$

$$0 = u \quad (3.40)$$

at  $x = 0$  and the natural boundary conditions

$$0 = h_{xxx}, \quad (3.41)$$

$$0 = C_x^s \quad (3.42)$$

at  $x = 0$ , and

$$\kappa = h_{xx}, \quad (3.43)$$

$$0 = h_{xxx}, \quad (3.44)$$

$$0 = (hu)_x, \quad (3.45)$$

$$0 = C_x^s \quad (3.46)$$

at  $x = 1$  must be fulfilled.

In order to formulate the weak problem, we have to define suitable spaces:

**Definition 7** Let  $\Omega = [0, 1]$ . Let the Sobolev space  $H^m(\Omega)$  be given analogously to Section 3.5.2 by

$$H^m(\Omega) = \{u \in L^2(\Omega); D^\alpha u \in L^2(\Omega); |\alpha| \leq m\}.$$

Then, define the spaces

$$\begin{aligned} V_h(\Omega) &= \{u \in H^2(\Omega); u_x(0) = 0\}, \\ V_u(\Omega) &= \{u \in H^1(\Omega); u(0) = 0\} \quad \text{and} \\ V_C(\Omega) &= H_1(\Omega). \end{aligned}$$

Moreover, let

$$V := V_h(\Omega) \times V_u(\Omega) \times V_C(\Omega).$$

Note that the essential boundary conditions (3.39) and (3.40) are integrated in  $V$ . We seek solutions  $\mathbf{X} : [0, T] \rightarrow V$ .

Multiplying the system (3.35) – (3.37) with a test function  $\Phi = (\phi_1, \phi_2, \phi_3)^\top \in V$  and integrating over  $\Omega$  yields the problem in weak form (applying the natural

boundary conditions):

$$\begin{aligned}
0 &= \int_0^1 h_t \phi_1 + \int_0^1 (uh)_x \phi_1 + \int_0^1 \delta h_{xxxx} \phi_1 + \int_0^1 u_t \phi_2 + \int_0^1 uu_x \phi_2 \\
&\quad - \int_0^1 \frac{4}{\text{Re}} u_{xx} \phi_2 - \int_0^1 \frac{4}{\text{Re}} \frac{h_x}{h} u_x \phi_2 + \int_0^1 \frac{2\text{Ma}\Sigma}{\varepsilon \text{Re}} \frac{C_x^s}{h} \phi_2 - \int_0^1 \frac{\varepsilon}{2\text{CaRe}} h_{xxx} \phi_2 \\
&\quad - \int_0^1 \frac{g}{\text{Fr}} e_{gx} \phi_2 + \int_0^1 C_t^s \phi_3 + \int_0^1 u C_x^s \phi_3 + \int_0^1 \frac{1}{1 + \frac{\varepsilon S \Lambda \text{Pe}}{2\Pi}} u_x C^s \phi_3 \\
&\quad - \int_0^1 \frac{(hC_x^s)_x}{\frac{2\Pi}{\varepsilon S \Lambda} + \text{Pe} h} \phi_3 \\
&= \frac{d}{dt} \int_0^1 h \phi_1 - \int_0^1 uh \phi_{1x} + u(1)h(1)\phi_1(1) + \delta \int_0^1 h_{xx} \phi_{1xx} - \delta \kappa \phi_{1x}(1) \\
&\quad + \frac{d}{dt} \int_0^1 u \phi_2 + \int_0^1 uu_x \phi_2 + \frac{4}{\text{Re}} \int_0^1 u_x \phi_{2x} + \frac{4}{\text{Re}} \frac{h_x(1)u(1)}{h(1)} \phi_2(1) \\
&\quad - \frac{4}{\text{Re}} \int_0^1 \frac{h_x}{h} u_x \phi_2 + \frac{2\text{Ma}\Sigma}{\varepsilon \text{Re}} \int_0^1 \frac{C_x^s}{h} \phi_2 + \frac{\varepsilon}{2\text{CaRe}} \int_0^1 h_{xx} \phi_{2x} - \frac{\varepsilon}{2\text{CaRe}} \kappa \phi_2(1) \\
&\quad - \frac{g}{\text{Fr}} e_{gx} \int_0^1 \phi_2 + \frac{d}{dt} \int_0^1 C^s \phi_3 + \int_0^1 u C_x^s \phi_3 + \int_0^1 \frac{1}{1 + \frac{\varepsilon S \Lambda \text{Pe}}{2\Pi}} u_x C^s \phi_3 \\
&\quad + \int_0^1 \frac{hC_x^s}{\frac{2\Pi}{\varepsilon S \Lambda} + \text{Pe} h} \phi_{3x} - \text{Pe} \int_0^1 \frac{hC_x^s h_x}{\left(\frac{2\Pi}{\varepsilon S \Lambda} + \text{Pe} h\right)^2} \phi_3 \\
&= \frac{d}{dt}(\mathbf{X}, \Phi) + F(\mathbf{X}, \Phi).
\end{aligned}$$

Thus, we can formulate the

**Weak problem** Find  $\mathbf{X} : [0, T] \rightarrow V$ , such that

$$\frac{d}{dt}(\mathbf{X}, \Phi) + F(\mathbf{X}, \Phi) = 0 \quad (3.47)$$

for all  $\Phi \in V$ , where

$$\mathbf{X}(0) = \mathbf{X}_0 \in V.$$

The corresponding finite-dimensional approximation reads:

**Finite element problem** Find  $\mathbf{X}_N : [0, T] \rightarrow V_N$ , such that

$$\frac{d}{dt}(\mathbf{X}_N, \Psi) + F(\mathbf{X}_N, \Psi) = 0 \quad (3.48)$$

for all  $\Psi \in V_N$ , where

$$\mathbf{X}_N(0) = \mathbf{X}_{N0} \in V_N.$$

$V_N$  denotes the finite-dimensional approximation space to  $V$ . There are multiple possibilities to define such a space that differ in their approximation qualities. For further information, we refer to [7]. The following is an exemplary approximation space  $V_N$  suitable for our problem.

**Remark** (3.48) is a finite-dimensional system of ordinary differential equations which can be solved using a standard ODE solver.

**Example** Define a grid

$$S_N := (0 = x_0, \dots, x_N = 1).$$

Moreover, define shape functions:

$$\psi_1 = \begin{cases} 1 + x & -1 \leq x \leq 0, \\ 1 - x & 0 < x \leq 1, \\ 0 & \text{else,} \end{cases}$$

$$\psi_{2a} = \begin{cases} (1 + x)^2(1 - 2x) & -1 \leq x \leq 0, \\ (1 - x)^2(1 + 2x) & 0 < x \leq 1, \\ 0 & \text{else,} \end{cases}$$

$$\psi_{2b} = \begin{cases} x(1 + x)^2 & -1 \leq x \leq 0, \\ x(1 - x)^2 & 0 < x \leq 1, \\ 0 & \text{else.} \end{cases}$$

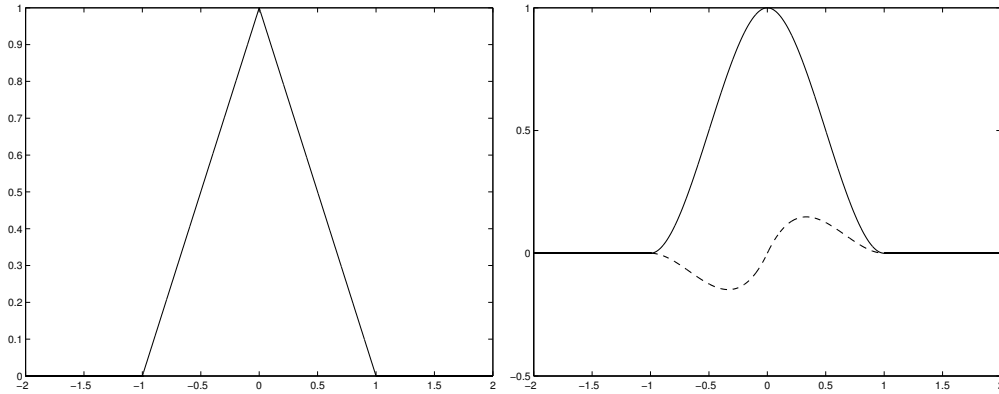


Figure 3.6: Shape functions. LEFT:  $\psi_1$ . RIGHT:  $\psi_{2a}$  (solid) and  $\psi_{2b}$  (dashed).

From these, one can easily derive functions  $\psi_{1,i}$ ,  $\psi_{2a,i}$  and  $\psi_{2b,i}$  corresponding to  $x_i$  with the following properties:

1.  $\psi_{1,i}$ ,  $\psi_{2a,i}$  and  $\psi_{2b,i}$  are compactly supported on  $[x_{i-1}, x_{i+1}]$  for all  $i = 1, \dots, N-1$ , on  $[x_0, x_1]$  for  $i = 0$  and on  $[x_{N-1}, x_N]$  for  $i = N$ .
2. The functions  $\psi_{1,i}$  fulfill

$$\psi_{1,i}(x) = \begin{cases} 1 & \text{if } x = x_i \\ 0 & \text{if } x = x_j, j \neq i. \end{cases}$$

3. For  $\psi_{2a,i}$ , the conditions

$$\begin{aligned} \psi_{2a,i}(x) &= \begin{cases} 1 & \text{if } x = x_i \\ 0 & \text{if } x = x_j, j \neq i \end{cases} \quad \text{and} \\ \psi_{2a,i,x}(x) &= 0 \quad \text{for } x = x_j, j = 1, \dots, N \end{aligned}$$

hold.

4. The functions  $\psi_{2b,i}$  have the properties

$$\begin{aligned} \psi_{2b,i}(x) &= 0 \quad \text{for } x = x_j, j = 1, \dots, N \\ \psi_{2b,i,x}(x) &= \begin{cases} 1 & \text{for } x = x_i \\ 0 & \text{for } x = x_j, j \neq i. \end{cases} \end{aligned}$$

As usual, the index  $x$  denotes the derivative with respect to  $x$ . The shape functions fulfill that  $\psi_{1,i}$  is continuous on  $\Omega = [0, 1]$  and  $\psi_{2a,i}$  and  $\psi_{2b,i}$  are continuously differentiable on  $\Omega$ .

We define the space  $V_N = V_N^h \times V_N^u \times V_N^{Cs}$  using these functions as basis, that is

$$\begin{aligned} V_N^h &= \text{span}(\Psi_{2a,i}, i = 0, \dots, N; \Psi_{2b,i}, i = 1, \dots, N), \\ V_N^u &= \text{span}(\Psi_{1,i}, i = 1, \dots, N), \\ V_N^{Cs} &= \text{span}(\Psi_{1,i}, i = 0, \dots, N). \end{aligned}$$

Then  $V_N$  is an approximation of  $V$  with the dimension  $M = 4N + 2$ .

**Remark** In the two-dimensional case, it is more difficult to define continuously differentiable basis functions. One possibility is the so-called Argyris element, which is a triangular element with basis functions that have continuous derivatives between mesh triangles. On each triangle, these functions are fifth-order polynomial with 21 degrees of freedom.

The practical computations have been done using the finite element package *Femlab*, versions 2.2 and 2.3, by *Comsol AB*, which allows the definition of nearly arbitrary PDE's. Therefore, we have split the operator and introduced the new variable  $d = \Delta h$ , such that we obtain a second order system for  $(h, d, u, v, C)^\top$ .

## 3.7 Discussion of the error

There are several sources for errors on the way from the physical model to the numerical solution. In the following, we will discuss the errors that are made at each step.

1. Basic simplifications: We consider a simplified model neglecting exterior forces and assuming the flow is controlled by the incompressible Navier-Stokes equations. Moreover, simple models are assumed for the description of the surfactant and volatile component, respectively. This first source for errors is difficult to quantify.
2. Thin film approximation: Using the ansatz  $\phi = \phi_0 + \varepsilon^2\phi_1 + \mathcal{O}(\varepsilon^4)$ , we make an error of the order  $\varepsilon^2$  since we only consider the leading order term.
3. Initial and boundary conditions: As we have discussed in Section 3.2, not all boundary conditions are straightforward. In some cases, we use approximations which is an additional error source. Moreover, the initial conditions prescribed are also approximations. A quantification of these errors is also difficult.
4. Physical parameters: Not all of the physical parameters are known.
5. Numerical approximation: This error can be controlled and estimated. It depends on the resolution of the grid and the approximation order of the basis functions.

As we can see, there are several sources for errors, and thus an estimate on the total error is obviously very difficult. Therefore, the final results of these computations must be considered with care. We mainly achieve qualitative results. However, in a real foam we are considering a large number of lamellae and are not particularly interested in the exact results for a single film. Moreover, the films obviously do not burst all at the same thickness, but we assume that this varies stochastically around a mean value. Hence, we want to obtain results in a statistical sense, i.e. compute the mean lifetime of films under given conditions.

By means of coupling the considered model with models for the foam drainage and transport of the foam, some of the errors might be reduced in future work. For example, more accurate boundary conditions could be obtained from a coupling with a model for the Plateau border, as discussed in Section 3.2. Some suggestions for such improvements are made in Chapter 5.

### 3.8 Summary

In this chapter, we have used the thin film equations derived in Chapter 2 to create a model for the dynamical behaviour of a fuel foam film. Suitable computational domains for the one- and two-dimensional problem have been determined and the equations have been equipped with conditions at the boundaries of these domains. Moreover, the physical parameters for the problem have been determined as far as they are known.

Altogether, a model has been derived that yields the thinning rate of a foam film and the time  $t_{crit}$  at which a critical thickness  $h_{crit}$  is reached. Therefore, the curvature  $\kappa$  of the Plateau border is needed as input variable by which the model can be coupled with a global foam model.

The existence and uniqueness of a solution for the linearized problem has been proven. Finally, a scheme for the numerical solution of the problem has been given.



## Chapter 4

### The limit $\varepsilon \rightarrow 0$

We have derived and analyzed a model describing the dynamics of a real thin foam film in the previous chapter. This model allows us to simulate the thinning of a lamella under the assumptions made in Section 3.1. In particular, it is required that the ratio  $\varepsilon$  between thickness and length of the lamella is small, such that the thin film approximations derived in Chapter 2 hold.

As we have discussed in Section 3.7, the approximation improves as  $\varepsilon$  decreases. On the other hand, if we consider very dry foams, the relative size of the Plateau border becomes smaller and its curvature larger. Since the crucial effects happen at the transition between lamella and Plateau border, it is important that this region is resolved very good by the numerical grid. Therefore, grid size and time step restrictions become more severe for smaller values of  $\varepsilon$ , such that the computational effort increases.

Moreover, there arise some stability issues with the solution in the case of a surfactant-stabilized lamella, which also lead to increased computational costs. We will discuss the reasons for this effect in Section 4.2.3.

However, one can make use of some special features of the film in the case of  $\varepsilon \rightarrow 0$  in order to further simplify the model. This approach is based on the splitting of the domain into regions in which some effects may be neglected such that simpler models can be derived for each subdomain. Such domain decompositions for foam lamellae have been applied before by Schwartz and Princen [34], Barigou and Davidson [3] and Braun et al. [8]. We will follow the approach of Breward [9], who divided the domain into three parts, the lamella, the Plateau border, and a matching region (or transition region) between the two (see Section 4.1).

We will shortly present this approach for the three cases of a pure liquid, a film stabilized by a surfactant and a film stabilized by the presence of a volatile

component for the inertia-free case in Section 4.2. Afterwards, we generalize the model and include inertia (Section 4.3). Finally, we are going to discuss in Section 4.4 in which way the approach may be extended to the two-dimensional problem.

## 4.1 Domain splitting approach

Consider a two-dimensional film in the  $x$ - $z$ -plane. It consists of a long lamella part with approximately spatially constant thickness and the Plateau border which has an approximately constant curvature. This can be used by splitting the film into three regions as shown in Figure 4.1. As the curvature is small in the lamella

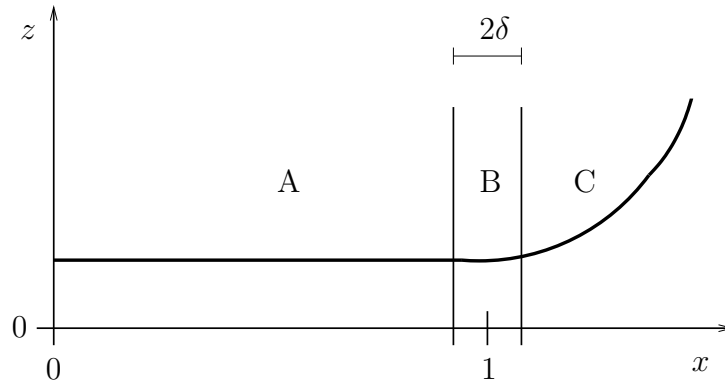


Figure 4.1: Splitting into lamella (A), Plateau border (C) and transition region (B) (sketch)

(A), we conclude that capillarity plays an inferior role there and thus can be neglected. For the Plateau border (C), capillarity is treated to be the dominant effect as discussed in Chapter 3. Since we assume that the radius of curvature in the Plateau border is of the order of the film thickness, this dominance becomes even stronger for thinner films.

In the transition region (B), the two solutions of the lamella and the Plateau border have to be matched. For the thin film approximations to be valid in the transition region, its thickness must be small compared to its length. If we assume that the length of this region is  $2\delta$  ( $2\delta L$  in dimensional variables), then this condition can be expressed in the form  $\varepsilon \ll \delta$ . Since the length of the transition region is small compared to that of the film, i.e.  $\delta \ll 1$ , this poses a more severe condition on the parameter  $\varepsilon$  than in Chapter 3, which is the reason why this approach is not used in general. A comparison between numerical results for the full problem defined in Chapter 3 and the following approximations  $\varepsilon$  will be done in Chapter 5.

The general procedure to get the solution at time  $t_i$  includes two steps (sketched for the case of a pure liquid):

1. Solve the transition region problem using the values  $h^{(i-1)}$ ,  $h_x^{(i-1)}$  and  $h_x^{(i-1)}x$  at the boundary to the lamella part from the previous time step  $i - 1$ . At the boundary to the Plateau border, the curvature  $\kappa$  obtained from the Plateau border has to be prescribed.

This yields the thickness  $h^{(i)}$  and velocity  $u^{(i)}$  in the transition region.

2. Solve the lamella problem using the velocity  $u^{(i)}$  obtained in Step 1 as boundary value.

This yields  $h^{(i)}$  and  $u^{(i)}$  in the lamella.

In the following, we will examine in detail how this idea can be implemented for the different cases. We henceforth neglect gravity and therefore assume the problem to be symmetric with respect to  $x = 0$ .

## 4.2 Inertia-free case

The cases considered in this section have been studied by Chris Breward in his dissertation [9]. We will use these examples to demonstrate the mechanisms involved in the splitting approach. Moreover, some limitations will be considered and improvements discussed. In Section 4.3, we will generalize these models by the inclusion of inertia.

### 4.2.1 General model

The general one-dimensional model including surfactant or volatile component, respectively, is given by (assuming  $\Pi \ll 1$ , see (2.71) – (2.81))

$$0 = h_t + (uh)_x + \frac{2\mathcal{E}}{\varepsilon}e, \quad (4.1)$$

$$0 = \frac{2\text{Ma}}{\varepsilon}\sigma_x + \frac{\varepsilon}{2\text{Ca}}hh_{xxx} + 4(hu_x)_x. \quad (4.2)$$

The gradient of the surface tension is computed by

$$\sigma_x = -\Sigma C_x^s, \quad (4.3)$$

$$0 = \left( \frac{2\Pi}{\varepsilon S\Lambda} + \text{Pe}h \right) (C_t^s + uC_x^s) + \frac{2\Pi}{\varepsilon S\Lambda}u_x C^s - (hC_x^s)_x \quad (4.4)$$

in the presence of a surfactant, and by

$$\sigma_x = -\widetilde{\Sigma}C_x^v, \quad (4.5)$$

$$0 = \widetilde{\text{Pe}}h(C_t^v + uC_x^v) + \frac{2\widetilde{\text{Pe}}\mathcal{E}}{\varepsilon}(1 - C^v)e - (hC_x^v)_x, \quad (4.6)$$

if the film is stabilized by a volatile component. Note that  $e \neq 0$  only holds in the latter case where evaporation plays a role. Otherwise the mass equation reduces to  $h_t + (uh)_x = 0$ .

### 4.2.2 Pure liquid

When neither surfactant nor volatile component are present, the system (4.1) – (4.6) reduces to

$$\begin{aligned} h_t + (uh)_x &= 0, \\ \frac{\varepsilon}{2\text{Ca}}hh_{xxx} + 4(hu_x)_x &= 0. \end{aligned}$$

#### Lamella

We consider the lamella region to correspond to the computational domain  $[0, 1]$ . We assume that the lamella is dominated by viscosity, i.e.  $\text{Ca} \gg \varepsilon$ , which corresponds to a high velocity scaling  $U$ . However, note that  $U$  is not uniquely determined by this condition. The governing equations are

$$h_t + (uh)_x = 0, \quad (4.7)$$

$$(hu_x)_x = 0. \quad (4.8)$$

Furthermore, we have the boundary conditions

$$u(0) = 0 \quad (\text{Symmetry}),$$

$$u(1) = u_1(t).$$

Let the lamella be initially of constant thickness, that is  $h(0, x) = h_0 = \text{const}$ . At time  $t = 0$ , the system (4.7), (4.8) reduces to

$$\begin{aligned} h_t + hu_x &= 0, \\ u_{xx} &= 0. \end{aligned} \quad (4.9)$$

This means that  $h_t$  does not depend on  $x$  at time  $t = 0$ , such that we obtain  $h_x = 0$  in the lamella for all  $t$ . If  $u_1(t)$ ,  $t \in [0, T]$  is given, this system can be solved and the solution is

$$\begin{aligned} h(t) &= h_0 e^{-\int_0^t u_1(\tau) d\tau}, \\ u(t, x) &= u_1(t)x. \end{aligned}$$

### Plateau border

It is assumed that the Plateau border is dominated by capillarity, which corresponds to a low velocity scaling. The momentum equation (4.2) simplifies to

$$h_{xxx} = 0,$$

which yields

$$h_{xx} = \kappa = \text{const.} \quad (4.10)$$

Equation (4.10) will be used as a boundary condition for the transition region problem.

### Transition region

Here, we have two scaling parameters which have to be determined, the velocity scaling  $U$  and the length scaling  $\delta$  of the transition region. These have to be chosen in such a way that capillary and viscous forces balance. Moreover, we require  $\delta$  to fulfill  $\varepsilon \ll \delta \ll 1$  according to Section 4.1.

We therefore define  $\delta := \sqrt{\varepsilon}$  and set  $U$  such that  $\text{Ca} = \delta = \sqrt{\varepsilon}$ . With  $x = 1 + \delta\xi$ , this leads to the system

$$(uh)_\xi = 0, \quad (4.11)$$

$$hh_{\xi\xi\xi} + 8(hu_\xi)_\xi = 0. \quad (4.12)$$

Note that due to the condition  $\delta \ll 1$ , the time-dependence drops out of the mass equation in leading order of  $\delta$ .

Integration of Equation (4.11) gives  $uh = Q$ , where  $Q$  is the (yet unknown) flux. Inserting this relation into (4.12) yields

$$(2hh_{\xi\xi} - h_\xi^2 - \frac{16Qh_\xi}{h})_\xi = 0. \quad (4.13)$$

Furthermore, we have given boundary conditions

$$\begin{aligned} h &\rightarrow h_L, \quad h_\xi \rightarrow 0, \quad h_{\xi\xi} \rightarrow 0 \quad \text{for } \xi \rightarrow -\infty, \\ h_{\xi\xi} &\rightarrow \delta^2\kappa \quad \text{for } \xi \rightarrow \infty. \end{aligned}$$

Using these, we can integrate Equation (4.13) once and obtain

$$2hh_{\xi\xi} - h_\xi^2 - \frac{16Qh_\xi}{h} = 0.$$

The analytical solution to this equation reads

$$\begin{aligned} \xi - C_2 &= \frac{2}{C_1} \sqrt{h} + \frac{2Q^{1/3}12^{2/3}}{9C_1^{4/3}} \ln \left( \sqrt{h} - \frac{Q^{1/3}16^{1/3}}{3^{1/3}C_1^{1/3}} \right) \\ &\quad - \frac{Q^{1/3}12^{2/3}}{9C_1^{4/3}} \ln \left( h + \frac{2Q^{1/3}18^{1/3}}{3C_1^{1/3}} \sqrt{h} + \frac{16^{2/3}Q^{2/3}}{3^{2/3}C_1^{2/3}} \right) \\ &\quad - \frac{2Q^{1/3}4^{2/3}3^{1/6}}{3C_1^{4/3}} \arctan \left( \frac{\sqrt{h}C_1^{1/3}}{2^{1/3}3^{1/6}Q^{1/3}} + \frac{1}{\sqrt{3}} \right). \end{aligned} \quad (4.14)$$

In this expression, there are still the unknown parameters  $C_1$ ,  $C_2$  and  $Q$ . We may set  $C_2 = 0$  due to translational invariance (the equation is autonomous).

In the limit  $\xi \rightarrow \infty$ , we obtain in leading order of  $\zeta = \xi^{-1}$

$$\frac{2}{C_1} \sqrt{h} = \xi,$$

since  $h$  has a quadratic behaviour in this limit due to the condition  $h_{\xi\xi} \rightarrow \delta^2\kappa$ . Using the latter, we obtain

$$C_1 = \sqrt{2\delta^2\kappa}.$$

In the limit  $\xi \rightarrow -\infty$ , the solution needs to fulfill the condition  $h \rightarrow h_L$ . The left hand side needs to be balanced by at least one of the terms on the right hand side, hence we analyze (4.14) under this aspect:

- $\sqrt{h}$  tends to a constant value and does not play a role for  $\xi \rightarrow -\infty$ .
- $\ln \left( \sqrt{h} - \frac{Q^{1/3}16^{1/3}}{3^{1/3}C_1^{1/3}} \right)$  tends to  $-\infty$  if the argument tends to zero. Hence, this term may balance  $\xi$  for  $\xi \rightarrow -\infty$ .
- $-\ln \left( h + \frac{2Q^{1/3}18^{1/3}}{3C_1^{1/3}} \sqrt{h} + \frac{16^{2/3}Q^{2/3}}{3^{2/3}C_1^{2/3}} \right)$  tends to a constant value since the argument tends to a positive constant.
- $\arctan(\cdot)$  is a bounded function.

Thus, the behaviour of the linear term on the left hand side can only be balanced by the second term on the left hand side, and only if

$$\sqrt{h} - \frac{Q^{1/3}16^{1/3}}{3^{1/3}C_1^{1/3}} \rightarrow 0 \quad \text{for } \xi \rightarrow -\infty.$$

This condition becomes

$$Q = \frac{3\sqrt{2\delta^2\kappa}}{16}h_L^{3/2},$$

which constitutes a relation between the lamella thickness  $h_L$  and the flow velocity  $u_L$  in the lamella limit by

$$u_L = \frac{3\sqrt{2\delta^2\kappa}}{16}h_L^{1/2}. \quad (4.15)$$

This velocity  $u_L$  is used as boundary condition for the lamella problem, which can then be solved for  $h$ .

Figure 4.2 shows the solution for  $h$  in the transition region for  $h_L = 1$  and  $\delta^2\kappa = 1$ .

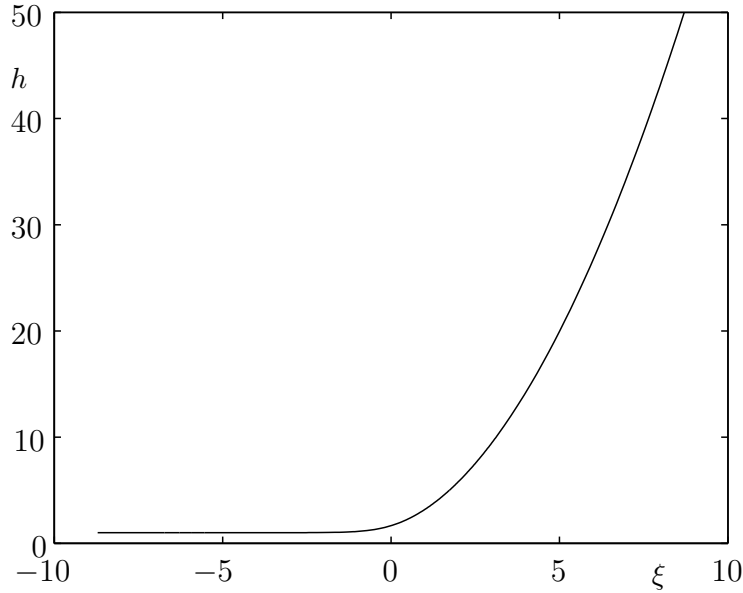


Figure 4.2: Film thickness in the transitions region for a pure liquid.

### Computation of the lamella thickness

Relation (4.15) yields the value of  $u_1$  by

$$u_1(t) = \frac{3\sqrt{2\delta^2\kappa}}{16}h(t)^{1/2}.$$

The velocity profile becomes

$$u(t, x) = \frac{3\sqrt{2\delta^2\kappa}}{16}h(t)^{1/2}x.$$

Plugging this into (4.9) yields

$$h_t + \frac{3\sqrt{2\delta^2\kappa}}{16}h^{3/2} = 0.$$

This ordinary differential equation (ODE) can be solved explicitly and we obtain

$$h(t) = \left( \frac{3\sqrt{2\delta^2\kappa}}{32}t + \frac{1}{\sqrt{h(0)}} \right)^{-2}. \quad (4.16)$$

Such a solution for  $h(0) = 1$  and  $\delta^2\kappa = 1$  is illustrated in Figure 4.3.

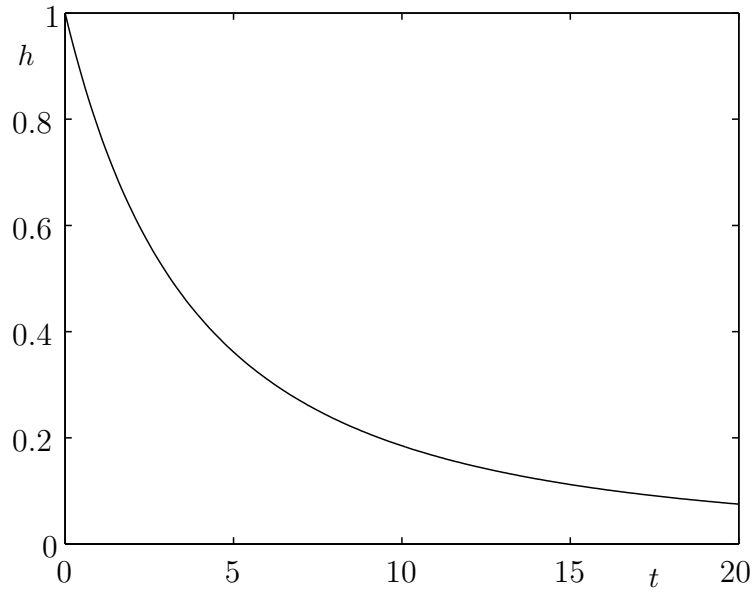


Figure 4.3: Film thickness vs. time in the lamella for a pure liquid.

### 4.2.3 Presence of a surfactant

In [9], viscosity is neglected in the presence of a surfactant and only Marangoni and capillary effects are regarded in the momentum equation. Therefore, the system (4.1) – (4.6) becomes

$$\begin{aligned} 0 &= h_t + (uh)_x, \\ 0 &= -\frac{2\text{Ma}\Sigma}{\varepsilon}C_x^s + \frac{\varepsilon}{2\text{Ca}}hh_{xxx}, \\ 0 &= \left(2\frac{\Pi}{\varepsilon S\Lambda} + \text{Pe}h\right)(C_t^s + uC_x^s) + \frac{2\Pi}{\varepsilon S\Lambda}u_x C^s - (hC_x^s)_x. \end{aligned}$$



We assume that the Plateau border is governed by capillary forces, such that we obtain the condition of constant curvature  $\kappa$  at this end of the transition region.

### Lamella model

The Marangoni effect is assumed to be dominant in the lamella. This relates to a low velocity scaling, but as in the previous case, it is not uniquely determined by this condition. The lamella model becomes

$$0 = h_t + (uh)_x, \quad (4.17)$$

$$0 = C_x^s, \quad (4.18)$$

$$0 = (1 + \mathcal{P}h) C_t^s + u_x C^s, \quad (4.19)$$

where  $\mathcal{P} = \frac{\varepsilon \text{PeSA}}{2\Pi}$  is of order  $\mathcal{O}(1)$ . Note that  $\mathcal{P}$  does not depend on the velocity scaling  $U$ .

We consider an initially constant thickness  $h(0, x) = h_0 = \text{const}$  in the lamella and find that

$$u_x(0, x) = - (1 + \mathcal{P}h_0) \frac{C_t^s(0)}{C^s(0)}$$

is independent of  $x$ . Hence,  $h_x(t, x) = 0$  for all  $t, x$ . We can compute the solution for the thickness as in the case without surfactant by

$$h(t) = h_0 e^{-\int_0^t u_1(\tau) d\tau}$$

if we know the velocity  $u_1(t)$  at the boundary ( $x = 1$ ).

Moreover, the combination of (4.17) and (4.19) yields

$$(1 + \mathcal{P}h)^{-1} \frac{h_t}{h} = \frac{C_t^s}{C^s}.$$

We solve this for  $C^s$ :

$$C^s = \frac{C_0^s (1 + \mathcal{P}h_0) h}{h_0 (1 + \mathcal{P}h)}.$$

$C_0^s = C^s(0)$  is the (constant) concentration at time  $t = 0$ . Thus,  $h$  and  $u$  are obtained independently from  $C^s$ , which is then computed from  $h$ .

### Transition region

We have to match Marangoni and capillary forces in the transition region. Since the velocity scaling  $U$  does not influence the relative magnitudes of these two,

we match them via the length scaling  $x = 1 + \delta\xi$ . Therefore, we choose  $\delta$  in such a way that  $\varepsilon^2 = 4\delta^2\text{CaMa}\Sigma$ . For the surfactant equation, it is assumed that diffusion, bulk convection and surface convection balance, which determines the velocity scaling by setting  $S = \frac{\delta\Pi}{\varepsilon\Lambda}$ . Hence, the velocity and length scalings are uniquely determined and we obtain in leading order of  $\delta$

$$\begin{aligned} uh &= Q, \\ C_\xi^s &= hh_{\xi\xi\xi}, \\ (uC^s)_\xi + \mathcal{P}uhC_\xi^s &= (hC_\xi^s)_\xi. \end{aligned}$$

Using  $u = Q/h$  and integrating the latter two equations, this system simplifies to

$$C^s - C_L^s = hh_{\xi\xi} - \frac{h_\xi^2}{2}, \quad (4.20)$$

$$hC_\xi^s = Q \left( \frac{C^s}{h} - \frac{C_L^s}{h_L} \right) + \mathcal{P}Q(C^s - C_L^s), \quad (4.21)$$

where  $h_L$  and  $C_L^s$  are the values of thickness and surfactant concentration, respectively, in the lamella.

We want to solve this problem such that the boundary conditions

$$\begin{aligned} C^s \rightarrow C_L^s, \quad h \rightarrow h_L, \quad h_\xi \rightarrow 0, \quad h_{\xi\xi} \rightarrow 0 \quad \text{for } \xi \rightarrow -\infty, \\ C^s \rightarrow C_{PB}^s, \quad h_{\xi\xi} \rightarrow \delta^2\kappa \quad \text{for } \xi \rightarrow \infty \end{aligned}$$

are fulfilled.

An asymptotic analysis for the limit  $\xi \rightarrow \infty$  yields (using translational invariance of the solution)

$$h = \frac{\delta^2\kappa}{2}\xi^2 + \frac{C_{PB}^s - C_L^s}{\delta^2\kappa} + \mathcal{O}(\xi^{-1}), \quad (4.22)$$

$$C^s = C_{PB}^s + \mathcal{O}(\xi^{-1}). \quad (4.23)$$

At the lamella side ( $\xi \rightarrow -\infty$ ) we make the ansatz

$$h = h_L + \alpha e^{\lambda\xi} + \mathcal{O}(e^{2\lambda\xi}),$$

$\lambda \in \mathbb{C}$ , in order to model the asymptotically constant behaviour. Plugging this into Equation (4.20), we obtain

$$C^s = C_L^s + h_L\alpha\lambda^2 e^{\lambda\xi} + \mathcal{O}(e^{2\lambda\xi}).$$

From (4.21) follows an equation for  $\lambda$ , namely

$$\lambda^3 - \lambda^2 \left( \frac{Q}{h_L^2} + \frac{\mathcal{P}Q}{h_L} \right) + \frac{QC_L}{h_L^4} = 0.$$

Assuming positive flux, i.e. liquid flows from the lamella into the Plateau border, this equation can be rewritten as

$$\lambda^3 - q\lambda^2 + p = 0,$$

with positive parameters  $p$  and  $q$ . This equation has one negative real root  $\lambda^*$  and two roots  $\lambda_1$  and  $\lambda_2$  with positive real parts. The condition for  $\xi \rightarrow -\infty$  dictates that the non-decaying mode  $\lambda^*$  vanishes, thus the solution in leading order is given by

$$h = h_L + \alpha e^{\lambda_1 \xi} + \beta e^{\lambda_2 \xi}, \quad (4.24)$$

$$C^s = C_L + \alpha \lambda_1^2 e^{\lambda_1 \xi} + \beta \lambda_2^2 e^{\lambda_2 \xi}. \quad (4.25)$$

Note that there are three degrees of freedom ( $\alpha$ ,  $\beta$  and  $Q$ ) in total for the third-order system of ODE's. In Section 4.2.4, the case of a third-order system with only two degrees of freedom occurs. Such a system is not solvable in general.

### Computation of a solution

We want to obtain a relation  $Q(h_L)$  between the flux  $Q$  in the transition region and the thickness  $h_L$  of the lamella. Then, the velocity profile in the lamella is given by  $u = \frac{Q(h)}{h}x$  and the thickness can be computed by solving

$$h_t + Q(h) = 0 \quad (4.26)$$

as in Section 4.2.2.

Hence, we need to find a numerical solution for the system (4.20), (4.21). However, there are several difficulties that arise:

- The system is defined on the unbounded domain  $\mathbb{R}$ . For practical computations, the computational domain  $[-\frac{1}{\varepsilon}, \frac{1}{\varepsilon}]$  is used.
- We are dealing with a boundary value problem (BVP), i.e. boundary values are given at both ends of the domain. In [9], the problem is solved using a simple shooting algorithm: a solution is computed starting from  $\xi = \frac{1}{\varepsilon}$  for some flux  $Q$ , then  $Q$  is varied until the desired behaviour of the solution at  $x = -\frac{1}{\varepsilon}$  is achieved.

However, the solution contains an unstable mode  $\lambda^*$ . Hence, the numerical solution of the ODE becomes unstable. Instead, we use a multiple shooting algorithm. The main idea behind this approach is the following: numerical errors due to machine precision increase exponentially for an unstable mode, hence this error becomes dominant for large domains. If the

computational domain is divided into smaller intervals and the differential equation is solved on each of these intervals, this error can be controlled by varying the size of the intervals. In order to solve the complete problem, transfer conditions between the intervals have to be fulfilled in addition to the boundary conditions. A detailed discussion of BVP's and the multiple shooting method can be found in [2].

Finally, we can solve the system in order to obtain the flux  $Q$  for each value of  $h_L$ , which is used to solve Equation (4.26). Some results for this approach will be discussed in Chapter 5.

#### 4.2.4 Presence of a volatile component

In [9], a model is given for a liquid in the presence of a volatile component. However, the resulting third order system of ODE's has only two degrees of freedom, such that a solution does not exist in general. We present an improved model with included viscosity that overcomes these difficulties. The relevant part of (4.1) – (4.6) is

$$0 = h_t + (uh)_x + \frac{2\mathcal{E}e}{\varepsilon}, \quad (4.27)$$

$$0 = -\frac{2\text{Ma}\tilde{\Sigma}}{\varepsilon}C_x^v + \frac{\varepsilon}{2\text{Ca}}hh_{xxx} + 4(hu_x)_x, \quad (4.28)$$

$$0 = \tilde{\text{Pe}}h(C_t^v + uC_x^v) + \frac{2\tilde{\text{Pe}}\mathcal{E}}{\varepsilon}(1 - C^v)e - (hC_x^v)_x. \quad (4.29)$$

This system is very similar to the surfactant case.

**Remark** *Apart from the inclusion of viscosity, we also take a different approach for the modelling of the evaporation process. We assume a constant evaporation  $e$ , while Breward uses a model in which  $e$  is proportional to the concentration of the volatile component.*

#### Lamella model

Evaporation must enter Equation (4.29) in leading order to have a stabilizing effect. We balance it by convection, which gives the velocity scaling  $U$  by setting  $2\mathcal{E} = \varepsilon$ . As in the surfactant case, the momentum equation (4.28) is considered to be dominated by the Marangoni force. This yields the equations

$$0 = h_t + (uh)_x + e, \quad (4.30)$$

$$0 = C_x^v, \quad (4.31)$$

$$0 = hC_t^v + (1 - C^v)e. \quad (4.32)$$

From Equations (4.31) and (4.32) follows  $h_x = 0$  for all  $t$ . Together with (4.30), we obtain  $u_{xx} = 0$ , such that the velocity profile is determined by its value at  $x = 1$  which can be obtained from the transition region as in Section 4.2.3. Therefore, we seek a relation  $Q(h)$  from the solution of the transition region model.

### Transition region

We match Marangoni and capillary forces in the momentum equation, scaling the length by  $x = 1 + \delta\xi$  where  $\varepsilon^2 = 4\delta^2\text{CaMa}\tilde{\Sigma}$ .

The velocity scaling has already been fixed by  $2\mathcal{E} = \varepsilon$ . Hence, there are three possible scenarios about which forces govern the equation for the volatile component:

- Convection is dominant in the transition region. This leads to  $C^v = \text{const}$ , such that the Marangoni effect plays no role and the film is not stabilized.
- The transition region is governed by diffusion. In this case  $hC_\xi^v = \text{const}$  and with the condition for  $\xi \rightarrow -\infty$  we obtain again  $C^v = \text{const}$ .
- The only scenario for which we obtain a non-trivial solution for  $C^v$  is a balance of convection and diffusion. Thus, we are only interested in this case.

Hence, we assume that the equation for the volatile component is governed by diffusion and convection and obtain the system

$$\begin{aligned} uh &= Q, \\ C_\xi^v &= hh_{\xi\xi\xi} + \frac{2\delta\text{Ca}}{\varepsilon}(hu_\xi)_\xi, \\ \tilde{\mathcal{P}}uhC_\xi^v &= (hC_\xi^v)_\xi, \end{aligned}$$

where  $\tilde{\mathcal{P}} = \delta\tilde{\text{Pe}}$ .

The momentum equation is integrated and  $u$  replaced by  $\frac{Q}{h}$ , such that the system simplifies to

$$C^v - C_L^v = hh_{\xi\xi} - \frac{h_\xi^2}{2} - \nu Q \frac{h_\xi}{h}, \quad (4.33)$$

$$hC_\xi^v = \tilde{\mathcal{P}}Q(C^v - C_L^v). \quad (4.34)$$

As before,  $h_L$  and  $C_L^v$  denote the values of thickness and concentration of the volatile component in the lamella, and  $\nu := \frac{2\delta\text{Ca}}{\varepsilon}$ .

We have the same boundary conditions as in the surfactant case, namely

$$\begin{aligned} C^v &\rightarrow C_L^v, \quad h \rightarrow h_L \quad \text{for } \xi \rightarrow -\infty \\ C^v &\rightarrow C_{PB}^v, \quad h_{\xi\xi} \rightarrow \delta^2\kappa \quad \text{for } \xi \rightarrow \infty. \end{aligned}$$

An asymptotic analysis for the limit  $\xi \rightarrow \infty$  yields

$$\begin{aligned} h &= \frac{\delta^2\kappa}{2}\xi^2 + \frac{C_{PB}^v - C_L^v}{\delta^2\kappa} + \mathcal{O}(\xi^{-1}), \\ C^v &= C_{PB}^v + \mathcal{O}(\xi^{-1}). \end{aligned}$$

For  $\xi \rightarrow -\infty$  we make the ansatz

$$h = h_L + \alpha e^{\lambda\xi} + \mathcal{O}(e^{2\lambda\xi}),$$

which yields with (4.33)

$$C^v = C_L^v + \left( h_L \alpha \lambda^2 - \frac{\alpha \nu \lambda Q}{h_L} \right) e^{\lambda\xi} + \mathcal{O}(e^{2\lambda\xi}).$$

Plugging these expressions into Equation (4.34), we obtain

$$\lambda^3 - \lambda^2 \left( \frac{\tilde{\mathcal{P}}Q}{h_L} + \frac{\nu Q}{h_L^2} \right) + \frac{\nu \tilde{\mathcal{P}}Q^2}{h_L^3} = 0.$$

This equation has the solutions

$$\lambda_1 = 0, \quad \lambda_2 = \frac{\tilde{\mathcal{P}}Q}{h_L}, \quad \lambda_3 = \frac{\nu Q}{h_L^2}.$$

For non-vanishing viscosity (that is  $\nu > 0$ ), we have two positive eigenmodes  $\lambda_2$  and  $\lambda_3$ , such that together with  $Q$ , the system has three degrees of freedom. Moreover, we obtain stability for  $\xi \rightarrow -\infty$ .

This marks a difference to the model derived in [9], where viscosity is neglected, i.e.  $\nu = 0$ . In that case, two of the eigenmodes become zero. Hence, only two degrees of freedom ( $\lambda_2$  and  $Q$ ) are left in the third-order system, which is in general not sufficient to obtain a solution.

In order to solve the film-thinning problem, we proceed analogously to the case of a film stabilized by a surfactant, i.e. we use a shooting algorithm to obtain the flux  $Q$  from the system (4.33), (4.34), which yields the boundary condition for the velocity  $u$  in the lamella problem. With this information, the evolution of  $h$ ,  $u$  and  $C^v$  in the lamella can be computed.

### 4.3 Non-planar lamella

One of the central assumptions in Section 4.2 is that inertia can be completely neglected. However, our considerations in Section 2.3 showed that this is in general not justifiable in our problem. We will observe that the inclusion of inertia leads to a non-constant lamella thickness  $h(t, x)$ , which is a major difference to the previous models. In particular, the transition region model of Section 4.2 explicitly uses the fact that the lamella has spatially constant thickness. Hence, it is no longer valid as we will see in Section 4.3.2.

For these reasons, we develop a more general splitting approach in Section 4.3.2, which can be applied for arbitrary lamella profiles. Subsequently, we discuss the solutions for our three cases (pure liquid, surfactant, volatile component) applying this new approach for the transition region and a more complex lamella model.

#### 4.3.1 Governing equations

The model equations for mass and momentum conservation including inertia are

$$0 = h_t + (uh)_x + \frac{2\mathcal{E}}{\varepsilon}e, \quad (4.35)$$

$$0 = \frac{2\text{Ma}}{\varepsilon}\sigma_x + \frac{\varepsilon}{2\text{Ca}}hh_{xxx} - \text{Re} h(u_t + uu_x) + 4(hu_x)_x. \quad (4.36)$$

For a pure liquid,  $\sigma$  is constant. If a surfactant is present, then it is described by

$$\sigma_x = -\Sigma C_x^s, \quad (4.37)$$

$$0 = \left( \frac{2\Pi}{\varepsilon S\Lambda} + \text{Pe} h \right) (C_t^s + uC_x^s) + \frac{2\Pi}{\varepsilon S\Lambda} u_x C^s - (hC_x^s)_x. \quad (4.38)$$

Similarly, for the volatile component the following equations hold:

$$\sigma_x = -\widetilde{\Sigma} C_x^v, \quad (4.39)$$

$$0 = \widetilde{\text{Pe}} h (C_t^v + uC_x^v) + \frac{2\widetilde{\text{Pe}}\mathcal{E}}{\varepsilon}(1 - C^v)e - (hC_x^v)_x. \quad (4.40)$$

#### 4.3.2 Generalized splitting approach

Let us analyze the effect of inertia on the lamella. While viscosity causes a levelling of differences in the flow, inertia has the opposite effect, i.e. it tries to

keep the flow in its current state. Hence, the capillary suction from the Plateau border does not affect the whole lamella uniformly, since it is not dominated by viscosity alone, such that a contraction forms at the transition between lamella and Plateau border.

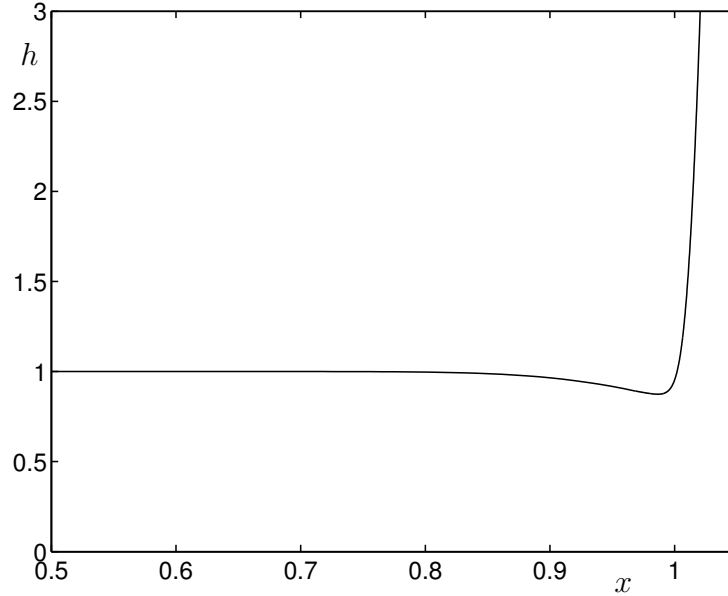


Figure 4.4: Formation of a contraction due to inertia.

In which way does this influence the model for the transition region? In Section 4.1, we had the boundary conditions  $h \rightarrow h_0$ ,  $h_\xi \rightarrow 0$  and  $h_{\xi\xi} \rightarrow 0$  for  $\xi \rightarrow -\infty$ . These conditions do not hold anymore, as the lamella thickness is not constant.

One possibility is to neglect this and proceed as in Section 4.2 anyway, matching only the thickness  $h$  in the transition region. However, we will take a more sophisticated approach and additionally match the derivative  $h_\xi$ . Obviously, we cannot match both  $h$  and  $h_\xi$  for  $\xi \rightarrow -\infty$ , but have to do this at some given point. Hence, we split the computational domain into a lamella part  $I_1 = [0, 1 - \delta]$  and a transition region  $I_2 = [1 - \delta, 1 + \delta]$ , where we demand that  $h$ ,  $h_x$ , and  $u$  are continuous at  $1 - \delta$ .

### 4.3.3 Pure liquid

We start with the simplest case of a pure liquid governed by capillary, viscous and inertial forces. We assume that capillary forces are negligible in the lamella and dominant in the Plateau border.



### Lamella

Inertia and viscosity balance in the lamella, hence the velocity scaling is determined by  $\text{Re} = \mathcal{O}(1)$ , while  $\text{Ca} \gg \varepsilon$ . The resulting system is

$$h_t + (uh)_x = 0, \quad (4.41)$$

$$\text{Re} h(u_t + uu_x) = 4(hu_x)_x. \quad (4.42)$$

Let us assume as in the inertia-free case that the lamella has a constant thickness initially. Then at time  $t = 0$  the system becomes:

$$h_t + hu_x = 0,$$

$$\text{Re}(u_t + uu_x) = 4u_{xx}.$$

Contrary to Section 4.2,  $u_{xx} \neq 0$  in general, such that  $h$  does not remain spatially constant. Hence, the full system (4.41), (4.42) must be solved. This is done using a simple finite difference method unwinding  $h$ .

### Transition region

We scale the length of the transition region in such a way that capillary and viscous forces balance, i.e. we define  $\delta$  such that  $\frac{\varepsilon}{\delta \text{Ca}} = 1$  and let  $x = 1 + \delta\xi$ . Instead of computing a solution on  $(-\infty, \infty)$  for a given behaviour for  $\xi \rightarrow \pm\infty$ , we now consider the interval  $[-1, 1]$  and demand transfer conditions at the boundaries. For the given scalings, we obtain

$$\delta u_t + (uh)_\xi = 0,$$

$$\frac{1}{2} h h_{\xi\xi\xi} - \delta \text{Re} h(\delta u_t + uu_x) + 4(hu_\xi)_\xi = 0.$$

In leading order of  $\delta$ , the inertia term vanishes and we get

$$uh = Q,$$

$$h h_{\xi\xi\xi} + 8(hu_\xi)_\xi = 0.$$

The boundary conditions that we associate with this system are

$$h, h_\xi \quad \text{at } \xi = -1,$$

$$h_\xi, h_{\xi\xi} \quad \text{at } \xi = 1.$$

The values at  $\xi = -1$  are obtained from the lamella problem, where we have to take into account that  $h_\xi = \delta h_x$ . We assume that  $h_{\xi\xi}(-1) = \delta^2 h_{Lxx}(1 - \delta)$  is small and can be neglected, where  $h_L$  is the solution in the lamella. At  $\xi = 1$ , we prescribe the curvature  $h_{\xi\xi}(1) = \delta^2 \kappa$  as well as  $h_\xi(1) = \delta^2 \kappa \cdot 1$ .

We can integrate the second equation once which gives

$$hh_{\xi\xi} - \frac{h_\xi^2}{2} - \frac{Qh_\xi}{h} = -\frac{h_\xi^2(-1)}{2} - \frac{Qh_\xi(-1)}{h(-1)} =: K. \quad (4.43)$$

Note that we have a non-zero right hand side  $K$  if  $h_\xi(-1) \neq 0$ . In this case, we do no longer obtain an analytic solution, but use a multiple shooting algorithm to solve the system for the flux  $Q$ .

A lower bound for the flux  $Q$  can be found by considering the initial value problem starting at  $\xi = -1$  for given values  $h(-1)$ ,  $h_\xi(-1)$  and  $h_{\xi\xi}(-1) = 0$ . As discussed in Section 4.3.2, we are interested in the case  $h > 0$ ,  $h_\xi(-1) \leq 0$ . Since we assume a quadratic behaviour for  $x \rightarrow \infty$ , the thickness  $h$  must have a minimum at a point  $\tilde{\xi} > -1$ , that is  $h_\xi(\tilde{\xi}) = 0$  and  $h_{\xi\xi}(\tilde{\xi}) \geq 0$ . Plugging these expressions into Equation (4.43), we obtain

$$K = h(\tilde{\xi})h_{\xi\xi}(\tilde{\xi}) \geq 0.$$

Thus, any solution must fulfill

$$Q \geq -\frac{h(-1)h_\xi(-1)}{2}.$$

### 4.3.4 Presence of a surfactant

#### Lamella

We assume that inertia enters the lamella problem in leading order and is balanced by the Marangoni force. This determines the velocity scaling by setting  $\frac{2Ma\Sigma}{\varepsilon} = \text{Re}$ . Moreover, we assume that the surfactant is dominated by convection, such that we obtain

$$\begin{aligned} 0 &= h_t + (uh)_x, \\ 0 &= C_x^s + h(u_t + uu_x), \\ 0 &= (1 + \mathcal{P}h)(C_t^s + uC_x^s) + u_x C^s, \end{aligned}$$

where  $\mathcal{P} = \frac{\varepsilon \text{Pe} S \Lambda}{2\Pi}$ . This is a hyperbolic system for the unknowns  $h$ ,  $u$  and  $C$  with the characteristic velocities  $\lambda_1 = u$ ,  $\lambda_{2/3} = u \pm \sqrt{f_1 f_2}$ , where  $f_1 = \frac{1}{h}$  and  $f_2 = \frac{C}{1 + \mathcal{P}h}$ . The corresponding characteristic variables are  $w_1 = u$ ,  $w_2 = u + C\sqrt{\frac{f_1}{f_2}}$  and  $w_3 = u - C\sqrt{\frac{f_1}{f_2}}$ .

If these velocities are all positive, we are dealing with a supersonic flow and no information can be prescribed at the right hand side of the lamella ( $x = 1 - \delta$ ).

Since we assume that the capillary suction from the Plateau border is the main effect responsible for the lamella thinning, this case bears no physical relevance, as the curvature of the lamella does not influence the lamella model at all.

If  $\lambda_3$  is negative, i.e. in the sub-sonic case, we have to prescribe a condition for  $w_3$  at  $(x = 1)$ . In characteristic variables, the three equations decouple and can be easily solved.

### Transition region

We scale the transition region with  $x = 1 + \delta\xi$ , where  $\delta$  is chosen in such a way that capillary forces enter the momentum equation in leading order, that is  $\varepsilon^2 = 4\delta^2\text{CaMa}\Sigma$ . Then we obtain

$$\begin{aligned} uh &= Q, \\ C_\xi^s + \frac{2\text{CaRe}\delta^2}{\varepsilon} h u u_\xi &= h h_{\xi\xi\xi}, \\ (uC^s)_\xi + \mathcal{P} u h C_\xi^s &= (hC_\xi^s)_\xi. \end{aligned}$$

Replacing  $u$  by  $Q/h$  and integrating, this becomes

$$\begin{aligned} h h_{\xi\xi} - \frac{h_\xi^2}{2} + \frac{h_\xi(-1)^2}{2} &= C^s - C^s(-1) + \frac{2\text{CaRe}\delta^2}{\varepsilon} Q^2 \left( \frac{1}{h} - \frac{1}{h(-1)} \right), \\ h C_\xi^s &= Q \left( \frac{C^s}{h} - \frac{C^s(-1)}{h(-1)} \right) + \mathcal{P} Q (C^s - C^s(-1)). \end{aligned}$$

This system is then solved as in Section 4.3.3

### Computation of a solution

We have to take into account that we are using the variables  $h$ ,  $u$  and  $C^s$  in the transition region, but the characteristic variables  $w_1$ ,  $w_2$  and  $w_3$  in the lamella. Hence, at each time step  $t_i$  we compute the solution by the algorithm:

1. Given  $h^{i-1}$ ,  $u^{i-1}$ ,  $C^{s,i-1}$ ,  $w_1^{i-1}$ ,  $w_2^{i-1}$  and  $w_3^{i-1}$  at time step  $t = t_{i-1}$  in the lamella and in the transition region.
2. Compute  $w_1^i$ ,  $w_2^i$  and  $w_3^i$  at  $t = t_i$  in the lamella using the boundary value  $w_3^{i-1}$  from the transition region at  $x = 1 - \delta$ .
3. Compute the corresponding solutions for  $h^i$ ,  $u^i$  and  $C^{s,i}$  in the lamella.

4. Compute  $h^i$ ,  $u^i$  and  $C^{s,i}$  in the transition region using the boundary values  $h^i$ ,  $h_\xi^i$ ,  $h_{\xi\xi}^i$  and  $C^{s,i}$  obtained from the lamella problem at  $\xi = -1$ .
5. Compute the corresponding solutions for  $w_1^i$ ,  $w_2^i$  and  $w_3^i$  in the transition region.

### 4.3.5 Presence of a volatile component

#### Lamella

We consider two different cases:

1. Inertial and Marangoni forces balance in the lamella. Thus, the velocity scaling is determined by  $\frac{2\text{Ma}\Sigma}{\varepsilon} = \text{Re}$ , which leads to the system

$$\begin{aligned} 0 &= h_t + (uh)_x + \frac{2\mathcal{E}}{\varepsilon}e, \\ 0 &= C_x^v + h(u_t + uu_x), \\ 0 &= h(C_t^v + uC_x^v) + \frac{2\mathcal{E}}{\varepsilon}(1 - C^v)e. \end{aligned}$$

As in the surfactant case (Section 4.3.4), this system is hyperbolic. However, all characteristic velocities are equal here, namely  $\lambda_i = u$  for  $i = 1, 2, 3$ . Hence, no information travels from the transition region to the lamella.

We deduce that this is not an appropriate model for the description of a real foam film, and that inertia does not play a role in this limit.

2. However, we are still interested in the case where no inertia is involved, but the lamella thickness is not constant initially. In order to obtain a closed model for this case, we have to advance to the next order of Equations (4.36) and (4.40) and get

$$\begin{aligned} 0 &= h_t + (uh)_x + \frac{2\mathcal{E}}{\varepsilon}e, \\ 0 &= C_x^v, \\ 0 &= hC_t^v + \frac{2\mathcal{E}}{\varepsilon}e(1 - C^v), \\ 0 &= \text{Re} h(u_t + uu_x) + \frac{2\text{Ma}\Sigma}{\varepsilon}C_{1x}^v - 4(hu_x)_x, \\ 0 &= C_{1t}^v + uC_{1x}^v. \end{aligned}$$

This system is then solved for  $h$ ,  $u$ ,  $C^v$  and  $C_1^v$ .

### Transition region

We have to solve the same system of equations as in Section 4.2.4, that is

$$\begin{aligned} uh &= Q, \\ C_\xi^v &= hh_{\xi\xi\xi} + \nu(hu_\xi)_\xi, \\ \tilde{\mathcal{P}}uhC_\xi^v &= (hC_\xi^v)_\xi. \end{aligned}$$

As in Section 4.3.3, this system is solved on the interval  $[-1, 1]$  with boundary conditions  $h = h_L$ ,  $h_\xi = h_{L,\xi}$  and  $C_L^v$  given at  $x = -1$  and  $h_\xi = \delta^2\kappa$ ,  $h_{\xi\xi} = \delta^2\kappa$  given at  $x = 1$ . Integrating the momentum equation and eliminating  $u$  yields

$$\begin{aligned} C^v - C_L^v &= hh_{\xi\xi} - \frac{h_\xi^2}{2} - \nu Q \frac{h_\xi}{h} + \frac{h_\xi^2(-1)}{2} + \nu Q \frac{h_\xi(-1)}{h(-1)}, \\ hC_\xi^v &= \mathcal{P}Q(C^v - C_L^v). \end{aligned}$$

This system of ODE's is solved as in the previous sections using a multiple shooting method.

## 4.4 Generalization to 2D

In the previous sections, we have shown how the one-dimensional film-thinning problem can be simplified in the case that  $\varepsilon \rightarrow 0$ . The main idea of this approach is that the domain is divided into a lamella part in which the film curvature is small and capillary forces can be neglected, a Plateau border part in which capillary forces are dominant, and a matching region.

A similar splitting can also be done in the two-dimensional case (see Figure 4.5). However, the geometry of the transition region is much more complicated than in the one-dimensional case.

We consider the limit of a dry film, where both  $(\kappa')^{-1}$  and  $\varepsilon$  tend to zero (recall that  $\kappa'$  is the dimensional film curvature in the Plateau border). As the curvature in the nodes is approximately the same as in the Plateau borders, the transition region tends to a polygon in this limit, and the influence of the nodes vanishes, as shown in Figure 4.5.

The transition region is thus composed of long rectangular areas of length  $L$  and thickness  $\delta L$ . We define the coordinate system as in Figure 4.6 and rescale it using  $x = 1 + \delta\xi$ . Neglecting boundary effects at the top and bottom boundary of the transition region, we recover the one-dimensional system from the previous sections.

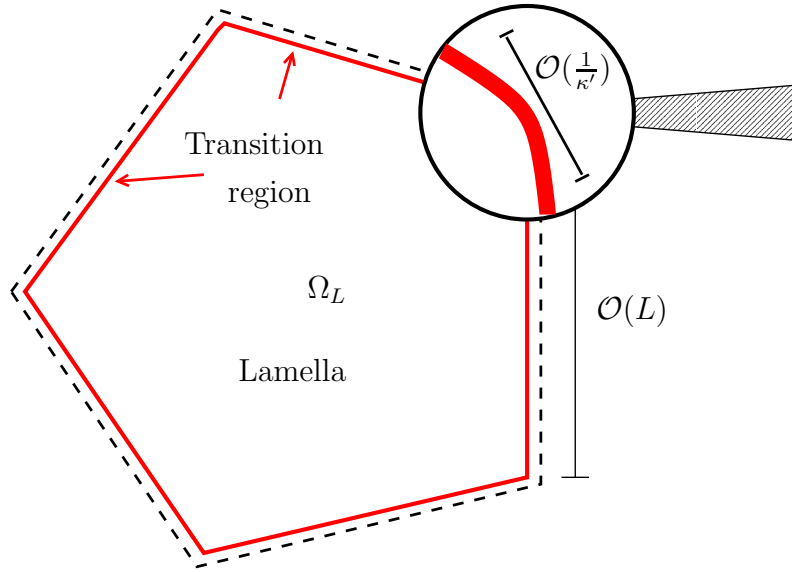


Figure 4.5: Geometry of the 3D problem

This can be used for the solution of the two-dimensional problem. The idea is to solve the quasi-one-dimensional transition region problem in order to obtain boundary conditions for the two-dimensional lamella problem. However, this approach only works if the thickness along the transition region is approximately constant. In the following, we will demonstrate this idea for the example of a lamella in the presence of a surfactant, neglecting inertia. An analogous approach can also be used for a volatile component instead of a surfactant.

#### 4.4.1 Example: Foam film stabilized by a surfactant

##### Lamella

The lamella is dominated by Marangoni forces, such that the resulting system becomes

$$\begin{aligned} 0 &= h_t + (uh)_x + (vh)_y, \\ 0 &= C_x^s, \\ 0 &= C_y^s, \\ 0 &= (1 + \mathcal{P}h)C_t^s + (u_x + v_y)C^s, \end{aligned}$$

where  $\mathcal{P} = \frac{\varepsilon \text{Pe} S \Lambda}{2\Pi}$ . Assuming  $h_x = h_y = 0$  at time  $t = 0$ , we conclude that  $u_x + v_y$  only depends on  $t$  and thus  $h = h(t)$  is independent of  $x$  and  $y$ . Therefore, the

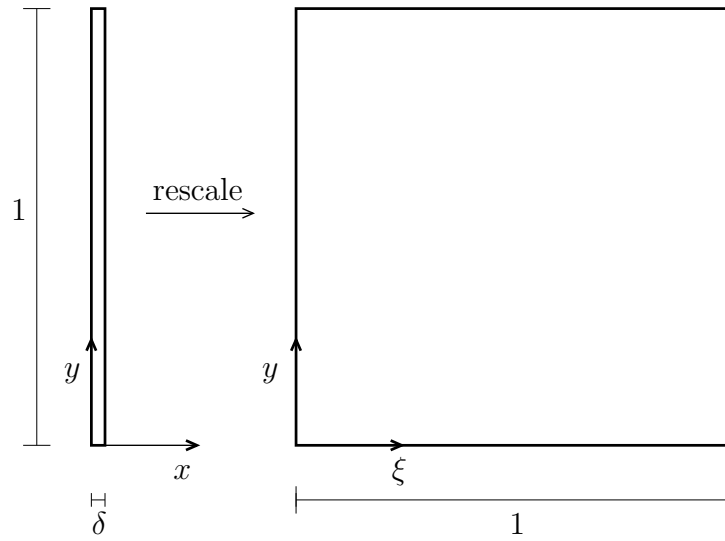


Figure 4.6: Rescaling of the transition region

evolution of the thickness is completely determined by the flux over the lamella boundary:

$$|\Omega_L| h_t \approx -|\partial\Omega_L| Q(h).$$

In this equation,  $|\Omega_L|$  denotes the area of the lamella,  $|\partial\Omega_L|$  the total length of the lamella boundary, and  $Q(h)$  the flux across the boundary obtained from the solution of the one-dimensional transition region problem.

# Chapter 5

## Results and applications

In the previous chapters, we have derived and analyzed models for the description and simulation of the dynamical behaviour of single foam films. We will now present and discuss results of these models, and point out in which way these results can be incorporated into a general foam model.

Moreover, we will discuss possible extensions to this work that may be topics of further studies in future.

### 5.1 General remarks

We consider problems in one and two dimensions. The one-dimensional problems are computed on the interval  $I = [0, 1.5]$ , where symmetry conditions are used at  $x = 0$  and Plateau border conditions are applied at  $x = 1.5$  (ref. Section 3.2). If not noted otherwise, we prescribe

$$h_0 = \begin{cases} 1 & ; x \leq 1 \\ 1 + \frac{\kappa}{2}(x - 1)^2 & ; x > 1 \end{cases}$$

and  $u_0 = 0$  as initial conditions for the thickness and the velocity. Note that we prolongate the Plateau border region artificially up to  $x = 1.5$ . By this we can examine if the solution fulfills the expected constant behaviour for the curvature and the concentrations of surfactant and volatile component.

The two-dimensional problem is computed on a triangular domain  $\Omega$  as shown in Figures 3.5 and 5.1. As initial value for  $h$ , we use

$$h_0 = \begin{cases} 1 & ; x \in \Omega_1 \\ 1 + \frac{\kappa}{2}(x - 1)^2 & ; x \in \Omega_2 \\ 1 + \frac{\kappa}{2}((x - 1)^2 + (y - \tan(\frac{\pi}{5}))^2) & ; x \in \Omega_3 \end{cases}$$



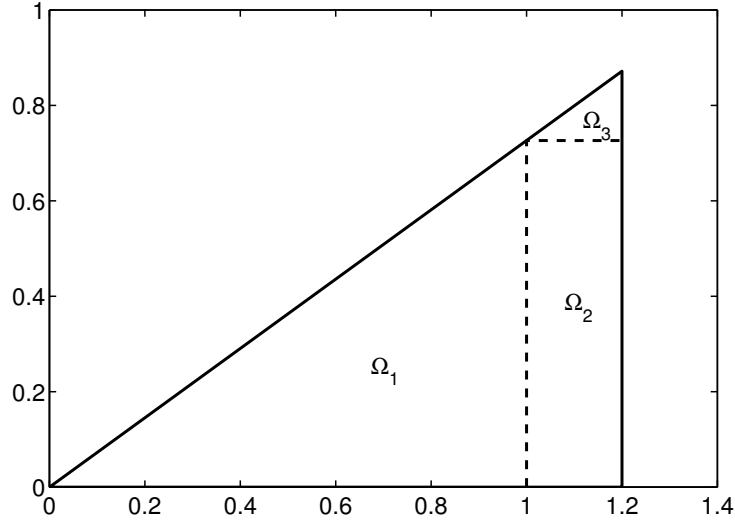


Figure 5.1: Computational domain  $\Omega$  for the two-dimensional problem.

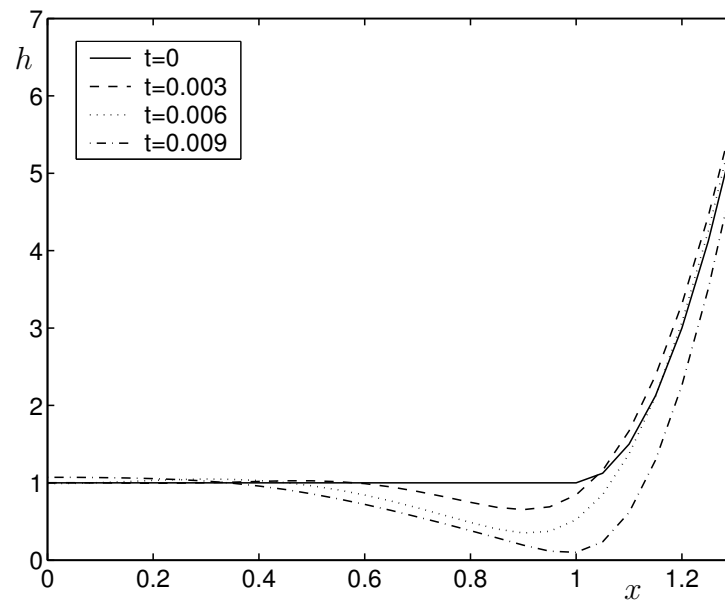
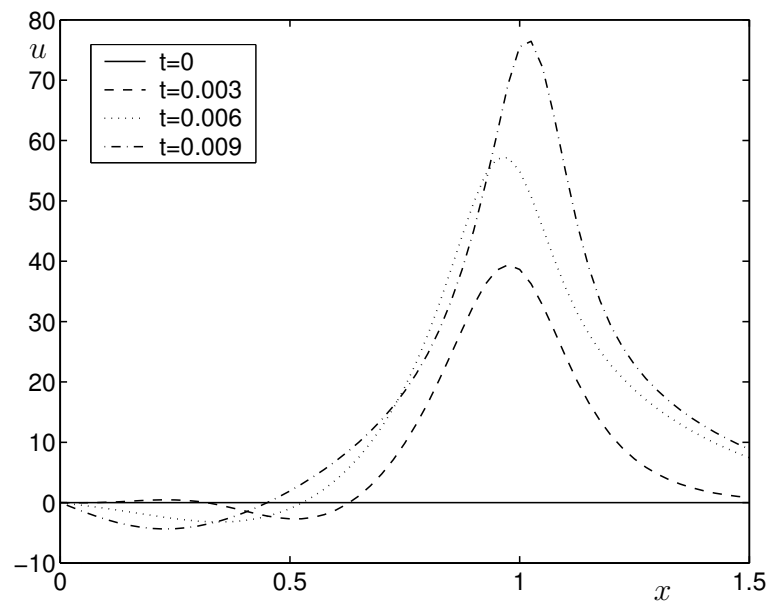
unless noted otherwise. The initial velocity is set to  $u_0 = v_0 = 0$ . As in the one-dimensional case, we use an artificially large Plateau border.

## 5.2 Pure liquid

We begin the discussion of numerical results by analyzing the simplest case of a pure liquid without surfactants or a volatile component. We neglect gravity, such that only viscous, inertial and capillary effects play a role here, simplifying the evaluation of their individual influences.

Consider the one-dimensional problem for the velocity scale  $U = 2 \cdot 10^{-3} m/s$ , the length scale  $L = 5 \cdot 10^{-4} m$  and the ration between film thickness and length  $\varepsilon = 10^{-2}$ . With the values given in Section 3.3, this corresponds approximately to the capillary number  $Ca = 10^{-4}$  and the Reynolds number  $Re = 1$  and is an example close to reality. Moreover, let  $\kappa = 100$ , i.e. the radius of curvature of the Plateau border is equal to  $L$ .

Figures 5.2 and 5.3 show the lamella thickness and the associated velocity profiles at times  $t = 0.003$ ,  $t = 0.006$  and  $t = 0.009$ . We clearly observe the influence of the acting effects, namely capillary, inertial and viscous forces. At the transition between lamella and Plateau border, the curvature of the interface rapidly increases from zero to 100, which triggers a flow of liquid into the direction of the Plateau border. Viscosity tries to extend this influence to the whole film, while inertia acts in the opposite way, i.e. tries to keep the film in its current state.

Figure 5.2:  $Re = 1$ : Lamella shape at different times  $t$ .Figure 5.3:  $Re = 1$ : Velocity profile at different times  $t$ .

The formation of a constriction of the film shows notably that inertia can not be neglected in this example.

We are particularly interested in the rate of thinning and the lifetime of films. Since in the case of a pure liquid, the lamellae are neither stabilized by surfactant nor by evaporation of a volatile component, we expect a very short lifetime of the films in the current cases.

Time is scaled by  $T = \frac{L}{U}$ , which yields  $T = 0.25s$  for the first example. Assuming that the lamella bursts at a thickness of approximately  $10^{-6}m$ , we obtain a film lifetime in the order of magnitude of  $\mathcal{O}(10^{-3}s)$ . Hence, we conclude that as anticipated no persistent foam is created without the stabilizing Marangoni effect, unless the stability is caused by effects not included in our model.

### 5.2.1 Influence of inertia

The effect of inertia to the flow can be observed even better if we consider for comparison a flow with an artificially low Reynolds number  $Re = 0.01$ , while  $Ca$ ,  $\varepsilon$  and  $\kappa$  are left as before. Note that this example corresponds to a typical length scale of  $L = 5 \cdot 10^{-6}m$ , and is therefore a rather theoretical study.

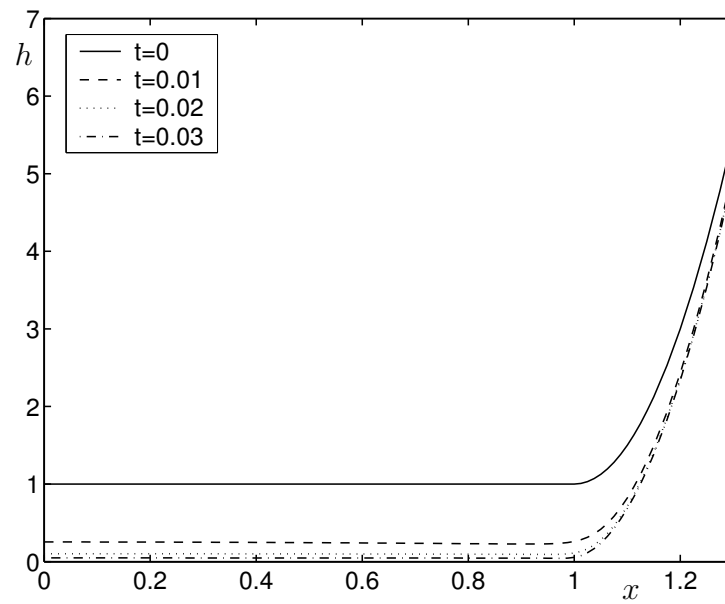
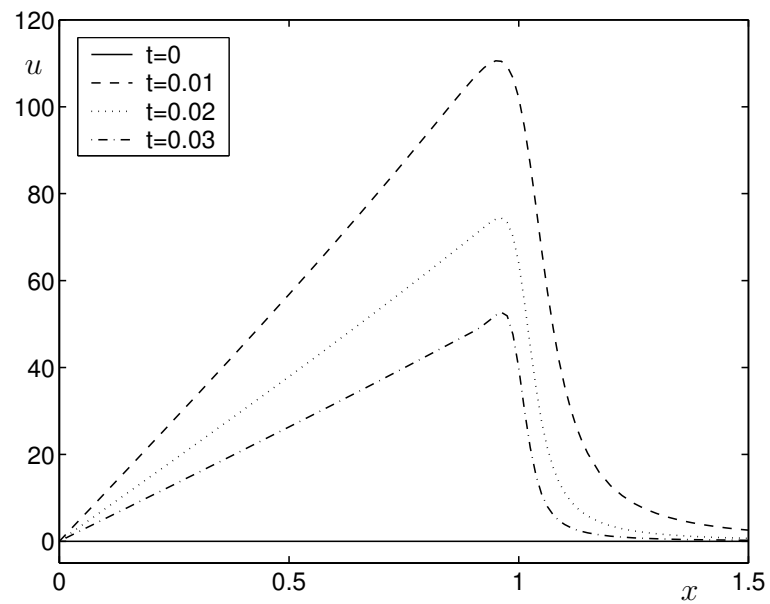
Results for  $h$  and  $u$  are shown in Figures 5.4 and 5.5 for the times  $t = 0.01$ ,  $t = 0.02$  and  $t = 0.03$ . Here, viscosity dominates the lamella part, such that very fast, a linear velocity profile is reached and the lamella thins uniformly as in Section 4.2.2.

Comparing the results illustrated in Figure 5.5 with those in Figure 5.3 clarifies the influences of inertia and viscosity. In the case  $Re = 0.01$ , viscosity dominates the lamella such that a linear velocity profile is assumed. For  $Re = 1$ , the flow is constricted to a smaller region in the vicinity of the transition between lamella and Plateau border. A comparison between solutions for different Reynolds numbers is shown in Figure 5.6.

### 5.2.2 Choice of initial conditions

So far, all computations have been performed for zero initial velocities. In a real foam however, films do not start out as thin lamellae but have a history of draining from thicker films.

In Section 5.2.1, we have observed that for problems with low inertia ( $Re \ll 1$ ), the velocity quickly reaches a quasi-steady state. We can use this to obtain an initial velocity profile for our problem by computing some time steps for the case

Figure 5.4:  $Re = 0.01$ : Lamella shape at different times  $t$ .Figure 5.5:  $Re = 0.01$ : Velocity profile at different times  $t$ .

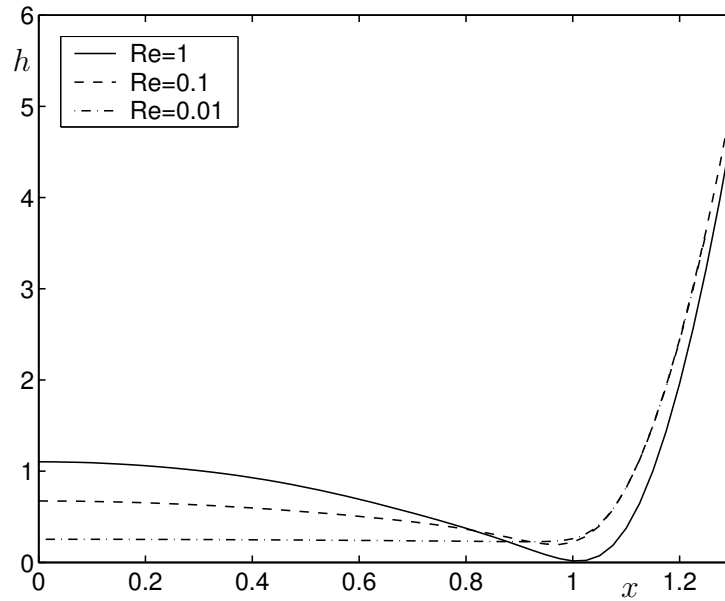


Figure 5.6: Influence of inertia on the solution; lamella profiles at  $t = 0.01$  for different Reynolds numbers.

of artificially low inertia. The result is taken as initial condition for the real problem.

We have to keep in mind that we can only guess the initial condition as long as we do not solve a much more complicated model including the creation of the foam and its draining up to the point where the thin film approximations can be applied. However, our approach is sufficient to obtain qualitative results for the film behaviour and its lifetime.

### 5.2.3 Dependence on $\kappa$

As the flow of liquid out of the lamella is mainly driven by capillary suction, it strongly depends on the curvature  $\kappa$  of the Plateau border. The parameter  $\kappa$  is also the one that couples our thin film model with the global foam model. Therefore, it is interesting to examine the influence of  $\kappa$  on the film lifetime. We have computed solutions for the case  $Ca = 10^{-4}$ ,  $Re = 0.1$  and  $\varepsilon = 10^{-3}$  for different values of  $\kappa$  using initial conditions obtained by the approach discussed in Section 5.2.2. The times  $T$  until the minimal thickness has reached  $h = 0.2$  (for an initial film thickness of  $h_0 = 1$ ) are listed in Table 5.1.

We observe that the lifetime of the film is approximately proportional to  $\sqrt{\kappa^{-1}}$ .

$\kappa$	1000	2000	4000	6000	8000	10000
$T$	0.032	0.0224	0.0164	0.013	0.011	0.0096
$T\sqrt{\kappa}$	1.01	1.00	1.04	1.01	0.98	0.96

Table 5.1: Dependence of film lifetime on  $\kappa$ 

This agrees very well with the observations made in Section 4.2.2 for the case  $\varepsilon \rightarrow 0$ , where we obtained a similar behaviour in Equation (4.16).

### 5.2.4 Behaviour for $\varepsilon \rightarrow 0$

In Chapter 4, we have discussed simplified models for the case when  $\varepsilon \rightarrow 0$ , i.e. when the thickness of the film becomes very small compared to its length. Here, we will compare results for these models based on a domain splitting approach to the results obtained from the full model.

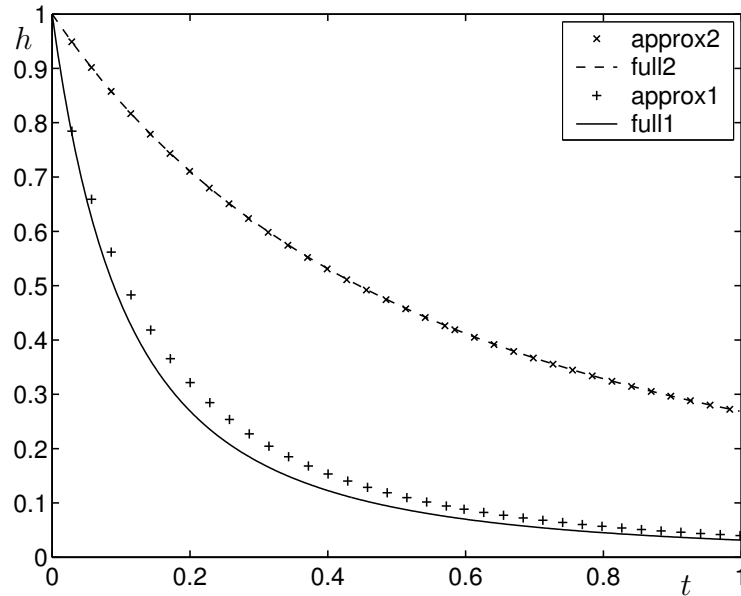


Figure 5.7: Comparison between full model and domain splitting approximation for  $\varepsilon = 0.01$  (approx1 and full1) and  $\varepsilon = 0.001$  (approx2 and full2).

We will first consider the case where inertia is negligible and the lamella is approximately planar. Let  $\text{Ca} = 0.0001$ ,  $\varepsilon = 0.01$ ,  $\kappa = 100$  and  $\text{Re} = 0.01$ , which is the problem we considered in Section 5.2.1. The evolution of the lamella thickness

with time is shown in Figure 5.7 for the solution of the full model (full1) and the solution of the splitting approach given by Equation (4.16) (approx1). (Note that the time has been rescaled in order to fit multiple solutions into one plot.) It can be seen that the general behaviour is sustained by the approximation. However, the thinning is slower by about 15%.

We expect that the approximation improves for smaller values of  $\varepsilon$ . We test this by examining the case  $\text{Ca} = 0.0001$ ,  $\varepsilon = 0.001$ ,  $\kappa = 10000$  and  $\text{Re} = 0.001$ . The results are also shown in Figure 5.7 (full2 and approx2) and it can be observed that the two solutions match very well. Hence, we conclude that for small values of  $\varepsilon$  the behaviour of the lamella is very well described by the model derived in Section 4.2.2.

In the examples above, we assumed that inertia can be neglected and the lamella thickness is spatially constant. However, this is in general not the case. In Section 4.3.3, we have therefore derived a generalized domain splitting approach for the computation of problems involving inertia and non-planar lamellae. We test this model for the case  $\text{Ca} = 0.0001$ ,  $\varepsilon = 0.001$ ,  $\kappa = 10000$  and  $\text{Re} = 0.3$ . The solutions at  $t = 0.038$  are plotted in Figure 5.8 for the full model, the basic domain splitting (DS) approach of Section 4.2.2 taking only the lamella thickness into account, and the improved DS approach derived in Section 4.3.3.

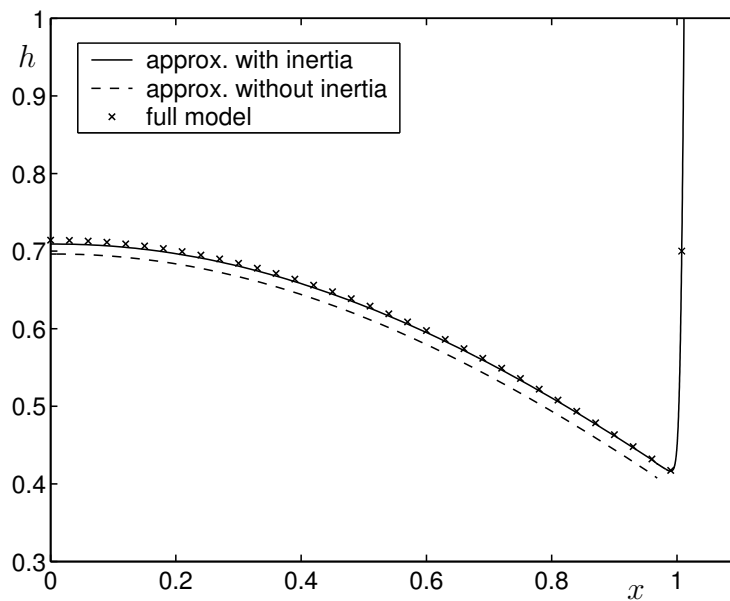


Figure 5.8: Solutions for full model, basic domain splitting (DS) approach and improved DS approach.

We observe that the generalized approach is a noticeable improvement to the

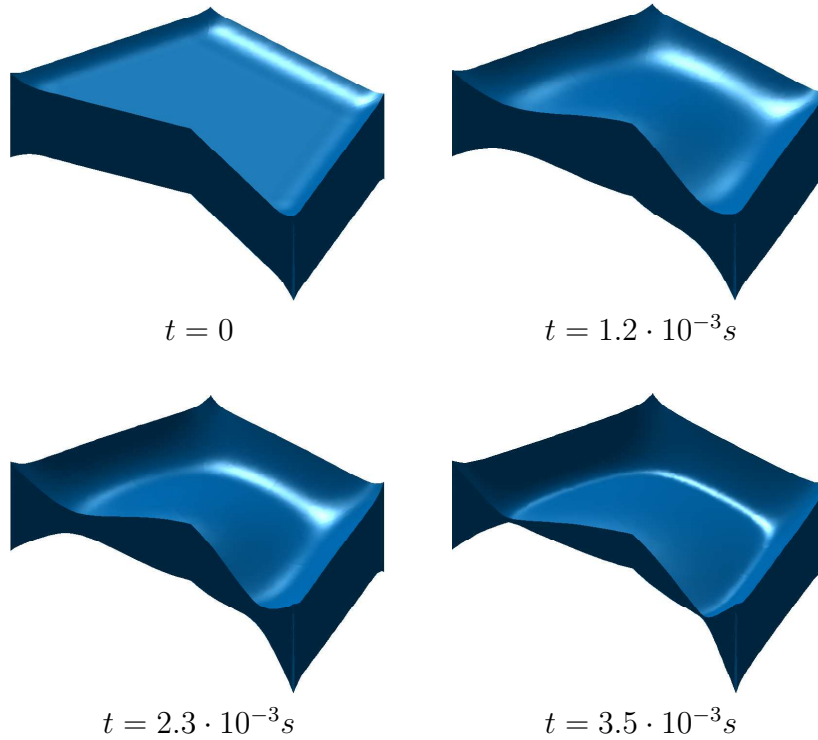


Figure 5.9: Evolution of the film profile for Case 1. The thickness of the films in the plots is scaled with a factor 3 compared to the dimensional values.

basic splitting approach if inertia is involved.

### 5.2.5 Two-dimensional problem

Finally for the case of a pure liquid in the absence of either surfactants or a volatile components, we examine solutions of the two-dimensional problem. We compare two cases:

1. A very thick lamella with a ratio  $\varepsilon = 0.1$ ,  $L = 5 \cdot 10^{-4}m$ ,  $U = 2 \cdot 10^{-2}m/s$  and Plateau border curvature  $\kappa = 0.1$ . This corresponds to  $Ca = 10^{-3}$  and  $Re = 10$ .
2. A rather thinner film with  $\varepsilon = 0.01$ ,  $L = 5 \cdot 10^{-4}m$ ,  $U = 2 \cdot 10^{-3}m/s$  and Plateau border curvature  $\kappa = 0.01$ . This corresponds to  $Ca = 10^{-4}$  and  $Re = 1$ .

The initial conditions are as defined in Section 5.1. Solutions for the thickness  $h$  at several time steps are shown in Figure 5.9 for Case 1 and Figure 5.10 for Case



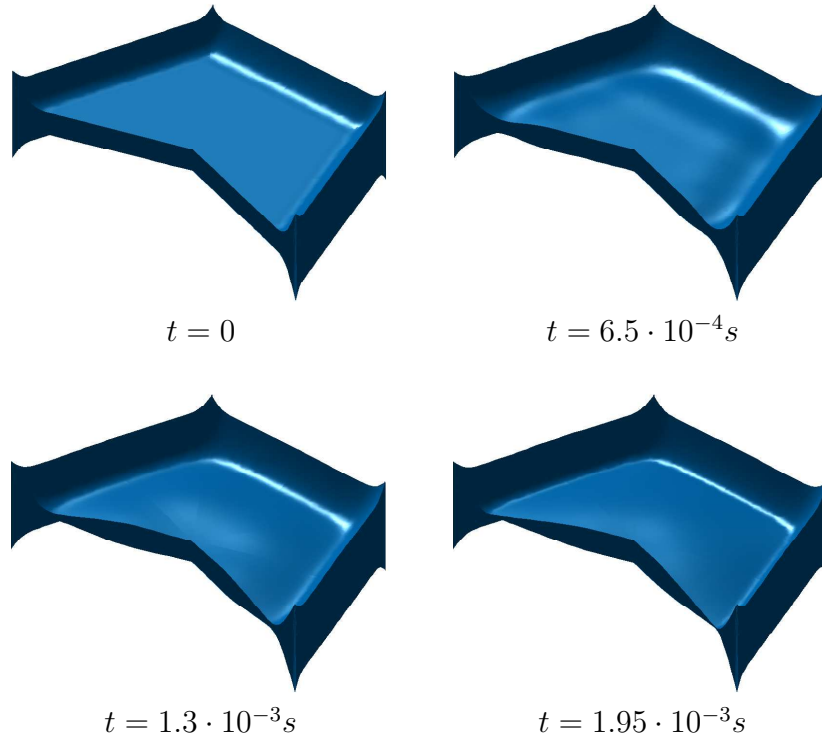


Figure 5.10: Evolution of the film profile for Case 2. The thickness of the films in the plots is scaled with a factor 10 compared to the dimensional values.

2. As expected, we obtain very similar results for the two-dimensional problem than we had before in the one-dimensional case. Capillary suction drives liquid from the lamella into the Plateau border, while a constriction forms along the border of the lamella due to the influence of inertia. However, the films thin faster in the two-dimensional case, with a lifetime of the film in Case 2 being about 0.84 times that of a one-dimensional film with the same characteristics. The reason for this is obvious: since the relative size of the lamella compared to the Plateau border is smaller in two dimensions, the influence of the Plateau border increases.

Another point we observe, which does not appear for the one-dimensional problem, is that the shape of the lamella depends on the parameter  $\varepsilon$ . We clearly note that the thicker lamella is more circular, while the shape of the lamella is much closer to a pentagon for the case  $\varepsilon = 0.01$ . We have already mentioned in Chapter 1 that foam bubbles tend to a polyhedral shape, if their liquid content  $\varphi$  tends to zero. This property is retained in our model.

This effect can be observed even better in Figures 5.11 and 5.12 which show the curvature  $\Delta h$  (visualized by the colours) and the velocity profile (denoted by the

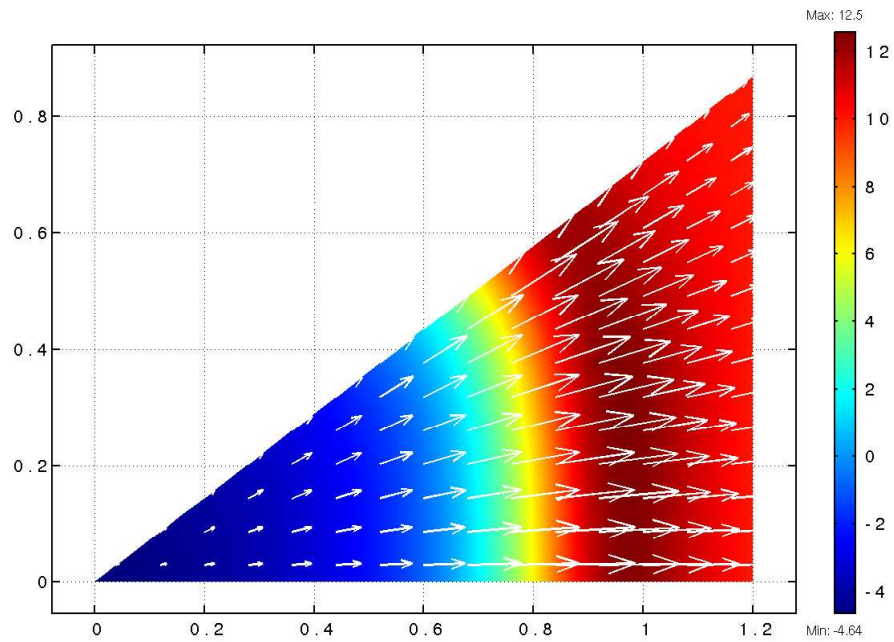


Figure 5.11: Case 1: Curvature of the interface ( $\Delta h$ ) (colour values) and velocity  $\mathbf{U}$  (arrows) at  $t = 2.3 \cdot 10^{-3} s$ .

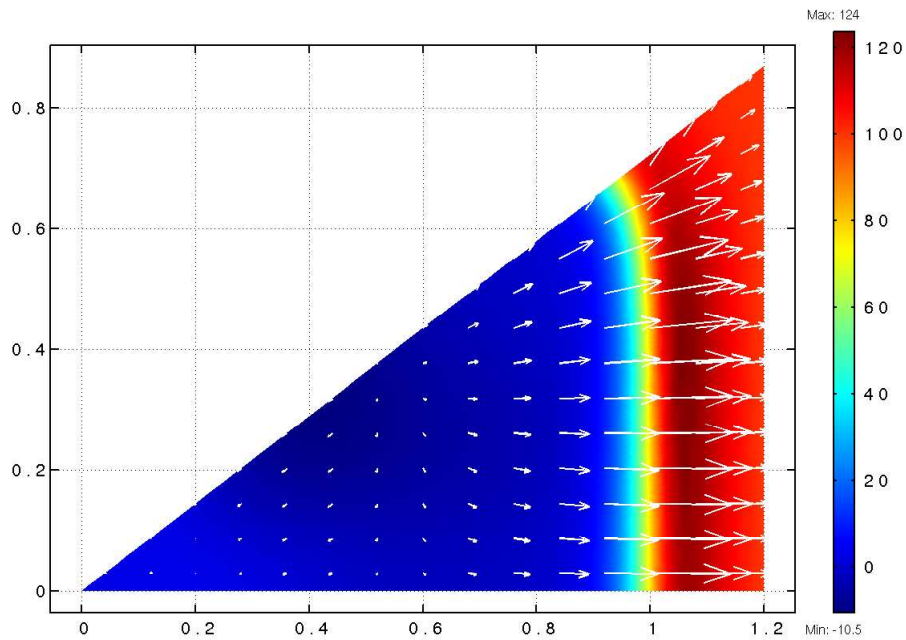


Figure 5.12: Case 2: Curvature of the interface ( $\Delta h$ ) (colour values) and velocity  $\mathbf{U}$  (arrows) at  $t = 1.3 \cdot 10^{-3} s$ .

arrows) for the two cases. We also note that, as expected, the transition between the lamella (with curvature zero) and the Plateau border (with curvature  $\kappa$ ) is much sharper for the thinner film in Case 2 ( $\varepsilon = 0.01$ ).

## 5.3 Influence of a surfactant

We now turn to the question of the influence of a surfactant on the stability of a film. We have seen in the previous section that lifetimes for films made of a pure Newtonian liquid are in the order  $\mathcal{O}(10^{-3}s)$ , and we expect much larger values for a foam stabilized by a surfactant.

### 5.3.1 Evolution of the film thickness

We simulate the evolution of a film with the characteristic parameters  $\varepsilon = 0.01$ ,  $\kappa = 100$ ,  $\text{Ca} = 0.0001$ ,  $\text{Ma} = 100$ ,  $\text{Re} = 1$ ,  $S = 2$ ,  $\text{Pe} = 1$ ,  $\Lambda = 0.1$ ,  $\Pi = 0.01$  and  $\Sigma = 1$ . The initial thickness is in this case given by

$$h_0 = \begin{cases} 10 & ; x \leq 1, \\ 10 + \frac{\kappa}{2}(x-1)^2 & ; x > 1. \end{cases}$$

The surfactant concentration at time  $t = 0$  is set to  $C_0 = 1$ , i.e. we start with a uniform distribution as in a freshly formed foam. Moreover, the film is motionless in the beginning, that is  $u_0 = 0$ .

A plot of the solution at  $t = 14$  is shown in Figure 5.13. The only major difference to the case of a pure liquid that we observe is that the lifetime of the lamella has been strongly increased. The time scale for the problem is  $T = 0.25s$ , such that the lifetime of the film has been increased to the order of seconds ( $\mathcal{O}(1s)$ ) by the presence of the surfactant. However, it is interesting to examine the evolution of the film in more detail. It can be divided into two phases:

Phase 1. There is an initial oscillatory phase in which the film seeks an equilibrium between capillary and Marangoni forces. Figure 5.14 shows the evolution of  $h$  at the points marked in Figure 5.13 in this phase.

Since we start with a constant surfactant concentration, capillary forces are dominant at the beginning, such that film thins very fast. Due to the flow of liquid and surfactant into the Plateau border, a gradient in the surfactant concentration arises which ultimately stops the thinning. Due to inertial effects, an equilibrium is not immediately reached, but the lamella shows an oscillatory behaviour in which liquid alternately flows back into the lamella and out again, until a quasi-equilibrium state is reached.

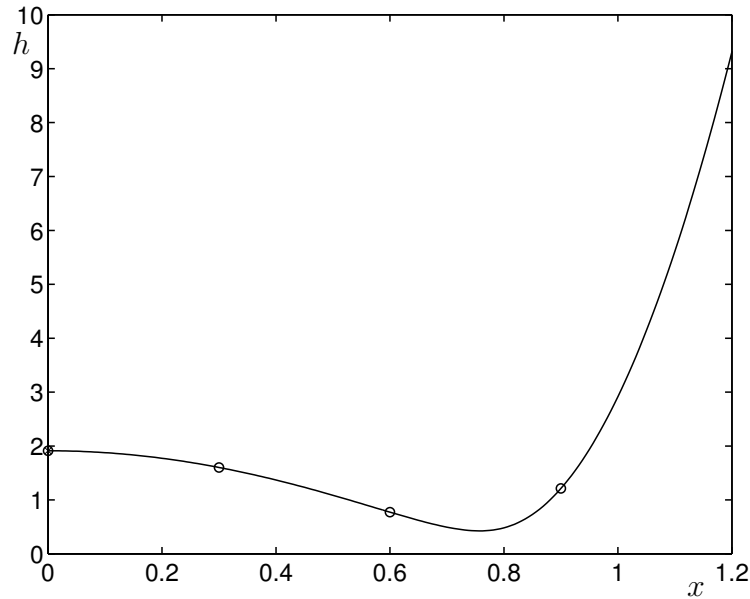


Figure 5.13: Solution  $h$  at  $t = 14$ .

Phase 2. At some point, a state is reached in which Marangoni and capillary forces are in a relative equilibrium. In this phase, the film drains on a much larger time scale than in the case of a pure liquid (ref. Figure 5.15).

The behaviour in the two phases is illustrated by comparing the solutions for the curvature  $\Delta h = h_{xx}$  of the film and the surfactant concentration  $C^s$ . Recall that the capillary force is proportional to the gradient of  $\Delta h$ , while the Marangoni force is proportional to the gradient of  $C^s$ . Hence, we expect a correlation between these two in the equilibrium state.

Figure 5.16 shows the solution for  $\Delta h$  and  $C^s$  at time  $t = 0.01$ , i.e. in the oscillatory phase. We observe no correlation of the two quantities, such that Marangoni and capillary effects are each dominant in different parts of the film. At later times, shown in Figure 5.17 for  $t = 14$ , the situation has changed. Both curvature and surfactant concentration behave very similarly, such that their effects are balanced over the complete domain.

### 5.3.2 Approximation for $\varepsilon \rightarrow 0$

The computational costs for the computation of the full model are very high for the surfactant problem. A reason for this is that the solution has unstable modes in the equilibrium state, as we have seen in Section 4.2.3, which leads to a

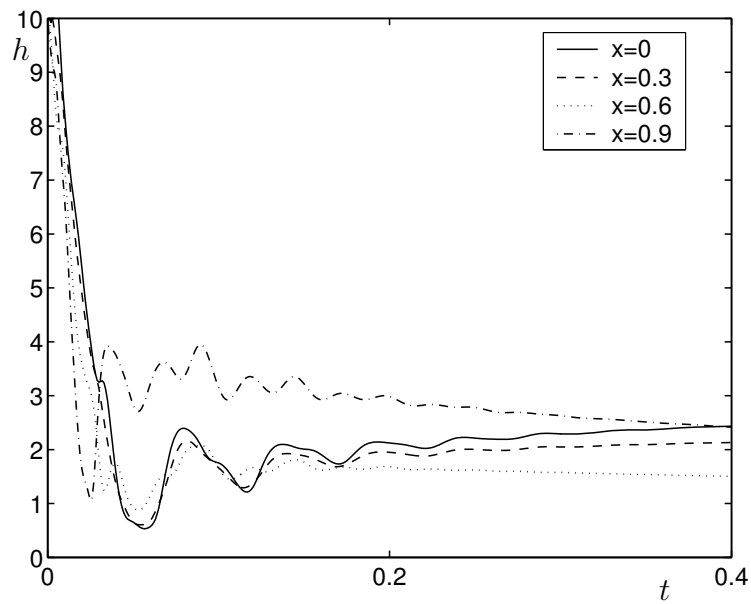


Figure 5.14: Evolution of the lamella thickness – Phase 1.

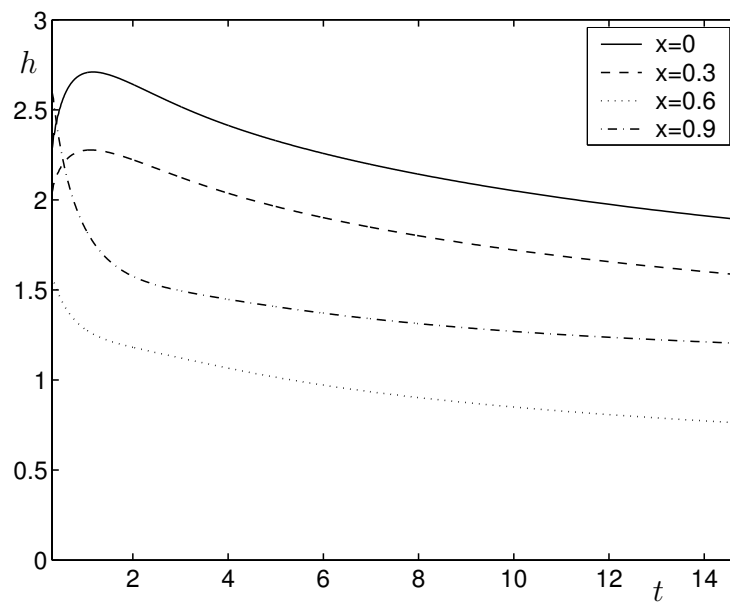


Figure 5.15: Evolution of the lamella thickness – Phase 2.

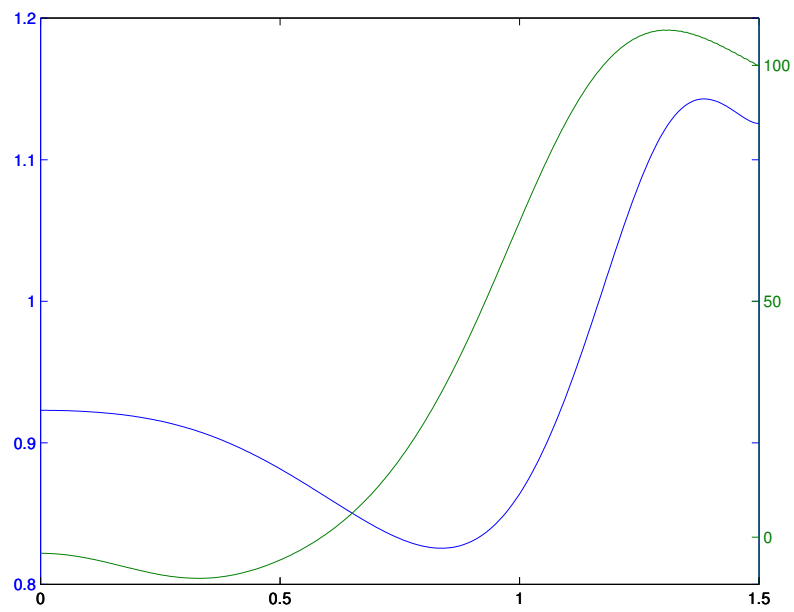


Figure 5.16: Curvature (green) and surfactant concentration (blue) in the film at  $t = 0.01$ .

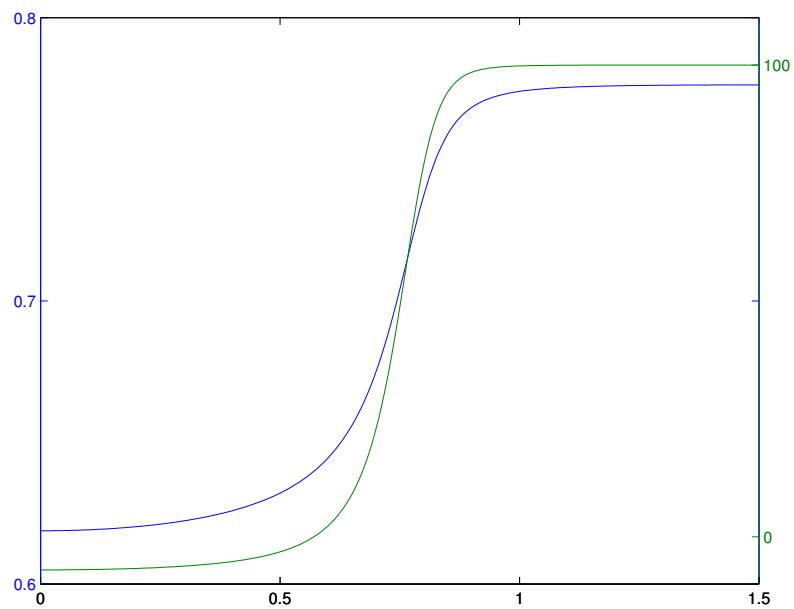


Figure 5.17: Curvature (green) and surfactant concentration (blue) in the film at  $t = 14$ .

severe time step restriction. An improved numerical scheme might overcome this problem.

However, for small values of  $\varepsilon$  we can apply the models derived in Chapter 4 to obtain approximate solutions and to study the behaviour of the flow in the quasi-equilibrium phase. Consider the inertia-free case with  $\varepsilon = 0.001$ ,  $\kappa = 10000$ ,  $\text{Ca} = 0.0001$ ,  $\text{Ma} = 100$ ,  $S = 2$ ,  $\text{Pe} = 1$ ,  $\Lambda = 0.1$ ,  $\Pi = 0.01$  and  $\Sigma = 1$ . The length scale of the transition region is computed as  $\delta = 0.005$ . Let the concentration of surfactant in the Plateau border be  $C_{PB}^s = 1$  and the initial concentration in the lamella be  $C_0^s = 0.6$ . Then the problem can be solved as in Section 4.2.3. The connection of the flux  $Q$  in the transition region and the lamella thickness  $h_L$  is shown in Figure 5.18. Using this, the lamella model is solved and the evolution of  $h_L$  computed (Figure 5.19).

Redimensionalizing the solution with  $T = 0.25s$  yields a lamella lifetime in the order  $\mathcal{O}(10s)$ , i.e. the stabilization is very strong in this case.

We observe that the influence of the lamella thickness on the flux is directly opposed to that of a pure liquid, i.e. the flux increases for thinner films, such that the rate of thinning of the lamella accelerates. To get a deeper insight into the correlations in the transition region, we examine the dependence of the flux  $Q$  on the curvature  $\kappa$  of the Plateau border, the surfactant concentration  $C_{PB}^s$  in the Plateau border (Figure 5.20) and the parameter  $\mathcal{P}$  describing the relation between surface and bulk convection (Figure 5.21).

An interesting observation is made in Figure 5.20 for the dependencies of the flux of  $\kappa$  and  $C_{PB}^s$ . An increase of  $\kappa$  leads to a higher gradient of the curvature  $\Delta h$  and thus to an increased capillary force in the direction of the Plateau border. However, the flux from the lamella decreases for increasing  $\kappa$ . Hence, we find that in the equilibrium the Marangoni force is increased even more than the capillary force. The same effect in inverse direction is noted for the relation of the flux and the concentration  $C_{PB}^s$ . A larger value of  $C_{PB}^s$  leads to a stronger Marangoni force; however, this does not lead to a reduced flux which we attribute to an ever stronger increase of the capillary force.

Finally, we note that the parameter  $\mathcal{P}$  does not influence the solution in a particularly strong way.

### 5.3.3 Two-dimensional problem

For a film stabilized by a surfactant, we have two main opposing forces, namely the capillary force and the Marangoni force. In the one-dimensional case, these two reach a relative equilibrium after an initial oscillatory phase. However, in

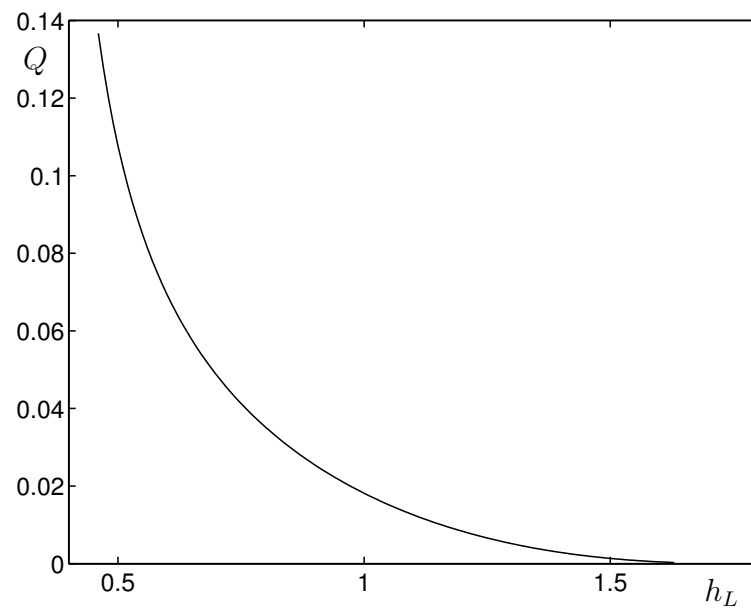


Figure 5.18: Dependence of the flux  $Q$  on the lamella thickness  $h_L$ .

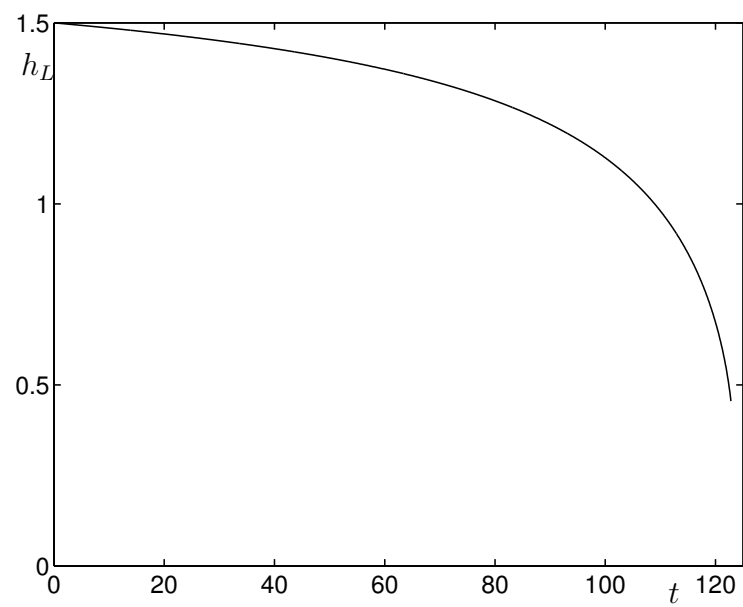


Figure 5.19: Evolution of the lamella thickness.



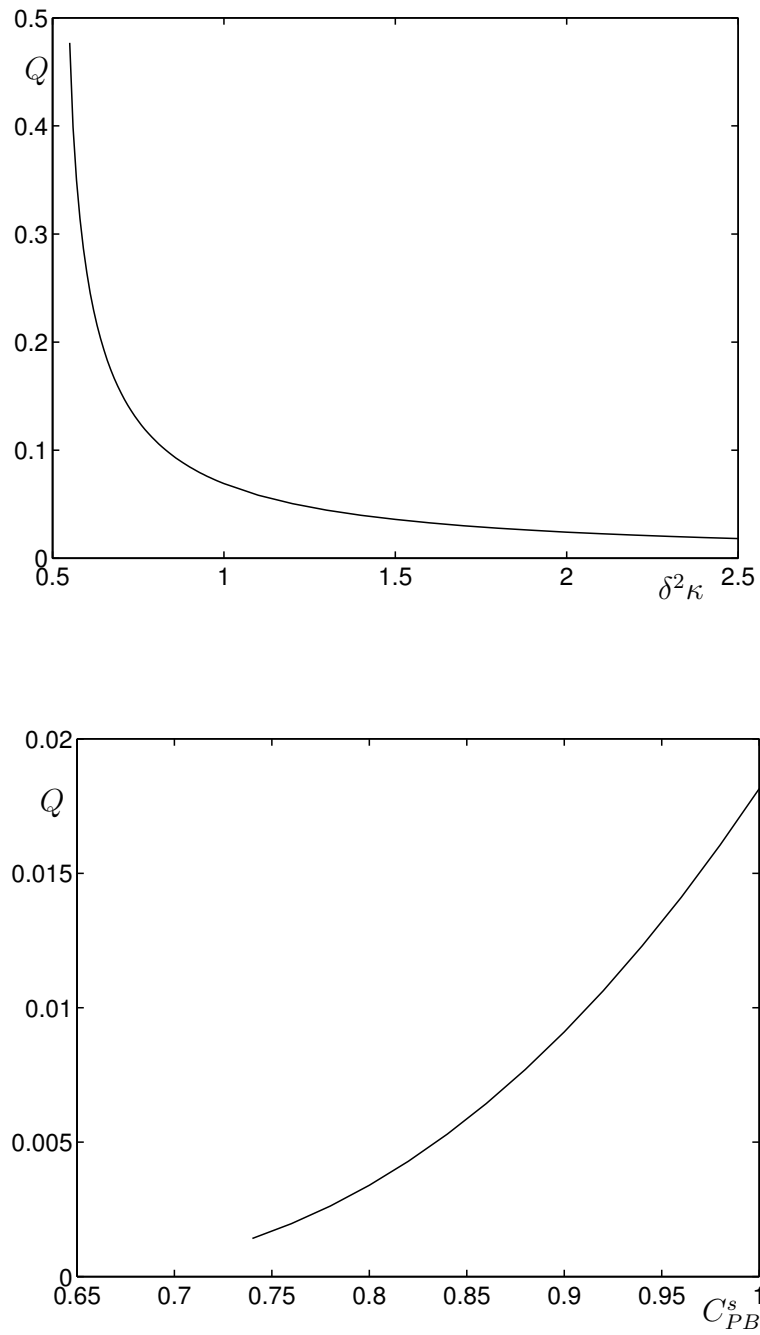


Figure 5.20: Dependence of the flux  $Q$  on the Plateau border curvature  $\kappa$  (top) and on the surfactant concentration in the Plateau border  $C_{PB}^s$  (bottom).

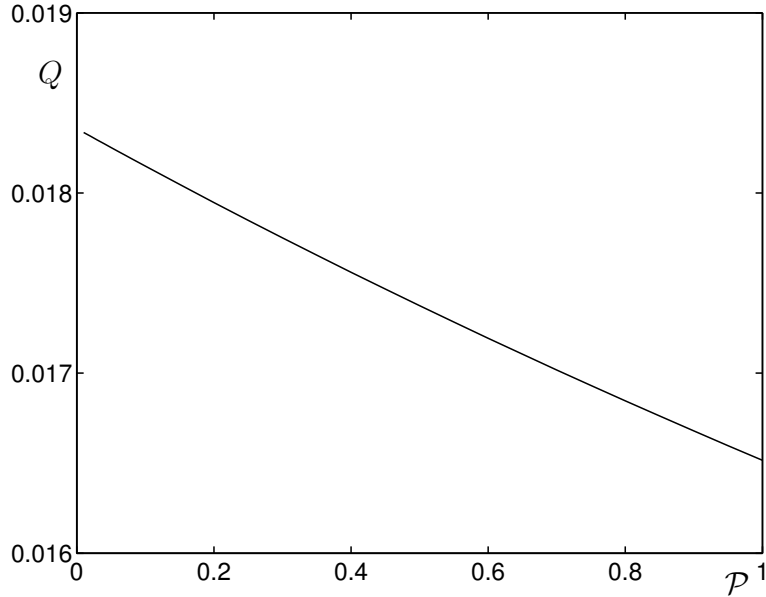


Figure 5.21: Dependence of  $Q$  on  $\mathcal{P}$ .

one dimension the two effects always act in exactly the opposite direction. In the two-dimensional case, there is another direction to which the flow may evade if it is influenced by two opposing forces. Therefore, it is not a priori clear if an equilibrium state is reached for the film.

In order to investigate this question, we consider a liquid film with the parameters  $\varepsilon = 0.01$ ,  $\kappa = 100$ ,  $\text{Ca} = 0.0001$ ,  $\text{Ma} = 100$ ,  $\text{Re} = 1$ ,  $\text{Pe} = 20$ ,  $S = 2$ ,  $\Lambda = 0.1$ ,  $\Pi = 0.01$  and  $\Sigma = 1$ . The initial condition for  $h$ ,  $u_0$  and  $v_0$  is defined as in Section 5.1,  $C_0^s$  is given by

$$C_0^s = \begin{cases} 0.8 & ; x \leq 0.8, \\ x & ; x > 0.8. \end{cases}$$

As in the one-dimensional case, we obtain an initial phase in which either of the effects struggles for dominance. Figure 5.22 compares the solutions for  $\Delta h$  and  $C^s$  at different time steps during this phase and shows the velocity profile in the film. We observe that in turn capillary (at  $t = 0.015$ ) and Marangoni (at  $t = 0.005$ ) forces dominate the flow, but eventually an eddy forms and a quasi-equilibrium state is reached.

This marks a significant difference to the one-dimensional case. Since the flow has an additional degree of freedom, i.e. an additional flow direction is possible, it can evade to that direction, which eventually leads to the formation of an eddy, marking the path of lowest resistance for the flow. The streamline plot of the

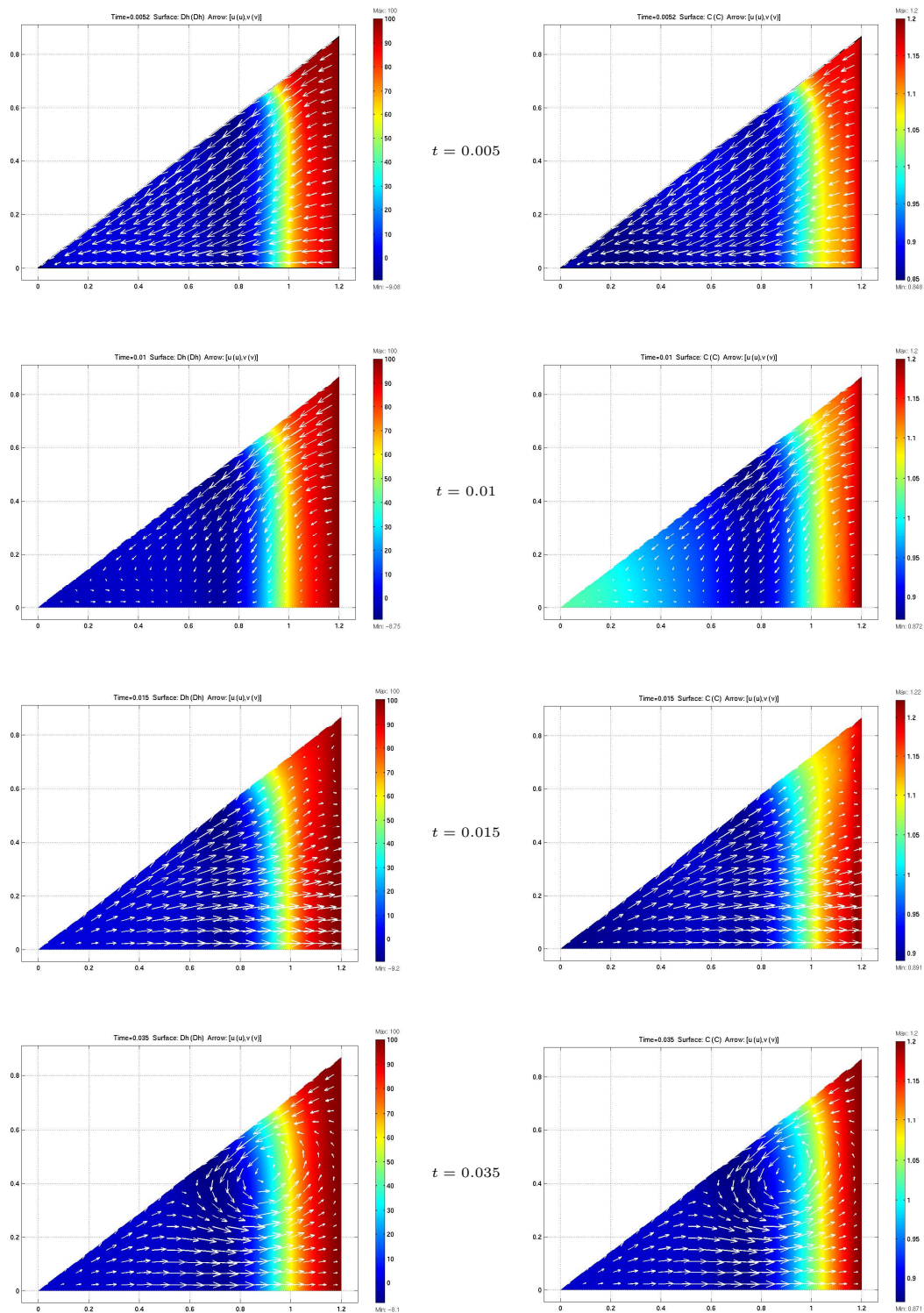


Figure 5.22: Solutions for  $\Delta h$  (left) and  $C^s$  (right) in the initial oscillatory phase at four different time steps. The arrows represent the velocity profile.

flow at a later time in Figure 5.23 clarifies this fact even more. Moreover, we observe that by and by a second eddy arises.

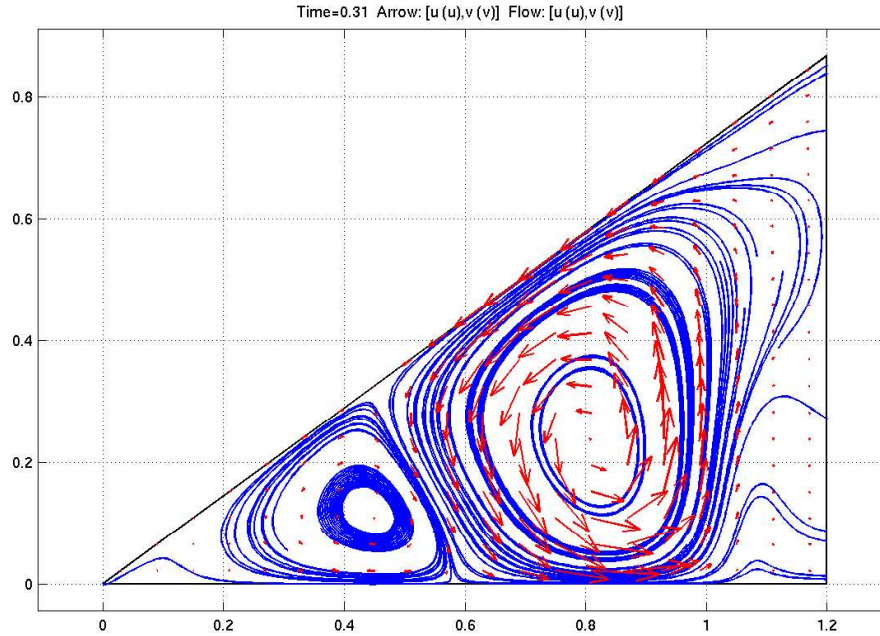


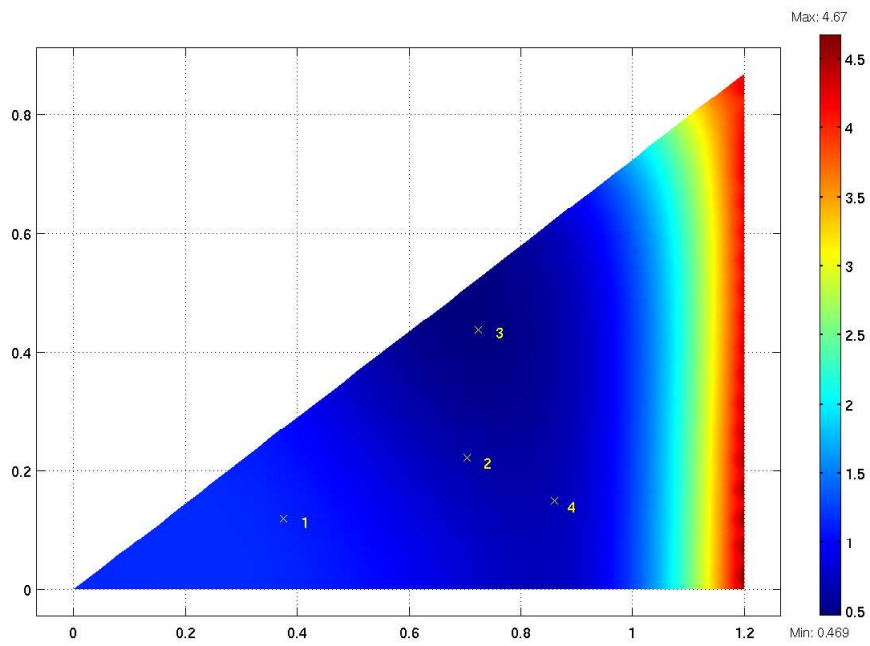
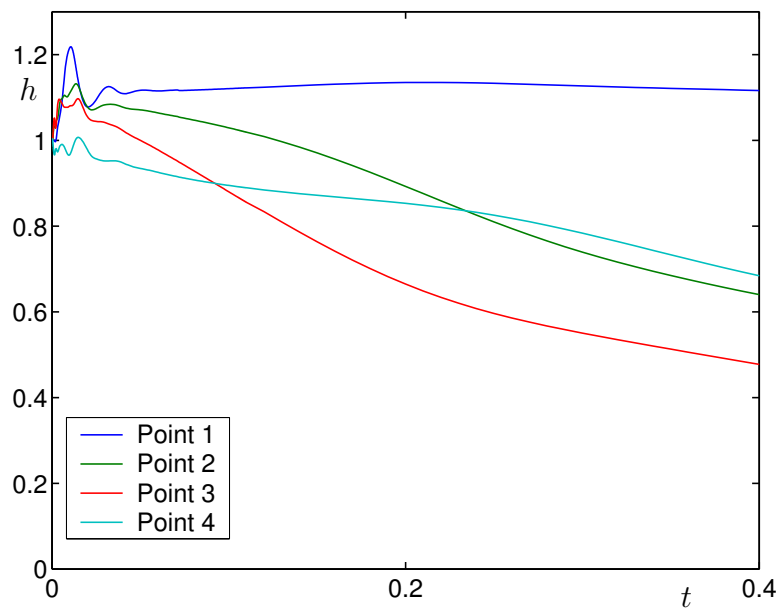
Figure 5.23: Streamlines and velocity profile of the solution at  $t = 0.4$ .

Finally, Figures 5.24 and 5.25 exhibit the profile of  $h$  in the film at time  $t = 0.4$  and its evolution at several points in the lamella. We observe again the two phases of the flow. Redimensionalizing the variables, we obtain  $T = 0.25s$  as in the one-dimensional case, such that the lifetime of the film is again of the order of seconds.

## 5.4 Influence of a volatile component

In the previous section, we examined the impact that the presence of a surfactant has on the stability of a foam film. We have seen that after an initial oscillatory phase, a quasi-stable equilibrium is adopted, leading to a very slow thinning. We are now interested in the influence of a volatile component, particularly if an analogous behaviour as in the surfactant case can be observed.

Let us therefore consider a film with the properties  $\varepsilon = 0.01$ ,  $\kappa = 100$ ,  $\text{Ca} = 0.0001$ ,  $\text{Ma} = 1000$ ,  $\text{Re} = 1$ ,  $\widetilde{\text{Pe}} = 1$ ,  $\mathcal{E} = 5 \cdot 10^{-6}$ ,  $e = 1$  and  $\Sigma = 1$ . The initial

Figure 5.24: Thickness  $h$  at  $t = 0.4$ .Figure 5.25: Evolution of  $h$  at the points determined in Figure 5.24.

condition is defined by

$$h_0 = \begin{cases} 10 & ; x \leq 1, \\ 10 + \frac{\kappa}{2}(x-1)^2 & ; x > 1, \end{cases}$$

$u_0 = 0$  and  $C^v = 0.5$ . Note that  $C_v$  always lies between 0 and 1, where  $C^v \equiv 1$  means that only the volatile component is present and no Marangoni effect can occur.

The evolution of the lamella thickness at the points  $x = 0$ ,  $x = 0.3$  and  $x = 0.6$  is shown in Figure 5.26. The Marangoni effect due to inhomogeneous evaporation is much weaker than that due to surfactants, at least for the parameter range which is of interest for us. As in the surfactant case, we notice an oscillatory behaviour at the beginning with decreasing oscillations.

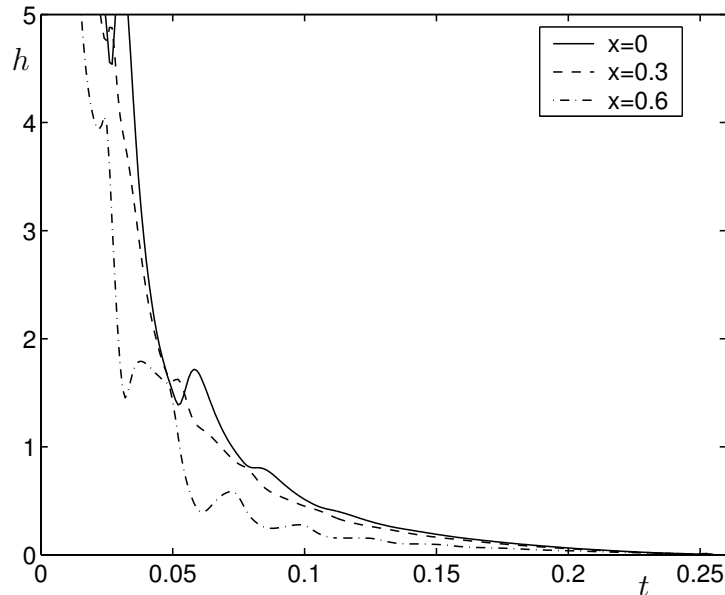


Figure 5.26: Evolution of  $h$  in the presence of a volatile component.

However, contrary to before, no stable equilibrium state is reached. This is confirmed by Figures 5.27 and 5.28, which show the profiles of velocity and concentration of the volatile component in the film at different time steps. While the velocity seems to settle down to an equilibrium initially, at approximately  $t = 0.25$  it suddenly destabilizes, leading to the breakdown of the lamella shortly afterwards.

The reason for this behaviour lies in the evaporation itself. Although it initially stabilizes the lamella by the Marangoni effect, the effect of the evaporation becomes stronger while the lamella thins. Eventually, the Marangoni effect becomes dominant leading to the destabilization of the film.

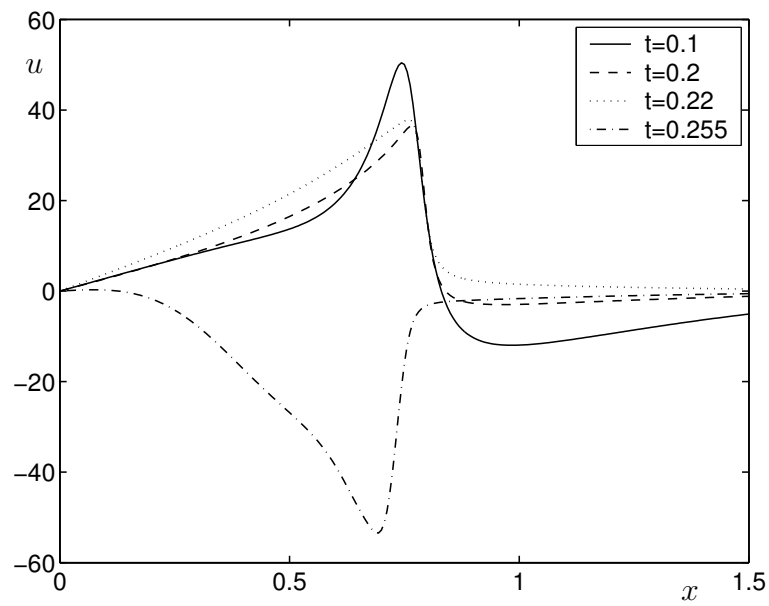


Figure 5.27: Solution for the velocity  $u$  at different times.

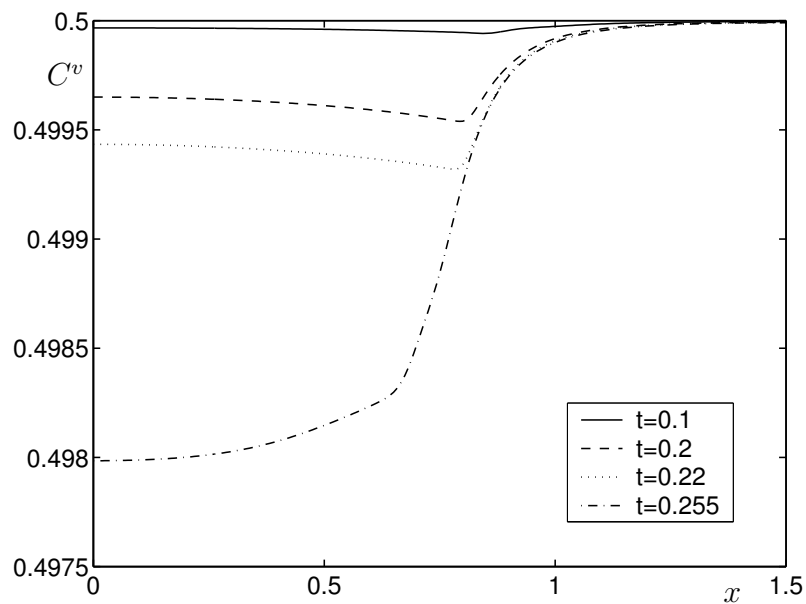


Figure 5.28: Solution for the concentration  $C^v$  of the volatile component at different times.

The lamella lifetime in dimensional values lies in the order  $\mathcal{O}(10^{-1}s)$ . Although the evaporation of a volatile component does not produce a long-lasting foam, it can nonetheless play a role in the filling of a car tank where we are dealing with relatively short-lived foam. A more detailed analysis could be conducted if more information about the composition and parameters of the fuel was available.

## 5.5 Extensions

We have derived a general model for the simulation of a foam lamella. Thereby, we have built a foundation to which any number of extensions can be added. At this point, we want to encourage some special enhancements.

### 5.5.1 Coupling with a global foam model

Ultimately, we are interested in building a global foam model which incorporates all of the relevant effects described by separate models. For that aim, we have to define an interface over which to communicate with this global model.

The main external parameters determining the lamella thinning are the curvature of the interface and the concentration of surfactant/volatile component in the Plateau border. A simple coupling can be done with the drainage model described in Section 1.5.5. The foam drainage equation (1.2) yields the liquid content of the foam at a given point. Using this information and the typical bubble size, an approximate value for the Plateau border curvature can be computed. Assuming the surfactant concentration to be constant along the network of Plateau borders and nodes, our lamella model can be used to compute a rate of decay depending on the position in the foam.

An improved version of the coupling approach is to use the flow of liquid from the lamella into the Plateau border as a source in the foam drainage model and derive an improved foam drainage equation.

Taking a more sophisticated approach, one can develop a model for the simulation of one or several Plateau borders and the neighbouring nodes. Coupling this with the lamella yields more exact boundary conditions for our model and thus improves its accuracy, as has been discussed in Section 3.2. However, this is paid by a greater computational effort. Moreover, a way must be found to incorporate the simulation of the Plateau border into the global foam model.



## 5.5.2 Application of an enhanced evaporation model

For the simulation made in this chapter, we have assumed a constant evaporation of the volatile component, i.e. we have considered the bubbles to be of infinite volume such that the vapour concentration does not increase over time. An improved evaporation model, which takes the finite volume of the bubbles into account, has already been discussed in Section 2.3.3. Depending on the parameters of the volatile component and on the bubble size, the evaporation rate in such a model may significantly decrease during the thinning of the lamella, which can lead to a distinctly different behaviour.

## 5.5.3 Continuous thermodynamics

In this work, we have considered a very simple fuel model consisting only of one or two different components. However, real gasoline or diesel is a compound of a large variety ( $> 100$ ) of components, all of which have a different boiling point. Hence, the behaviour can be different particularly in the case of evaporation.

Taking each of the components of the fuel under account leads to a very high-dimensional problem, whose solution is too computationally expensive. *Continuous Thermodynamics* [35] is an alternative approach which reduces the complexity of the model by making use of the type of composition of the fuel. The components of the fuel can be classified into few families, namely *paraffins* and *aromatics* for gasoline, and *paraffins*, *aromatics* and *naphthalenes* for diesel. The members of each family have very similar properties differing only within a small range. The basic idea is to consider each family as a continuous probability density function instead of a mixture of discrete components.

In a future work, the lamella model can be extended using this approach, such that more exact statements about the behaviour of a film under the influence of evaporation can be made.

## Conclusion

In the present thesis, a model for the behaviour of a foam lamella under the influences of inertial, viscous, gravitational, capillary and Marangoni forces has been developed. The underlying physical behaviour of such lamellae is described by the incompressible Navier-Stokes equations in combination with free interfaces between liquid and gas phase at either side of the film. An asymptotic analysis with respect to the lamella thickness leads to a simpler model by reducing the spatial dimension of the problem and thereby eliminating the free interfaces.

The high surface curvature causes a lower capillary pressure in the adjacent Plateau borders and triggers a liquid flow leaving the lamella. This leads to thinning and eventual rupture. The principal stabilizing influence is the Marangoni effect caused by the presence of surfactants or volatile components in the film. Spatial variations in the concentration of these substances result in a gradient of the surface tension, leading to an attenuation of the flow. Therefore, additional models for their description and interaction with the flow have been derived.

In order to close the models, boundary conditions at the threshold to the Plateau borders have been determined. Therefore, a simple Plateau border model has been derived and converted into suitable boundary conditions for the lamella problem. The formulation of the central film-thinning problem for the case of a fuel foam is possible after the assignation of the relevant parameters and the evaluation of the magnitudes of the individual forces.

In the resulting central model, the flow is governed by a highly nonlinear third-order system of partial differential equations. Existence and uniqueness of a solution to the linearized problem have been proven using a variational approach. Due to the complexity of the problem, such a statement remains open for the general nonlinear case and may be an interesting challenge for further investigation.

A further approximation of the problem based on a domain decomposition approach is possible for the case of a very thin film. The corresponding models have been derived for an inertia-free film under the assumption of planar lamellae. On their basis, an extended model has been developed for the general case of a non-planar lamella and the inclusion of inertial forces.

The derivation of a Galerkin scheme for the numerical examination of the model and its application to the film-thinning problem with particular attention to the influence of surfactants and volatile components have provided a deeper understanding of the mechanisms involved in this process. The model that we have developed in this work provides a basis for the simulation of the flow inside of a foam film. A number of extension can be made in further work in order to improve the accuracy and performance of the model and the numerical scheme, and to investigate other interesting questions, such as the coupling with a macroscopic foam model.



# Nomenclature

We have used a large number of notations for different variables, parameters, etc. throughout this thesis. This overview is intended to facilitate keeping track of all those symbols. As general conventions, scalar-valued quantities are denoted by normal-sized letters ( $x$ ), vectors by bold face letters ( $\mathbf{n}$ ) and matrices by capital letters ( $A$ ). Moreover, derivatives are usually denoted by subscripts ( $h_x$ ).

Furthermore, we have used the following notations:

## Variables and geometrical parameters

$x$	x-coordinate
$y$	y-coordinate
$z$	z-coordinate
$H$	center-face of the film
$h$	film thickness
$\Delta h$	Laplacian of the film thickness
$u$	velocity in x-direction
$v$	velocity in y-direction
$w$	velocity in z-direction
$p$	pressure
$C^s$	surfactant concentration
$\Gamma$	surfactant concentration at the interface
$j$	flux of surfactant to the interface
$C^v$	concentration of volatile component
$\sigma$	surface tension
$e$	evaporation
$\mathcal{T}$	stress tensor
$\mathbf{n}$	Normal vector to the interface
$\mathbf{t}_{1/2}$	Tangential vectors at the interface
$\kappa$	Curvature of the interface
$\varepsilon$	Ratio of film thickness and length

**Physical parameters (ref. page 51f)**

$\varphi$	liquid fraction of the foam
$L$	length scale of the lamella
$U$	velocity scale of flow out of lamella
$T$	time scale of film-thinning process
$\rho$	liquid density
$\mu$	dynamic viscosity of the liquid
$g$	gravitational acceleration on earth
$\gamma, \Delta\gamma$	typical surface tension, surf. ten. variation
$\gamma_{v/l}$	surface tension of volatile/non-volatile component
$\kappa$	curvature of the interface in the Plateau border
$C^*$	typical surfactant concentration in the bulk
$\Gamma^*$	typical surf. conc. at the interface
$D_s$	diffusivity of surfactant in the bulk
$D_\Gamma$	diffusivity of surfactant at the surface
$\Gamma_\infty$	surfactant saturation concentration at the interface
$k_{1/2}$	Langmuir parameters
$\tilde{C}^*$	typical concentration of volatile component, $\tilde{C}^* = 1$
$e^*$	typical evaporation
$D_v$	diffusivity of volatile component
$R$	universal gas constant
$\Theta$	temperature of the liquid

**Similarity parameters (ref. page 54)**

Re	Reynolds number, $\text{Re} = \frac{\rho LU}{\mu}$
Fr	Froude number, $\text{Fr} = \frac{U^2}{L}$
Ca	Capillary number, $\text{Ca} = \frac{\mu U}{\gamma}$
Ma	Marangoni number, $\text{Ma} = \frac{\Delta\gamma}{\mu U}$
Pe	Péclet number for surfactant, $\text{Pe} = \frac{UL}{D_s}$
$\text{Pe}_\Gamma$	Péclet number at the interface, $\text{Pe} = \frac{UL}{D_\Gamma}$
$S$	Replenishment number, $S = \frac{D_s C^*}{U \Gamma^*}$
$\Lambda$	$\Lambda = \frac{\Gamma^*}{\Gamma_\infty}$
$\Pi$	$\Pi = \frac{C^*}{k_2}$
$\tilde{\text{Pe}}$	Péclet number for volatile component, $\tilde{\text{Pe}} = \frac{UL}{D_v}$
$\mathcal{S}$	relation between evaporation and diffusion, $\mathcal{S} = \frac{Le^*}{D_v \tilde{C}^{star}}$
$\mathcal{E}$	relation between evaporation and convection, $\mathcal{E} = \frac{e^*}{U}$
$\Sigma$	$\Sigma = \frac{R\Theta\Gamma_\infty}{\Delta\gamma}$
$\tilde{\Sigma}$	$\tilde{\Sigma} = \frac{\gamma_l - \gamma_v}{\Delta\gamma}$

**Sets and spaces**

$\mathbb{R}$	set of real numbers
$\mathbb{C}$	set of complex numbers
$\Omega$	computational domain
$\partial\Omega$	boundary of the computational domain
$L^2(\Omega)$	space of Lebesgue integrable functions on $\Omega$
$H^m(\Omega)$	Sobolev space, $H^m(\Omega) = \{u \in L^2(\Omega) : D^\alpha u \in L^2(\Omega),  \alpha  \leq m\}$
$V, H$	real, separable Hilbert spaces

## References

- [1] ADAMS, R.A., *Sobolev spaces*, Academic Press (1978)
- [2] ASCHER, U.M., MATTHEIJ, R.M. AND RUSSELL, R.D., *Numerical solution of boundary value problems for ordinary differential equations*, SIAM (1995)
- [3] BARIGOU, M. AND DAVIDSON, J.F., *Soap film drainage: Theory and experiment*, Chem. Eng. Sci. 49, 1807–1819 (1994)
- [4] BERTOZZI, A.L. AND PUGH, M., *The lubrication approximation for thin viscous films: regularity and long-time behaviour of weak solutions*, Comm. Pure Appl. Math. 49, 85–123 (1996)
- [5] BIKERMAN, J.J., *Foams*, Springer (1973)
- [6] BRAKKE, K., *The surface evolver homepage*,  
<http://www.susqu.edu/facstaff/b/brakke/evolver>
- [7] BRAESS, D., *Finite Elemente: Theorie, schnelle Löser und Anwendungen in der Elastizitätstheorie*, 2. Auflage, Springer (1997)
- [8] BRAUN, R.J., SNOW, S.A. AND PERNISZ, U.C., *Gravitational drainage of a tangentially immobile thick film*, J. Coll. Int. Sci. 219, 225–240 (1999)
- [9] BREWARD, C.J.W., *The mathematics of foam*, Dissertation, Oxford (1999)
- [10] BREWARD, C.J.W. AND HOWELL, P.D., *The drainage of a foam lamella*, J. Fluid Mech. 458, 379–406 (2002)
- [11] BUDIARTO, E., *Mathematical simulation of liquid-vapor phase transition*, Master thesis, Kaiserslautern (2000)
- [12] DAUTRAY, R. AND LIONS, J.-L., *Mathematical analysis and numerical methods for science and technology*, Springer (1992)



- 
- [13] EGGLETON, C.D. AND STEBE, K.J., *An adsorption-desorption controlled surfactant on a deforming droplet*, J. Coll. Int. Sci. 208, 68–80 (1998)
- [14] ENGELBERG, S., *An analytical proof of the linear stability of the viscous shock profile of the Burgers equation with fourth-order viscosity*, SIAM J. Math. Anal. 30, 927–936 (1999)
- [15] FEISTAUER, M., *Mathematical methods in fluid dynamics*, Longman Scientific and Technical (1993)
- [16] GLAZIER, J.A. AND WEAIRE, D., *The kinetics of cellular patterns*, J. Phys. Cond. Mat. 4, 1867 (1992)
- [17] GRÜN, G. AND RUMPF, M., *Simulation of singularities and instabilities arising in thin film flow*, Euro. J. Appl. Math. 12, 293–320 (2001)
- [18] HALES, T.C., *The honeycomb conjecture*, Discrete Comput. Geom. 25, 1–22 (2001)
- [19] HALES, T.C., *The Kepler conjecture*, arXiv:math.MG/9811071–9811078
- [20] JÜNGEL, A. AND TOSCANI, G., *Exponential time decay of solutions to a nonlinear fourth-order parabolic equation*, Z. angew. Math. Phys. 54, 377–386 (2003)
- [21] KOEHLER, S.A., STONE, H.A., BRENNER, M.P. AND EGGERS, J., *Dynamics of foam drainage*, Physical Review E, 58, 2097 (1998)
- [22] KOEHLER, S.A., HILGENFELDT, S. AND STONE, H.A., *A generalized view of foam drainage: experiment and theory*, Langmuir 16, 6327–6341 (2000)
- [23] KRAYNIK, A.M., *Foam drainage*, Sandia Report 83-0844 (1983)
- [24] KRAYNIK, A.M., *Foam flows*, Ann. Rev. Fluid Mech. 20, 325–357 (1988)
- [25] KUHNERT, J., *General smoothed particle hydrodynamics*, PhD thesis, Fachbereich Mathematik, Universität Kaiserslautern (1999)
- [26] KUHNERT, J. AND TIWARI, S., *Finite pointset method based on the projection method for simulations of the incompressible Navier-Stokes equations*, Technical report, Fraunhofer ITWM (2001)
- [27] LADYŽENSKAJA, O.A., SOLONNIKOV, V.A. AND URAL’CEVA, N.N., *Linear and quasilinear equations of parabolic type*, AMS (1968)
- [28] LEVEQUE, R.J., *Numerical methods for conservation laws*, Second edition, Birkhäuser (1992)

- [29] MYSELS, K.J., SHINODA, K. AND FRANKEL, S., *Soap films: studies of their thinning*, Pergamon (1959)
- [30] O'BRIEN, S.B.G. AND SCHWARTZ, L.W., *Theory and modelling of thin film flows*, Encyc. Surf. Coll. Sci, 5283–4297 (2002)
- [31] OLEĬNIK, O.A., *Discontinuous solutions of non-linear differential equations*, Am. Math. Soc. Transl. S. 2, 26, 95–172 (1963)
- [32] ORON, A., DAVIS, S.H., AND BANKOFF, S.G., *Long-scale evolution of thin liquid films*, Rev. Mod. Phys. 69, 931–980 (1997)
- [33] OTTO, A., *Methods of numerical simulation in fluids and plasmas*, Lecture notes, <http://what.gi.alaska.edu/ao/sim/> (2003)
- [34] SCHWARTZ, L.W. AND PRINCEN, H., *A theory of extensional viscosity for flowing foams and concentrated emulsions*, J. Coll. Int. Sci. 118, 201–211 (1987)
- [35] TAMIM, J. AND HALLETT, W.L.H., *A continuous thermodynamics model for multicomponent droplet vaporization*, Chem. Eng. Sci. 50, No. 18, 2933–2942 (1995)
- [36] TAYLOR, J.E., *The structure of singularities in soap-bubble-like and soap-film-like minimal surfaces*, Ann. Math. 103, 489–539 (1976)
- [37] THOMSON, W., LORD KELVIN, *On the division of space with minimum partitional area*, Phil. Mag. 24, 503 (1887)
- [38] VAYNBLAT, D., LISTER, J.R., AND WITELSKI, T.P., *Symmetry and self-similarity in rupture and pinchoff: a geometric bifurcation*, Euro. J. Appl. Math. 12, 209–232 (2001)
- [39] VERBIST, G., WEAIRE, D. AND KRAYNIK, A.M., *The foam drainage equation*, J. Phys.: Condens. Matter 8, 3715 (1996)
- [40] WALTER, W., *Gewöhnliche Differentialgleichungen*, 7. Auflage, Springer (2000)
- [41] WEAIRE, D. AND PHELAN, R., *A counterexample to Kelvin's conjecture on minimal surfaces*, Phil. Mag. Lett. 69, 107–110 (1994)
- [42] WEAIRE, D., HUTZLER, S., VERBIST, G. AND PETERS, E., *A review of foam drainage*, Adv. Chem. Phys. 102, 315–374 (1997)
- [43] WEAIRE, D. AND FORTES, M.A., *Stress and strain in liquid and solid foams*, Adv. Phys. 43, 685–738 (1994)

- 
- [44] ZUIDERWEG, F.J. AND HARMENS, A., *The influence of surface phenomena on the performance of distillation columns*, Chem. Eng. Sci. 9, 89–108 (1958)

# Index

- Argyris element, 72
- Asymptotic expansion, 20
- Boundary condition, 44
- Bubble, *see* Foam bubble
- Capillary number, 19
- Cell, *see* Foam cell
- Coarsening, *see* Foam coarsening
- Coercivity, 61
- Colloidal dispersion, 1
- Continuous Thermodynamics, 123
- Dispersion, *see* Colloidal dispersion
- Domain splitting, 76
- Drainage
  - Film, *see* Film drainage
  - Foam, *see* Foam drainage
- Emulsion, 1
- Evaporation rate, 35
- Femlab, 72
- Film, *see* Foam film
- Film drainage, 12
- Finite element method, 68
- Foam, 1
  - bubble, 1
  - cell, 1
  - coarsening, 11
  - creation, 8
  - decay, 11
  - drainage, 11
    - equation, 11
  - Dry, 2
  - film, 3
  - geometry, 9
  - Liquid, 1
    - rheology, 10
  - Solid, 1
    - stability, 5
    - wet, 2
- Froude number, 19
- Frumkin equation, 29
- Galerkin method, 68
- Hölder's inequality, 61
- Initial condition, 44
- Kelvin cell, 9
- Kelvin problem, 9
- Kepler problem, 9
- Kugelschaum, 3
- Lamella, 3
- Langmuir isotherm, 28
- Langmuir-Hinshelwood equation, 27
- Laplace's law, 4
- Liquid content, 1
  - macroscopic scale, 4
- Marangoni force, 5
- Marangoni negative, 6
- Marangoni number, 19
- Marangoni positive, 6
- mesoscopic scale, 4
- microscopic scale, 3
- Navier-Stokes equations, 16
- Newtonian fluid, 16
- Node, 3
- Péclet number, 30

- 
- PDE classification, 56  
Plateau border, 3  
Plateau's laws, 4  
Polyederschaum, 3
- Replenishment number, 31  
Reynolds number, 19  
Riemann problem, 57
- Sobolev space, 58  
Stress tensor, 18  
Surface viscosity, 8  
Surfactant, 5, 26  
von Szyckowski equation, 29
- TFE, *see* Thin film equations  
Thin film equations, 15  
Transition region, 75
- Volatile component, 6, 33
- Weaire-Phelan cell, 10  
Weak formulation, 58



# Curriculum Vitae

27. June 1975	Born in Alzey (Rheinland-Pfalz)
1981 – 1985	Attendance at the Grundschule Wörrstadt
1985 – 1994	Attendance at the Gymnasium am Römerkastell, Alzey
June 1994	Abitur
Oct. 1995 – Oct. 2000	Study of technomathematics at the University of Kaiserslautern
Oct. 1997	Vordiplom in technomathematics
Sept. 1998 – March 1999	Study of technomathematics at Chalmers University, Göteborg
Oct. 2000	Diplom in technomathematics
Jan. 2001 – April 2004	PhD student of the Department of Mathematics at the University of Kaiserslautern in co-operation with the Fraunhofer ITWM, Kaiserslautern